NUMERICAL SOLUTIONS FOR FINITE STRAIN CRACK TIP FIELDS IN SOFT INCOMPRESSIBLE SOLIDS

A Dissertation

Presented to the Faculty of the Graduate School

of Cornell University

In Partial Fulfillment of the Requirements for the Degree of

Doctor of Philosophy

by

Venkat Ramanan Krishnan

January 2009

NUMERICAL SOLUTIONS FOR FINITE STRAIN CRACK TIP FIELDS IN SOFT INCOMPRESSIBLE SOLIDS

Venkat Ramanan Krishnan, Ph. D.

Cornell University 2009

This dissertation concerns itself with problems involving cracks under finite deformation in incompressible hyperelastic materials with special application to soft materials. The main focus is on using numerical methods, in particular the finite element method (FEM), to find the solution of crack tip fields under applied far field loads, in materials undergoing axisymmetric, plane stress and plane strain deformations. In the first chapter a large strain finite element analysis is used to study the deformation of an incompressible Neo-Hookean half space in contact with a flat rigid cylindrical punch. Adhesion is assumed between the elastic solid and punch and the deformation is studied as the punch is retracted. Two interface conditions, frictionless and no slip, are considered. Numerical results are compared with prediction of small strain linear elastic (SSLE) theory. The results show that many aspects of the deformation are not captured by the SSLE theory. For example, the interfacial normal stress at the punch edge is much higher for the case with frictionless boundary condition. The deformation profiles are also very different. The results give important insights on how soft adhesives deform when they detach from a hard surface.

The second chapter makes use of a finite element model to study the behavior of the large deformation field near the tip of a crack in a soft incompressible plane stress fracture specimen loaded in Mode I. Results are obtained for the case of a Neo-Hookean solid (ideal rubber) and a hyperelastic solid with exponentially hardening

behavior. In contrast to the predictions of linear elastic fracture mechanics (LEFM), the near tip stress fields are dominated by the opening stress which shows a *1/R* singularity for the Neo-Hookean material and a *-1/RlnR* singularity for the exponential hardening solid. The results show very similar qualitative behavior in the near tip stress fields despite the very large difference in strain hardening behavior of the two material models. Further, the results show that the near tip opening stress is controlled by the far field energy release rate for large applied loads.

The third chaper presents a numerical study of finite strain deformation fields near the tip of an interface crack between a rigid substrate and an incompressible hyperelastic solid using the finite element method (FEM). The FEM simulations make use of a remeshing scheme to overcome mesh distortion. Analyses are carried out by assuming that the crack tip is either "*pinned*", i.e., the elastic material is perfectly bonded (*full friction*) to the rigid substrate, or *frictionless*. The focus is on a material which hardens exponentially.

For both the frictionless interface and the pinned crack under plane stress deformation, it is found that the true stress field directly ahead of the crack tip is dominated by the normal stress (T_{22}) and the crack face opens up smoothly. This is also true for an interface crack along a frictionless boundary in plane strain deformation. However, for a pinned interface crack under plane strain deformation, the true opening normal stress (T_{22}) is found to be lower than the shear stress (T_{12}) and the transverse normal stress (T_{11}). Also, the crack opening profile for a pinned crack under plane strain deformation is completely different from those seen in plane stress and in plane strain (frictionless boundary condition). The crack face flips over and the tip angle is almost tangential to the interface. The results suggest that interface friction can play a very important role in interfacial fracture of soft materials on hard substrates.

BIOGRAPHICAL SKETCH

The author was born in Hyderabad, India on January 29, 1982. After completing his schooling from HAL Higher Secondary School (Balanagar) and later Little Flower Junior College (Uppal) in Hyderabad, the author was admitted into the Bachelor of Technology program at the Indian Institute of Technology (IIT), Bombay in 1999, from where he received his degree in Civil Engineering in May 2003. In August 2003, the author was admitted into the MS program in the Department of Civil Engineering at Cornell University with a research assistantship, from where he has a Masters degree. He later transferred to the department of Theoretical & Applied Mechanics in January 2005 to continue on a Ph.D. program which he successfully completed on Sept. 26, 2008. That is the just the short of it!

It was the "pen-penultimate" day of the end of the first month, in the 35th year of Indian independence; Dark was the night and weird the atmosphere. It rained from time to time. Between thunderclaps could be heard the crying of babies in the neighboring wards. But the newborn swerved not; Venkat Krishnan was born in the lineage of the great sage Vishwamithra! When he was 3 years old, his mother, already tired of his mischief mongering at home, wasted no time in enrolling him in school. School was monotonous and boring, and to make it worse, the pedantic teachers made the author's life miserable by ever drawing comparisons with his sister who was a goody two shoes. The only respites were the lunch breaks, the games periods and the Sanskrit classes, Sanskrit being the author's favorite subject. The author disliked English, mostly because the English teachers were too phony and the grammar is funny. His school years were also memorable on account of the numerous fights with his sister over access to the TV, sweetmeats and mostly just for fun. After 15 years of high school, when the author had finally begin to master the not so gentile art of gully

cricket, thanks largely to the countless after school hours in the sun with likeminded chums, he was forced through a major transition. The following 2 years in junior college were spent in the company of nerds and wannabe nerds whose lunch time discussions revolved around the physics problems in “Irodov”. Understandably, the best times for the author then were the rides to and fro in the college bus when he had chirpy company. His favorite subject in college again was Sanskrit, mostly because the Sanskrit lecturer was a hilarious guy who displayed unabashed favoritism towards pupils good at the subject. Not so curiously, the good old vice-principal who taught English took a liking to the author and often gave him permission to leave his lecture, sometimes within minutes of the class starting. The author’s pet peeves in college also included chemistry, thanks largely to the lab which forever reeked of Sulphur. At the end of those 2 years, the author, mentally sharper from all the time spent avoiding the company of geeks, appeared for the all India joint entrance exam for the IITs and sneaked through, despite a forgettable performance in chemistry.

The next 4 years in IIT Bombay passed as if a dream. The author played a lot of Cricket, Table Tennis, Squash, Basketball and Volleyball. He made the hostel team in almost every sport, even swimming, though mostly only due to lack of enough team players! Academically, the author did well in mechanics and set forth to Cornell for graduate studies in computational mechanics, dooming himself into spending cold dark winters for the next five years. The time spent far away from civilization has however helped the author enhance his non academic skills. In addition to his numerous other talents, the author can now boast of tennis, skiing, windsurfing, and boxing! The author’s only regret as he leaves Cornell, is not to have taken a course in Sanskrit. Nonetheless, he hopes to go back to his first academic love in the near future.

to my dear sister, Priya Kannan.

ACKNOWLEDGMENTS

I am grateful to many people for their help and support in the completion of this dissertation and the research associated with it. I would like to specially thank my advisor, Professor Herbert Hui for his support and guidance over the last 2 years. He readily accepted me in his research group after my ex-advisor Prof. Katerina Papoulia left Cornell in 2005. He always has time for his students and has a unique ability to inspire them with his wonderful curiosity for any and everything under the sun. I will always cherish the time spent with him academically and otherwise; discussions on tennis, sports, politics etc in the T&AM lounge during lunch in particular, were real fun. I would also like to thank my special committee members, Professors Alan Zehnder and Leigh Phoenix; their courses provided valuable knowledge and skills during the course of my Ph.D. work.

Outside my committee, I would like to acknowledge professors Katerina Papoulia and Steve Vavasis, both now in the Univ. of Waterloo, who were really helpful during the formative years of my Phd. Their intensive numerical computing courses imparted valuable knowledge and mathematical skills needed for my research. I would like to thank Michelle Seitz and Prof. Kenneth Shull of Northwestern University whose experiments motivated this work. I am also thankful to my groupmates Lulin, Jingjou and Rong with whom I have shared a lot of brain storming sessions during our weekly group meetings.

I would like to thank the all the members (faculty, staff and students) in the department of Theoretical and Applied Mechanics for making my stay in Cornell very enjoyable; special thanks to Cindy, Dan and Neil who were always around for help. I am grateful to T&AM for supporting me through a teaching assistantship during my fourth and fifth years at Cornell. I am also thankful to the Cornell theory center, now

CAC, for providing me with access to ABAQUS. This research was conducted using the resources of the Cornell University Center for Advanced Computing, which receives funding from Cornell University, New York State, the National Science Foundation, and other leading public agencies, foundations, and corporations.

I would also like to acknowledge several discussions with my friends and roommates Dr. Sethuraman Sankaran and Dr. Veera Sundararaghavan, who were of great help with the numerical aspects of my research. Tennis and cooking sessions with Sethu will be unforgettable, and so will the time I spent with the Cornell Cricket and Table Tennis teams during practice and tournaments. I am also glad to have met Aruna and the rest of the TBC gang. Aruna is a wonderful friend and I wish her all the best for her Phd in MIT.

Finally, I cannot fail to mention the calming influence of Carnatic music during the past few years! The effect that Semmangudi's scintillating "Marubalka" in raga Sriranjani, Madurai Mani's divine Rama nee samanam" in Kharaharapriya and MDR's majestive "Giripai" in sahana have on me is beyond words. They never fail to lift my spirits in the most testing of times. I am eternally grateful to the bard saint Tyagaraja for composing such masterpieces. I am also thankful to Lord Krishna for everything! His Bhagavad Gita always has and will guide me through life. I also express my deepest gratitude to my parents, sister and grandmother for their boundless support, patience and sacrifice through these five years.

TABLE OF CONTENTS

LIST OF FIGURES

LIST OF ABBREVIATIONS

NH……..Neo-Hookean

PSA……pressure sensitive adhesive

FEM……...finite element method

GK…….…….Guebelle & Knauss

KS…….…..Knowles & Sternberg

PREFACE

This dissertation includes two chapters that originally were written independently as separate papers. The references to these papers are given as footnotes in the beginning of each chapter. The third and final chapter is based on a working paper which will be sent out for publication shortly. Symbols referring to mathematical or physical quantities should be checked carefully for meaning within the text. Although effort was made to use consistent notation throughout, some symbols may have different meanings in different chapters.

CHAPTER 1

LARGE DEFORMATION OF SOFT ELASTIC MATERIALS IN ADHESIVE CONTACT WITH A RIGID CYLINDRICAL FLAT PUNCH[1]

1.1 Introduction

A fundamental problem in adhesive contact mechanics is the deformation of a linear elastic half space caused by the retraction of a flat cylindrical rigid punch. The solution is often attributed to Boussinesq [1]. A good review on how this solution can be used to study axisymmetric adhesion tests and contact mechanics for soft materials can be found in work by Shull [2]. It should be noted that the solutions and models presented by Shull [2] are all based on small strain linear elastic (SSLE) theory.

Soft materials, such as pressure sensitive adhesives (PSAs) and polymer gels deform readily under moderate stresses, and this property makes them good candidates to bond to surfaces where only van der Waals surface interactions are available. From the point of view of the numerical or analytical prediction of the deformation however, the low modulus of these materials is a mixed blessing, because the SSLE assumption breaks down for many problems of practical interest. For example, the modulus of most polymer gels is of the order of kPa. For materials with such a low modulus, even relatively weak forces can cause very large deformations. In particular, the deformation near stress concentrators, such as the tip of a crack or the edge of an indenter, can be so extensive that the solution cannot be addressed by the usual SSLE theory. The recent 3-D experiments of Yamaguchi *et al.* [3] show clearly that the

[1] Reproduced by permission of the royal society of chemistry. http://www.rsc.org/delivery/_ArticleLinking/ArticleLinking.cfm?JournalCode=SM&Year=2008&ManuscriptID=b804340j&Iss=9

deformation of the soft material is well into the non-linear regime and involves large changes in geometry.

The SSLE assumption breaks down in two ways, first, the geometry of deformation is incorrectly described by small strain theory, second, the material behavior is no longer linear, that is, the deformation (strain) is no longer linearly proportional to the stress. However, despite growing interest in the mechanical behavior of soft materials, there has been almost no large deformation analysis of how these materials behave during indentation and retraction. An exception is the recent work by Lin and Chen [4], who carried out a large deformation analysis of the Johnson–Kendall–Roberts (JKR) theory [5]. It turns out that the computational difficulty of the present problem is much greater than the large deformation JKR problem, since the deformation can be much larger. A discussion of the importance of large deformation analysis to soft material problems can be found in a recent article by Shull [6]. In this paper, we study the retraction of a rigid cylindrical flat punch which is in adhesive contact with an incompressible Neo-Hookean half space. The undeformed reference geometry is shown schematically in figure 1.1a. To put our results into perspective, we briefly review the SSLE solution. The half space is assumed to be homogeneous, isotropic, incompressible and linearly elastic. In addition, its surface is in *frictionless contact* with the flat cylindrical rigid punch. The contact pressure σ_{zz} is [7]:

$$\sigma_{zz}(r < a, z = 0) = P/\left(2\pi a\sqrt{a^2 - r^2}\right) \tag{1.1}$$

where a is the punch radius, P is the normal force acting on the punch, r is radial distance from the center of the contact circle (O) and z is the vertical axis of a

cylindrical coordinate system centered at O. The punch displacement Δ is related to the normal force P by

$$\Delta = CP \tag{1.2}$$

where C is the compliance and G is the shear modulus of the half space. The compliance is [7]

$$C = 1/(8Ga). \tag{1.3}$$

In this work, we focused on incompressible elastic solids, e.g. elastomers. Also, we adopt the standard notation that tensile stress is positive, i.e., $P > 0$ during retraction. Note that equation (1.1) predicts that the interfacial normal stress at the contact edge ($r = a$) has an inverse square root singularity. The intensity of the singularity is given by the stress intensity factor K_I, which is

$$K_I = P/2a\sqrt{\pi a} = 4G\Delta/\sqrt{\pi a}\,. \tag{1.4}$$

The SSLE result given by (1.4) states that contact stress at the edge of the punch has an inverse square root singularity; identical to the stress field directly ahead of a Mode I crack in an elastic solid. Indeed, because the punch is rigid, one can replace it with a rigid half space (e.g. by adding (rigid) material to the sidewall of the punch) provided that none of the added material is in contact with the elastic half space. Thus, the problem of retracting a punch from the substrate is equivalent to the problem illustrated in figure 1.1b, that is: A uniform displacement in the z direction, $\Delta > 0$, is applied to the rigid upper half space. The lower half space $z < 0$ is occupied by an incompressible linear elastic solid. An external interface crack occupies the region $z = 0, r > a$.

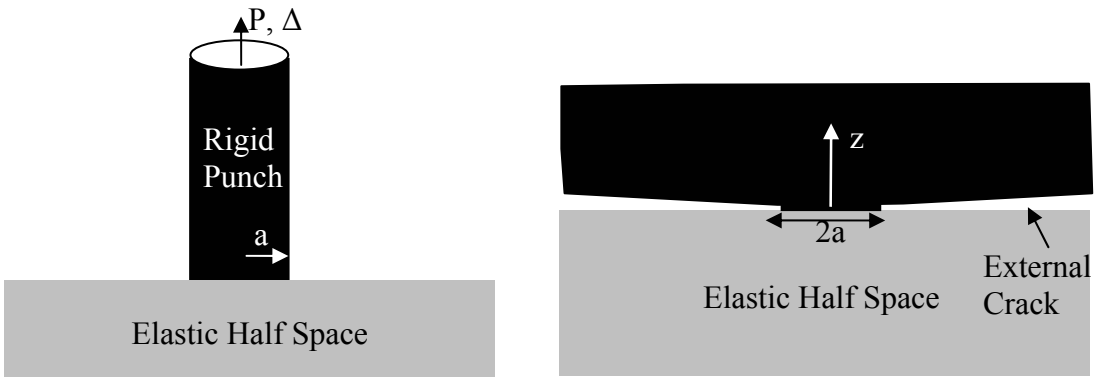

(a) (b)

Figure 1.1a shows a flat rigid punch with a circular cross-section (radius = *a*), in adhesive contact with an infinite substrate of a soft incompressible material. b: For $P > 0$ (tension), the punch can be substituted by a rigid half space with an external crack as shown, that is, the circular edge of the punch can be viewed as the front of an external crack that is infinite in extent. (r, z) are the co-ordinates in the axisymmetric problem.

It should be noted that the Boussinesq solution given in (1.1) assumes frictionless contact, that is, the shear stress on the interface is zero. In practice, the no slip condition, where sliding of the contacting surfaces is not allowed, is much more realistic. Fortunately, as long as the punch is *rigid* and the elastic material *incompressible and its spatial dimensions are large compared with the punch radius*, the interfacial shear stress will vanish even if the no slip condition is imposed. Furthermore, the normal interfacial stress is the same (given by (1.1)) whether or not the interface slips. It should be noted that this result is only valid when the strains are *small*. For large deformation, the two boundary conditions will give very different results, as we shall see below.

A test that is relevant to this work is the classical probe tack test [8, 9]. In this test, the thick elastic substrate considered in this work is replaced by a thin layer of PSA, one side of which is bonded to a rigid substrate. The cylindrical punch (in this case a steel probe) is brought into intimate contact with the exposed surface of the elastic layer and then retracts at a fixed rate (see figure 1.2a). Because the elastic layer is thin and incompressible, punch retraction give rise to high hydrostatic stress which promote growth of cavities from small crack-like defects on the interface between the punch and the PSA (see figure 1.2b). Experiments have shown that when the adhesive is debonded from a high energy surface [10, 11], the crack fronts of these defects do not propagate along the interface but are pinned, which allows them to grow into cavities shown schematically in figure 1.2d. Figure 1.2d show that the deformed crack surface has rotated about the pinned tip, so that the angle (θ) between the rotated crack face and the interface is almost 180^0. Following this development, the cavity starts to grow, resulting in the formation of a thin wall of material (fibrils) between neighboring cavities. The profile of the deformed crack face (or cavity) in figure 1.2d is referred to as "the foot of the fibril" in the work of Glassmaker et al

[12]. It is difficult to explain this phenomenon using SSLE theory. For example, SSLE theory will predict a completely different surface profile during the growth of these crack-like defects (see figure 1.2c). Specifically, SSLE theory predicts that the crack opening displacement is proportional to $\sqrt{d}$ (see figure 1.2b,c), where d is the distance behind the crack tip, which means that $\theta \approx 90^0$; whereas the actual θ is almost 180^0 (see figure 1.2d). In addition, the energy release rate in the SSLE theory is proportional to the square of the punch displacement. Since adhesion is primarily due to van der Waals interaction, the work of adhesion is on the order of $0.1 J/m^2$. Even if one takes into account of viscoelastic deformation, it is hard to explain how the crack front remains pinned despite the fact that the energy release rate increases as the square of the punch displacement. This apparent paradox can be explained by crack blunting and stress relaxation, as we will demonstrate below.

It is also interesting to examine the case of weak adhesion. Zhang et al [13-14] and Léger et al [15] in particular, have shown in beautiful peel tests with fluorescent probes that when a PSA is detached from a non-adhesive surface, such as a silicone surface, the peel force is controlled by the resistance to slippage of the interface. If the adhesive macroscopically slips, the peel force is low, while if the adhesive does not slip the adhesive is sheared and the adhesive force is high. It should be noted that these peel tests were carried out with a very small peel angle and the adhesive was almost loaded in pure mode II.

The plan of this chapter is as follows. In section 1.2 we specify the material model and the normalization schemes used to present our results. A discussion of the finite element method (FEM) is given in section 1.3. Finite element results will be presented in section 1.4 which is followed by a discussion and summary. This work was reported in Krishnan et al (2008).

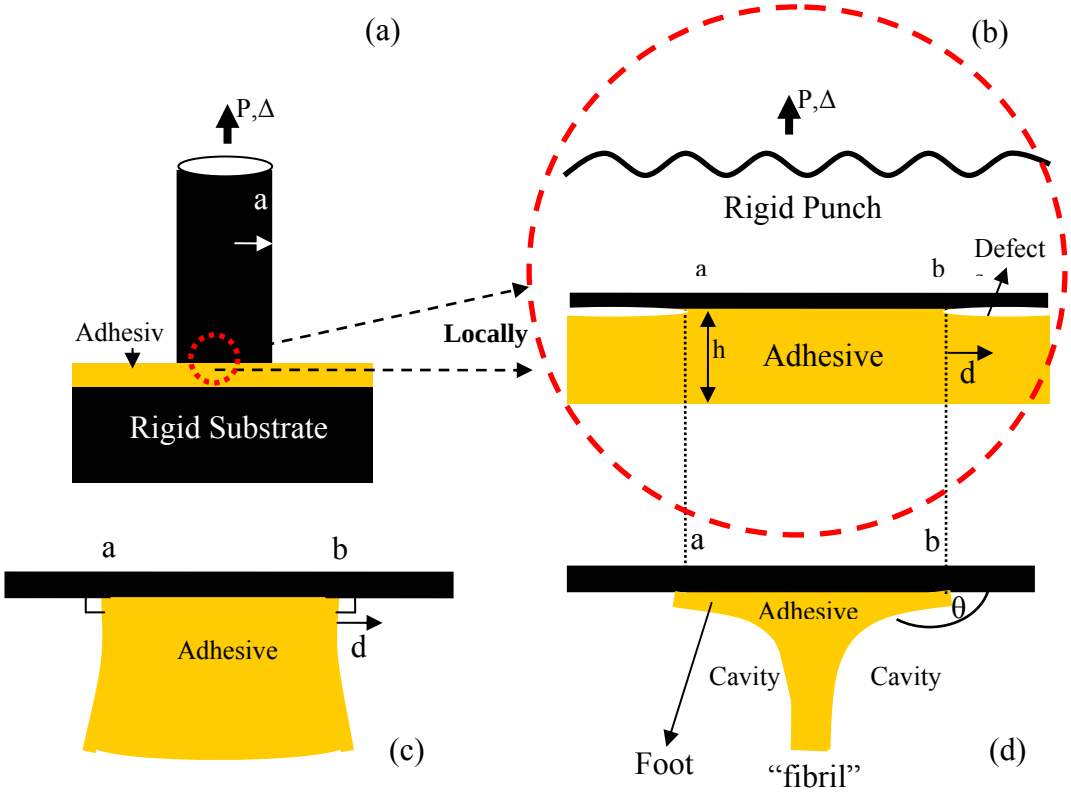

Figure 1.2: (a) A schematic of a tack test. The rigid flat punch is in adhesive contact with a thin layer of soft adhesive. It is then pulled upwards in the vertical direction. (b) An expanded view of the interface region: the applied load causes crack-like defects on the punch–adhesive interface to grow. In good adhesives, the tips of these defects are pinned between points a and b. (*d* is the distance behind the crack front.) (c) A close up view of the deformation near the pinned crack predicted by SSLE theory, note that the angle θ made by the adhesive with the punch surface is 90°. (d) Observed deformation, the angle θ made by the adhesive with the punch surface is close to 180°. The foot refers to the thin layer of material attached to the interface.

1.2 Material Property

All simulations are conducted using a Neo-Hookean solid (an ideal rubber) which has universal appeal. A weakness of this model is that it underestimates the stresses at very large deformations, since real polymer chains have a finite extensibility. We emphasize that simulations can also be performed using more realistic strain energy functions which model the deformation more accurately for a particular material. The strain energy function W for a Neo-Hookean solid is

$$W = G(I_1 - 3)/2 \tag{1.5}$$

where G is the small strain shear modulus and $I_1 = \sum \lambda_i^2$ *(i = 1,2,3)*, is an invariant which is the sum of the square of the principal stretches λ_i. In an uni-axial test of a straight bar in the *1* direction ($\lambda_2 = \lambda_3 = 1/\sqrt{\lambda_1}$), the true (Cauchy) stress σ for a Neo-Hookean solid is related to the axial stretch $\lambda = \lambda_1$ by

$$\sigma = G\left(\lambda^2 - \lambda^{-1}\right) \tag{1.6}$$

Dimensional analysis implies that the indenter load P must be related to the indenter displacement Δ by

$$P/8Ga^2 = \phi\left(\Delta/a\right), \tag{1.7}$$

where ϕ is an unknown dimensionless function. The numerical factor of *8* in equation (1.7) is inserted so that $\phi(\Delta/a \to 0) \to \Delta/a$ as required by SSLE theory (see (1.2) and (1.3)). Equation (1.7) states that the normalized load depends *only* on the normalized displacement. Using (1.7), the compliance $C = \Delta/P$ is

$$C = \frac{\Delta / a}{8Ga\phi(\Delta / a)}. \tag{1.8}$$

Equation (1.7) suggests defining a normalized load $\bar{P}$ and a normalized displacement $\bar{\Delta}$ by

$$\bar{P} = \frac{P}{8Ga^2}, \qquad \bar{\Delta} = \Delta / a. \tag{1.9}$$

Likewise, the normalized compliance

$$\bar{C} \equiv 8GaC = \bar{\Delta} / \phi(\bar{\Delta}) \tag{1.10}$$

is a function of the normalized displacement only.

We are interested in the true stress (Cauchy stress) distribution, particularly the traction in the contact region. In the following, stresses will be normalized by G and lengths will be normalized by a, the punch radius. Two kinds of interface conditions are considered: no slip and frictionless.

1.3 Finite element Method

The problem was solved using an axisymmetric finite element model in ABAQUS [16]. According to our normalization, the punch radius was chosen to be 1 unit. The half space is approximated by a square 100 unit in length. We have verified that this is sufficient to simulate the half space, that is, the result of our simulation do not change in any significant way if we increase the size of the square. To simulate retraction, a uniform normal displacement was imposed on the contact zone. For the no slip case, the shear displacement is zero in the contact zone and a uniform vertical

displacement is applied on the interface. For the frictionless case, only a vertical uniform displacement is applied and the shear traction on the interface is zero. The elastic "half space" was modeled using *hybrid quadrilateral* elements which have a pressure degree of freedom in addition to the usual displacement degrees of freedom. This extra degree of freedom accounts for incompressibility. A typical simulation has about 40000 nodes. Because of the high stresses near the contact edge and the large deformation imposed, very large mesh distortion results even for very small applied displacements ($\Delta / a \approx 0.1$) . Therefore, simulations are carried out in multiple steps and adaptive meshing is used.

For quasi-static problems, ABAQUS does not have an automated adaptive tool to reduce mesh distortion. A Python script was coded to automate the adaptive meshing. Details of our coding effort will be reported in chapter 3. Briefly, in a step, an incremental displacement is applied. This increment is taken to be sufficiently small so that mesh distortion does not affect the results near the contact edge. The deformed geometry is then re-meshed and the old solutions (stresses and deformation) are re-mapped to the new mesh. Specifically, the stress and deformation gradient is extracted from the integration points of the old mesh and applied to the integration points of the new undistorted mesh at the corresponding locations. Hence the new mesh will inherit the previous stresses before the new incremental displacement is applied on the boundary. This procedure is successively applied until the desired degree of punch displacement is achieved. We have validated this procedure for some simple problems where the analytical solutions are known. We also validated our finite element method by solving a plane strain crack problem and comparing the near tip stress fields with the asymptotic solutions of Stephenson [17].

1.4 Results

In the following, all stresses reported are Cauchy or true stresses. Recall that the normalized solution (normalized load, normalized stresses) depends on the single dimensionless parameter $\bar{\Delta}$ (normalized punch displacement). The normalized punch force $\bar{P}$ versus normalized punch displacement $\bar{\Delta}$ is plotted in figure 1.3. The dashed line is for the frictionless interface whereas the solid line is for the no slip case. The SSLE theory ($\bar{P}=\bar{\Delta}$) is also plotted in figure 1.3 for comparison. During retraction, the computed compliance is significantly larger than the prediction of SSLE theory for $\bar{P}>1$. Using the results in figure 1.3, we obtain polynomial fits (error less than 0.5% for $\bar{\Delta}\le 4$) for the compliance functions for the no slip (C_{ns}) and frictionless (C_s) boundary conditions. These functions are normalized by the compliance of the SSLE theory *1/8Ga* and are given by equations (1.11a, b)

$$8GaC_{ns}\left(\bar{\Delta}\right)=0.0045\bar{\Delta}^4-0.0462\bar{\Delta}^3+0.1570\bar{\Delta}^2-0.0530\bar{\Delta}+1, \quad \text{(no slip)} \tag{11a}$$

$$8GaC_{s}\left(\bar{\Delta}\right)=0.0028\bar{\Delta}^4-0.029\bar{\Delta}^3+0.0788\bar{\Delta}^2+0.1031\bar{\Delta}+1, \quad \text{(frictionless)} \tag{11b}$$

Although the compliances are not significantly affected by large deformation, the deformations and stresses are. To study the evolution of the normal stress profile in the contact zone, we marked a sequence of points (*a, b, c*, etc.) on the force displacement curve in figure 1.3. The corresponding normal contact stress profiles are plotted in figure 1.4 (no slip, solid line). Figure 1.4 shows that when sliding is not permitted, the normal stress singularity at the interface near the contact edge disappears. Specifically, the normal contact stress at a fixed material point close to the contact edge initially increases with the applied displacement, reaches a maximum, and then decreases for sufficiently large displacements. The maximum normal stress occurs directly above the blunted crack tip, which lies below the interface. This result

explains why interface cracks in a tack test remain pinned despite increases in applied displacement (see figure 1.2c). This result is at odds with the SSLE theory, which predicts that the stress at the edge should be governed by an inverse square root singularity given by (1.1); in addition, the magnitude of this singularity should increases linearly with the applied punch displacement. Figure 1.4 shows that the normal stress oscillates in the region close to the contact edge after its maximum value. We believe that this oscillation is real and is not due to numerical instability (see discussion).

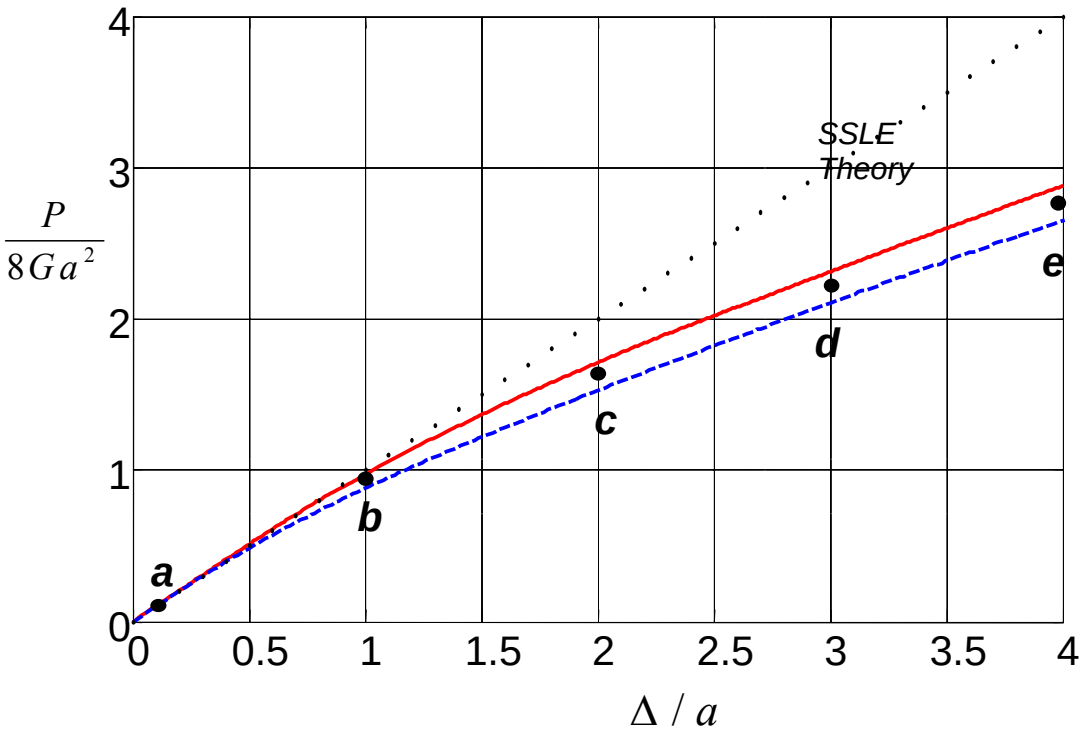

Figure 1.3: Normalized load *versus* normalized displacement. ━━(no slip), – – – (frictionless), ···(SSLE prediction); a, b, c, d and e show different stages of applied displacement.

To gain insight into how the interfacial normal stress near the edge relaxes despite increase in applied displacement, we examine the local deformation by tracking the evolution of the deformed profile of the elastic material surrounding the contact zone. These profiles corresponding to different stages of deformation are shown in figure 1.5 (no slip). The no-slip case clearly shows the evolution of the "foot" referred by Glassmaker et al [12] (see Fig 1.2d). Intuitively, the foot shape geometry reduces the stress concentration at the contact edge. Since the contact edge can be regarded as the front of an interface crack before load application (see introduction), the development of the "foot" corresponds to crack blunting. Indeed, during deformation, the blunted crack tip moves inwards and away from the interface. At very large applied displacements, the elastic material surrounding the edge deforms into the surface of a "drawn" fibril, similar to those observed in a tack test (see figure 1.2d). The fact that the normal stress relaxes at the contact edge implies that the strains are also small there, suggesting that the deformation there is primarily due to rigid body rotation. The relaxation of interfacial normal stress is compensated by high interfacial shear stress, which builds up rapidly from zero to its maximum near the edge. This is shown in figure 1.6 for different applied normalized punch displacements. Note that the peak interfacial shear stress occurs much closer to the contact edge than the maximum interfacial normal stress. The maximum interfacial shear stress can actually be higher than the maximal interfacial normal stress. The maximum principal stress along the blunted crack front is plotted in figure 1.7 for different values of normalized punch displacements. These plots show that the stretch along the crack front becomes more evenly distributed as it blunts.

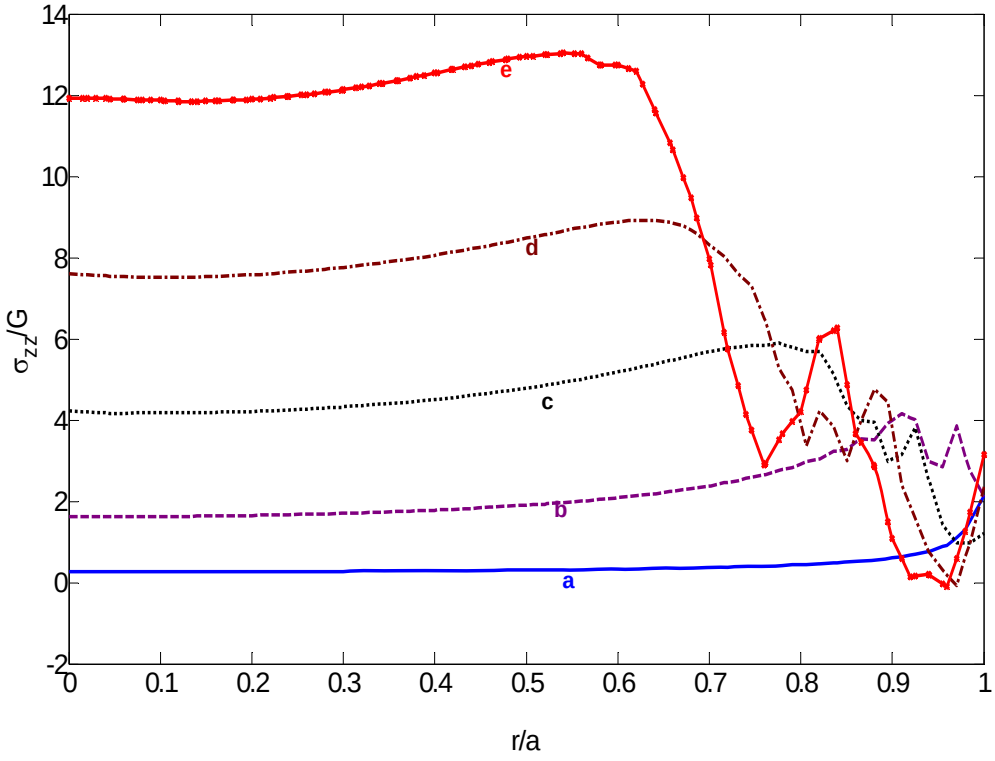

Figure 1.4: Normalized interfacial normal stress profile (no slip). (a, b, c, d and e correspond to Δ/a = 0.2, 1.0, 2.0, 3.0 and 4.0 respectively, see figure 1.3.)

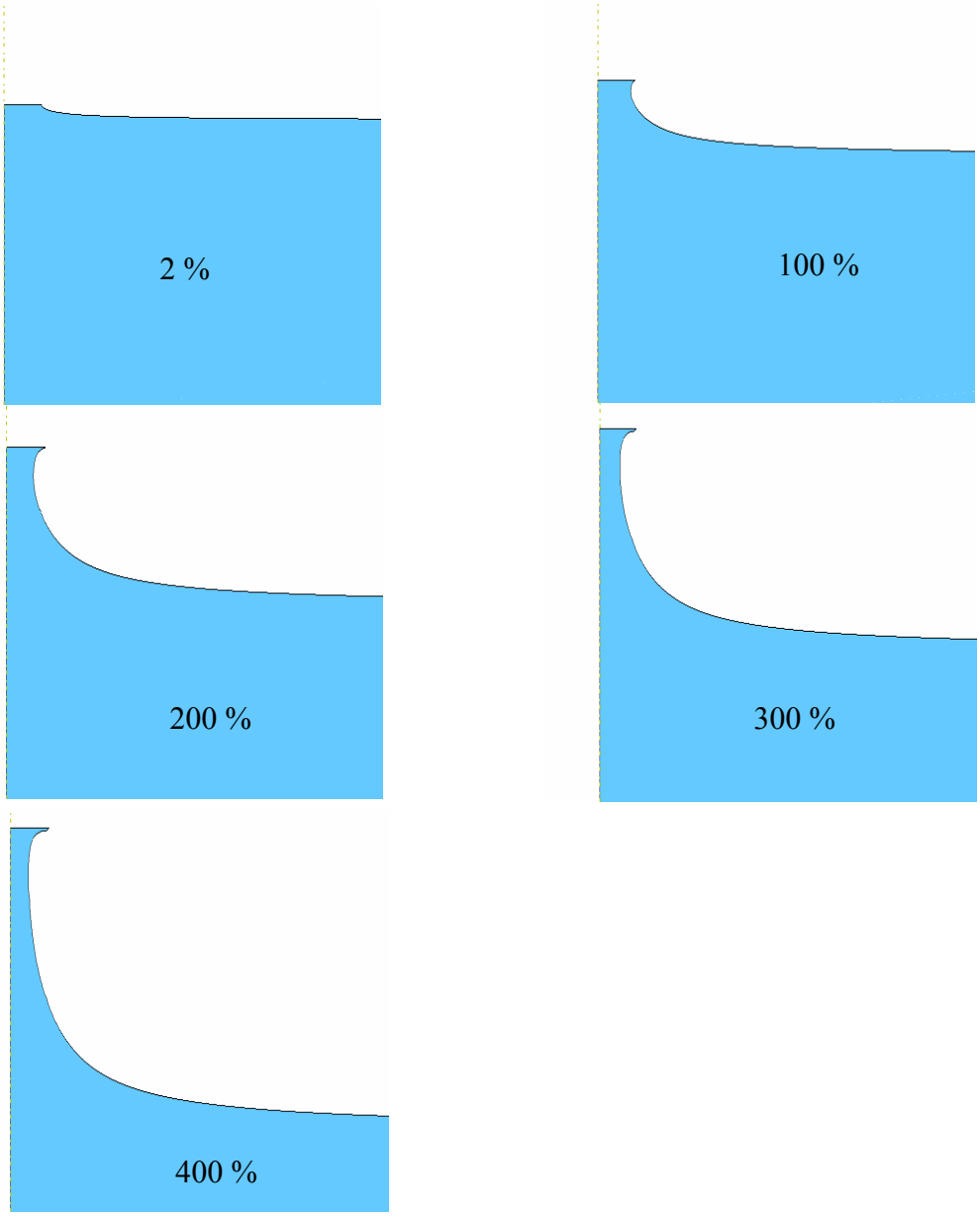

Figure 1.5: Deformation profiles for no slip contact. The percentage applied strain is also shown.

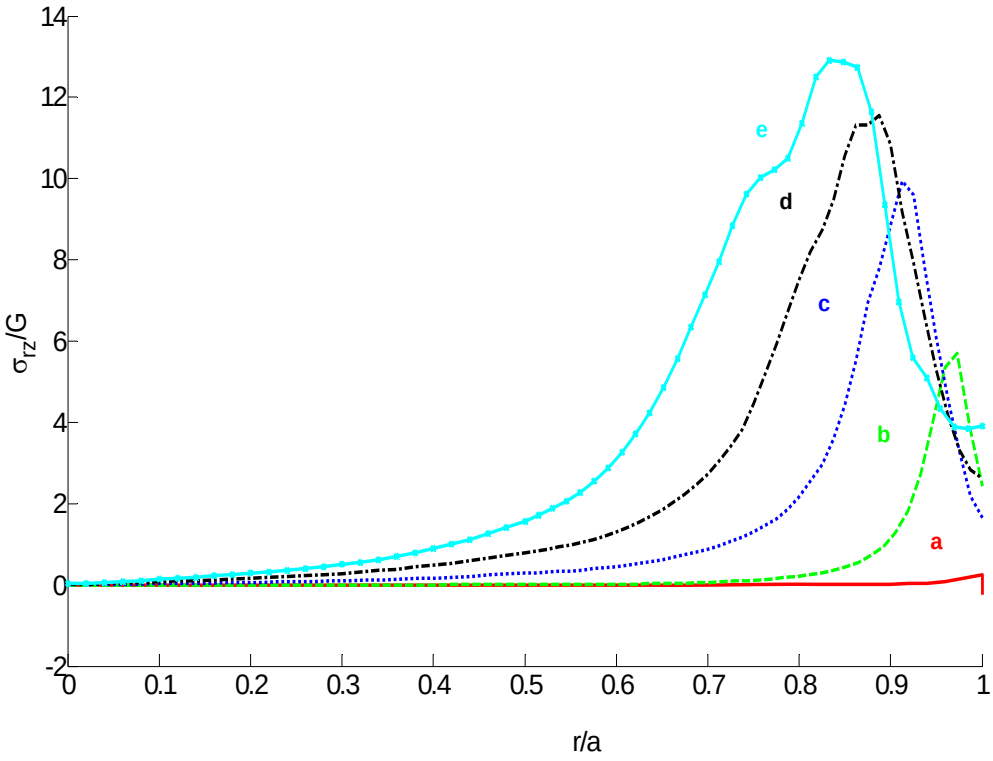

Figure 1.6: Normalized interfacial shear stress profile (no slip). (a, b, c, d and e correspond to Δ/a = 0.2, 1.0, 2.0, 3.0, 4.0 respectively, see figure 1.3.)

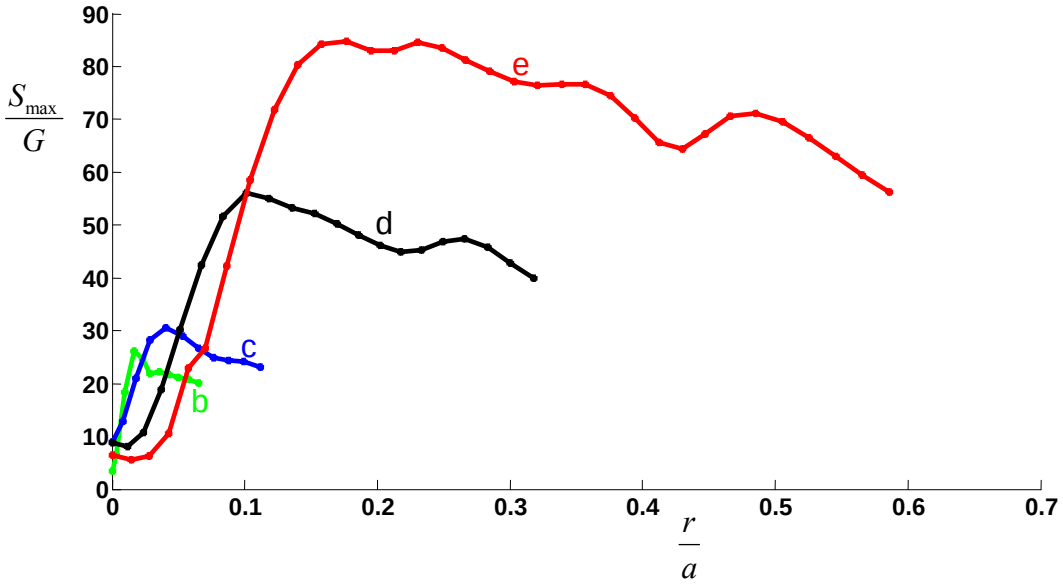

Figure 1.7: Normalized maximum principal stress along the blunted crack front for different values of applied displacements (no slip). (b, c, d and e correspond to Δ/a = 1.0, 2.0, 3.0, 4.0 respectively, see figure 1.3.)

The situation is quite the opposite when the interface is allowed to slide (frictionless), the normal interfacial stress seems to exhibit a singularity which increases with the applied displacement, as shown in figure 1.8. Indeed, figure 1.10 shows that the contact edge remains vertical to the punch's flat surface. Intuitively, this gives rise to the high interfacial normal stress at the contact edge and will cause the crack to propagate. This is indeed observed experimentally in probe tests [18, 19]. It should be noted that, due to slip, the contact radius r_c is less than the punch radius a. In other words, the contact edge is no longer the punch edge. A comparison of figure 1.4 and figure 1.8 shows that there are significant differences in the magnitude of interfacial normal stresses between the no slip and the frictionless boundary condition, in contrast to the prediction of the SSLE theory. Recall that there is no stress concentration at the contact edge for the no slip case.

One may think that because the normal force at the same applied displacement is higher for the no slip case (see figure 1.3), the normal stresses should be higher. However, this reasoning is flawed because the increase in normal force due to slip cannot compensate for the reduction in contact area, hence the normal stresses in the no slip case are actually lower. The normalized contact radius r_c/a is plotted against the normalized applied displacement in figure 1.9, which shows a significant reduction of the contact radius due to slip ($\approx 50\%$ at $\bar{\Delta} = 4$). A numerical fit of the normalized contact radius as a function of the normalized punch displacement is shown in the same figure. The fact that in the no slip case, the contact radius remains equal to the punch radius implies that interfacial shear stress must develop as shown in figure 1.4. Note that this result also contradicts the SSLE theory which predicts the interface shear stress is zero for both cases.

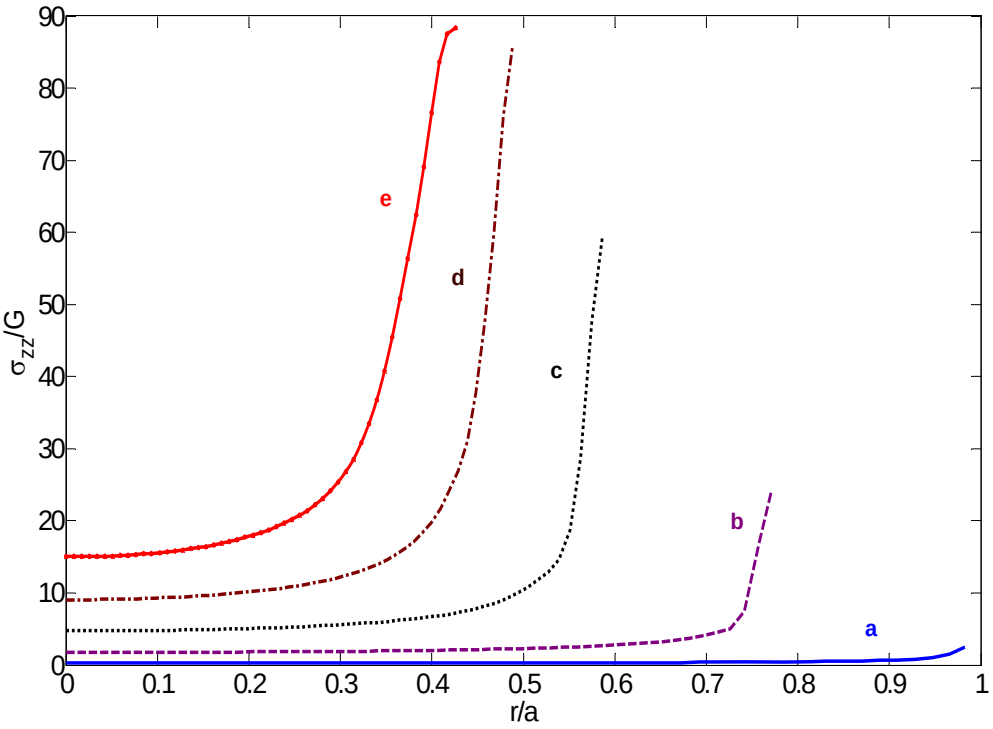

Figure 1.8: Normalized interfacial normal stress (σ_{yy}/G) profile (frictionless case). (a, b, c, d, e correspond to Δ/a = 0.2, 1.0, 2.0, 3.0, 4.0 respectively, see figure 1.3).

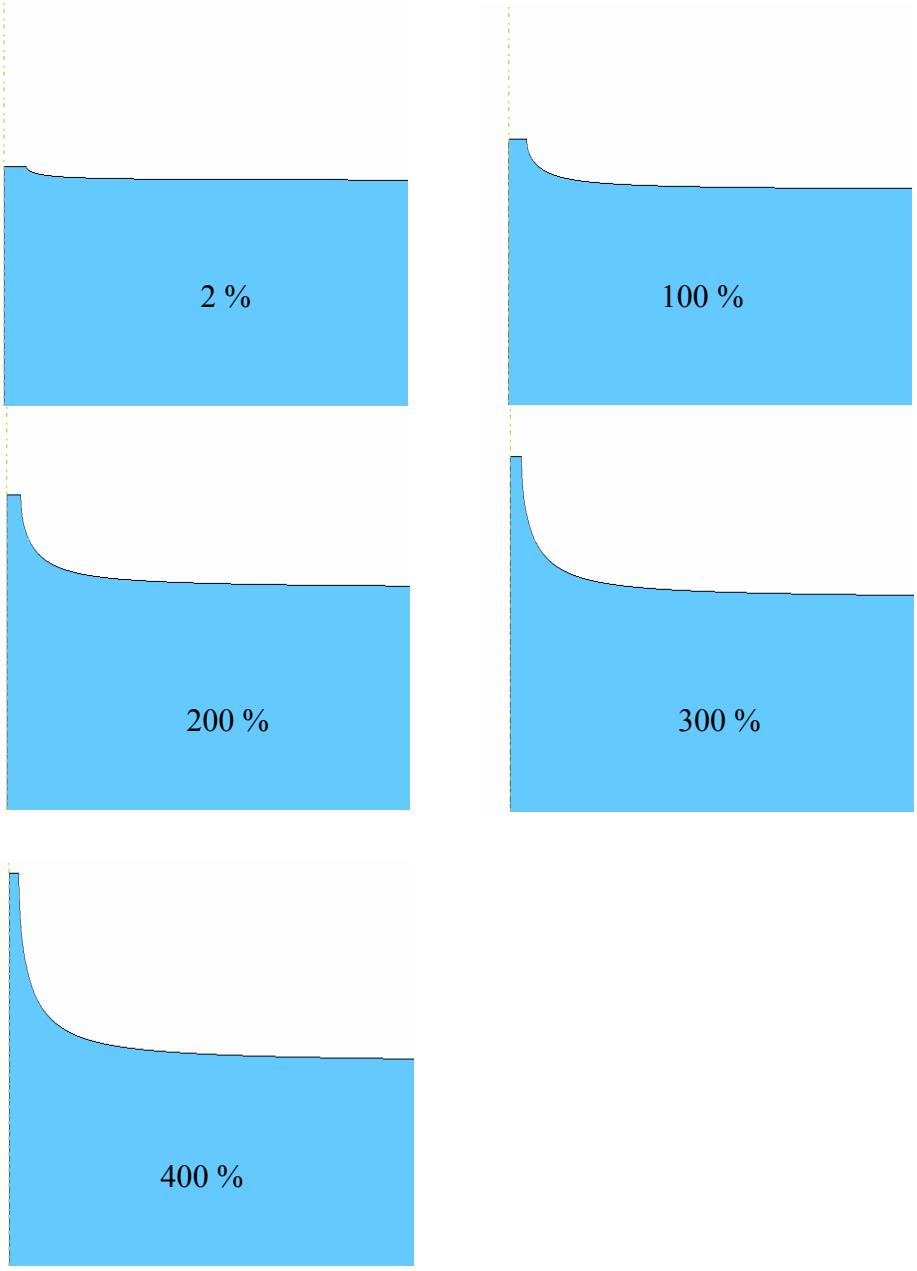

Figure 1.9: Deformation profiles for frictionless contact. The percentage applied strain is also shown.

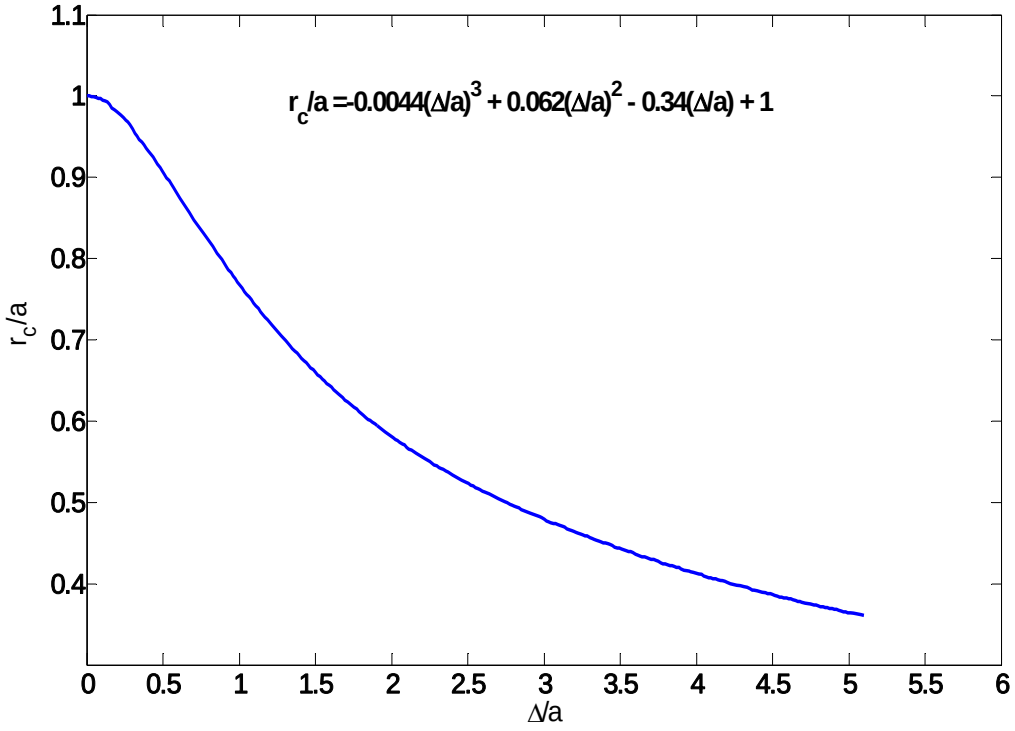

Figure 1.10: Normalized contact radius *versus* normalized punch displacement for frictionless contact.

1.5 Summary and Discussion

We carried out large deformation simulations for a rigid flat circular punch retracting from an elastic half space and computed the normalized compliance and contact stresses for both indentation and retraction. The interfacial normal stress for the no slip case is bounded at the punch edge but it shows oscillations after the peak stress, which occurs almost directly above the blunted crack tip. We believe that the oscillations are real and not numerical instabilities. We have refined our mesh to the finest mesh size allowed in Abaqus ($5x10^{-5}$) and found that oscillations still persist. To confirm the accuracy of the finite element code and the remeshing procedure, we carried out a simulation of a plane strain crack in a Neo-Hookean solid. Specifically, we studied the stress field near the tip of a plane strain crack in a homogeneous Neo-Hookean solid. The main difference between this plane strain problem and the punch problem studied above is the presence of a bimaterial interface in the punch problem. Thus, in the plane strain problem, the crack tip can move as a result of deformation, whereas in the punch problem, the crack tip is pinned for the case of no slip. The asymptotic stress field for the plane strain problem was worked out by Stephenson [17]. He showed that the σ_{22} component of the true stress tensor has a $1/r$ singularity, where r is the distance from the crack tip. Also, the true shear stress (σ_{12}) has a $1/\sqrt{r}$ singularity, while the transverse true normal stress (σ_{11}) is bounded as $r \to 0$. We confirmed these analytical results using our FEM method. More relevant to the issue of oscillations, we found that if the crack tip was pinned in the plane strain problem, that is, if we fixed the crack tip position in our FEM calculations, oscillations are also observed in the normal true stress ahead of the crack tip. This result is consistent with the finding in our punch problem.

The simulation in this work assumes that the material is Neo-Hookean, which underestimates the stresses at large deformation. Hence, in order to convince

ourselves that the qualitative nature of our result is preserved for hardening solids also, we performed a limited number of simulations on a strongly hardening material with strain energy density of the form

$$W = \left(\frac{GI_m}{2}\right)\left(\exp\left\{\frac{(I_1 - 3)}{I_m}\right\} - 1\right), \tag{1.12}$$

where I_m is a hardening parameter and equals 1.17 in our finite element simulations. The work function (1.12) reduces to (1.5) for small deformations. Motivation and details about this large deformation hyperelastic model will be presented elsewhere. Our simulations show that the stress distributions and the deformed shape of the cavity are similar to the Neo-Hookean case for both the frictionless and no slip conditions. The difference being, the stresses are higher for the same deformation in the hardening model.

A word about energy release rate. If we assume that the interface is frictionless and that crack growth occurs along the interface (that is, the punch fails by the growth of an interface crack at the edge), then it is possible to compute the energy release rate of the interface crack which is

$$G = \left.\frac{\partial \Gamma}{\partial A}\right|_{\Delta} \tag{1.13a}$$

where $A = \pi a^2$ is the punch area and $\Gamma = \int_0^{\Delta} P(\Delta', A)\, d\Delta'$ is the elastic strain energy of the system. A straightforward calculation using the definition of compliance C (see (1.8)) shows that

$$G = \frac{-1}{2\pi a}\int_0^{\Delta}\left(\frac{\Delta'}{C^2(a,\Delta')}\right)\frac{\partial C(a,\Delta')}{\partial a}\, d\Delta' \tag{1.13b}$$

The integral in (1.13b) can be evaluated using the expression given by (1.11a, b). However, it is important to note that the energy release rate may not be a sufficient criterion for interface failure. In general, interface failure will also be dependent on the relative amount of interfacial normal and shear stresses.

In summary, our analysis shows that there are significant differences between the contact stresses for the no slip and frictionless boundary conditions, in contrast to the prediction of SSLE theory. Specifically, for the no slip case, the normal contact stress singularity at the punch edge vanishes as the crack blunts, in contrast to the frictionless case, where a singularity persist at the contact line. This result explains why interface cracks in a tack test on a sticky surface get pinned, which is a necessary condition for stable cavity growth in the direction of the applied displacement, while interface cracks propagate on a slippery surface. Our result is also consistent with the experimental observation that fibrils between cavities eventually fail due to sliding of the "foot" along the interface (ref Glassmaker [12]). Indeed, our analysis shows that crack blunting initially reduces stress concentration on the interface, allowing stable cavity growth. As deformation continues, shear stress builds up on the interface, which eventually slides. Finally, sliding enhances normal stress at the receding contact line, which subsequently causes the detachment of fibrils from the interface. This conclusion is entirely consistent with recent experiments [18-20].

REFERENCES

[1] J. Boussinesq, Application des potentials a l'etude de l'equilibre et due mouvement des solides elastique, Gauthier-Villars, 1885**,** Paris;

[2] K.R. Shull, Contact Mechanics and the Adhesion of Soft Soids, Mat. Sci. and Eng. R*.,* 2002*,* 36**,** *1-45*

[3] T. Yamaguchi, K. Koike and M. Doi, In situ observation of stereoscopic shapes of cavities in soft adhesives, Europhys. Lett., 2007, 77, 64002.

[4] Yu-Yun Lin and Hsin-Yang Chen, Effect of Large deformation and material nonlinearity on the JKR (Johnson–Kendall–Roberts) test of soft elastic materials, J. Polym. Sci., Part B: Polym. Phys., 2006, 44–19, 2912–2922.

[5] K. L. Johnson, K. Kendall and A. D. Roberts, Surface energy and the contact of elastic solids, Proc. R. Soc. London, Ser. A, 1971, 324, 301–13.

[6] K. R. Shull, Fracture and adhesion of elastomers and gels: large strains at small length scales, J. Polym. Sci., Part B: Polym. Phys., 2006, 44, 3436–3439.

[7] K. L. Johnson, Contact Mechanics, Cambridge University Press, Cambridge, 1985.

[8] K. R. Shull and C. Creton, Deformation behavior of thin, compliant layers under tensile loading condition, J. Polym. Sci., Part B: Polym. Phys., 2004, 42, 4023–4043.

[9] A. Zosel, Adhesion and tack of polymers: influence of mechanical properties and surface tensions, Colloid Polym. Sci., 1985, 263, 541– 553.

[10] H. Lakrout, P. Sergot and C. Creton, Direct observation of cavitation and fibrillation in a probe tack experiment on model acrylic pressure-sensitive adhesives, J. Adhes., 1999, 69(3–4), 307– 359.

[11] K. Brown, J. C. Hooker and C. Creton, Micromechanisms of tack of soft adhesives based on styrenic block copolymers, Macromol. Mater. Eng., 2002, 287, 163–179.

[12] N. J. Glassmaker, C. Y. Hui, T. Yamaguchi and C. Creton, Detachment of stretched viscoelastic fibrils, Eur. Phys. J. E, 2008, 25 (3), 253-266.

[13] B. M. Z. Newby and M. K. Chaudhury, Effect of Interfacial Slippage on Viscoelastic Adhesion, Langmuir, 1997, 13(6), 1805–1809.

[14] B. M. Z. Newby, M. K. Chaudhury and H. R. Brown, Macroscopic evidence of the effect of interfacial slippage on adhesion, Science, 1995, 269, 1407–1409.

[15] N. Amouroux, J. Petit and L. Le´ger, Role of interfacial resistance to shear stress on adhesive peel strength, Langmuir, 2001, 17, 6510– 6517.

[16] Hibbit Karlsson and Sorensen Inc., ABAQUS Manuals, Hibbit Karlsson and Sorensen Inc., Providence, RI, 2007, Abaqus 6.6.

[17] R. Stephenson, The equilibrium field near the tip of a crack for finite plane strain of incompressible elastic materials, J. Elasticity, 1982, 12, 65–99.

[18] C. Creton, J. C. Hooker and K. R. Shull, Bulk and interfacial contributions to the debonding mechanisms of soft adhesives, Langmuir, 2001, 17, 4948–4954.

[19] G. Josse, P. Sergot, M. Dorget and C. Creton, Measuring interfacial adhesion between a soft viscoelastic layer and a rigid surface using a probe method, J. Adhes., 2004, 80, 87–118.

[20] L. Le´ger and C. Creton, Adhesion mechanisms at soft polymer interfaces, Philos. Trans. R. Soc. London, Ser. A: Math. Phys. Eng. Sci., 2008, 366, 1425–1442.

CHAPTER 2

FINITE STRAIN CRACK TIP FIELDS IN SOFT INCOMPRESSIBLE ELASTIC SOLIDS UNDER PLANE STRESS[†]

2.1 Introduction

Fracture of soft materials such as gels has recently been of interest to physicists and chemists. The physical structure of these materials consists of a dense network of polymer chains in a liquid matrix giving rise to a high degree of elasticity, incompressibility and strain hardening. However, their fracture behavior is not very well understood. Recent works on gel fracture has focused mainly on covalent hydrogels [1-4] or biopolymer gels such as gelatin [5-6]. As experimentalists have pointed out, gels made from polymerization of monomers in a cross-linking reaction are usually brittle with few dissipative mechanisms. On the other hand, double network (DN) gels have shown recently to possess high fracture toughness [7], because of their ability to transmit stress concentrations at crack tips between the cross-linking networks. However, DN gels are not very elastic and show hysteresis on repeated loading due to structural changes during loading [8]. Recently, there have been several efforts to perform carefully designed fracture experiments on well characterized, elastic polymer gels. For example, using a fracture specimen with a strip geometry (see figure 2.1), Baumberger et al [9] studied the fracture behavior of gelatin gels. They found that gelatin is very elastic at small strains. No systematic large strain measurement was done and fracture images suggest that gelatin is highly dissipative above a certain level of strain. A similar fracture study using the same

[†]Reproduced with permission from Langmuir, in press. Unpublished work copyright [2008] American chemical society.

specimen made with an acrylic triblock copolymer gel was carried out by Seitz et al [10].

The nature of cracks in soft elastic materials is qualitatively very different from those in metals and other commonly known brittle materials such as polymer glass and ceramics, in that soft materials exhibit very large deformation and a high degree of strain hardening as deliberated by Shull [11]. However, theoretical models of the stress and deformation fields near the tips of cracks in soft materials are mostly based on the assumption of small deformations and linear elastic behavior. Although there have been some beautiful analyses on the nonlinear deformation fields near cracks in Hyperelastic solids [12-16], these analyses are very mathematical and are not easily accessible to material scientists and chemists. There are also very few numerical studies of crack tip fields in real fracture specimens. An example of such a study is Ravichandran and Knauss [17]. They used a Lagrangian based FEM to study the finite strain field of an interface crack between two infinite Hyperelastic sheets.

One may question our choice of studying a Neo-Hookean solid since real gels or rubber exhibits finite extensibility and strain hardens much more than this idealized model. There are several reasons to study the Neo-Hookean solid. First, it is one of the few elastic materials which have universal appeal and where an exact closed form solution of the crack tip fields is known. Furthermore, even for this simple material, the solution is not readily accessible in the literature. For example, the results presented in literature do not determine the true stress fields near the crack tip in the deformed coordinates. Second, this solution allows us to validate the accuracy of our numerical method. In section 2.3.4, the same numerical technique is used to study the stress fields in a real hydrogel specimen. Finally, by comparing the Neo-Hookean solution with the numerical solution of a severe strain hardening material, we discover

many aspects of the Neo-Hookean solution are universal and therefore allow us to gain insight in the fracture mechanics of soft materials.

In this chapter, we address the nonlinear deformation of the crack tip fields in soft elastic solids in a way that is accessible to experimentalists who are interested in the fracture of soft materials. In section 2.2, we focus attention on a Neo-Hookean solid. We determine the stress fields near the crack tip and relate these stresses to the external applied load of a fracture specimen. Our results on the near tip fields are based on the analysis of Guebelle and Knauss [16]; we also included many features of their solutions which have not been discussed previously and which are of practical relevance. The full-field solution for the Neo-Hookean solid is new and is obtained using a nonlinear finite element analysis. In section 2.3, we study the crack tip field in the strip specimen using a constitutive model that has very severe strain hardening. Summary and discussion is given in section 2.4.

2.2 Fracture mechanics of a Neo-Hookean solid under Plane stress

2.2.1 A Strip Specimen

To put our problem into perspective, we focus on the fracture specimen used by Baumberger et al [9] and Seitz et al [10] to study the fracture of gels. The specimen consists of a long elastic strip of width 2L with height 2h, L >> h. The out of plane thickness of the strip t, is assumed to be much smaller than h so that the strip is loaded in plane stress. A schematic of the un-deformed reference configuration of the specimen is shown in Fig 2.1a. An in-plane Cartesian coordinate system (x_1, x_2) is placed at the un-deformed crack tip. Before deformation, the crack is a slit of length L and is located at the mid-plane $x_2 = 0$. The sample is stretched by applying a spatially uniform vertical displacement $u_2 = \pm\Delta$ at the top and bottom faces $(x_2 = \pm h)$ resulting in a uniform stretch ratio of $\lambda_a = 1 + \Delta / h$ at distances far ahead of the crack tip.

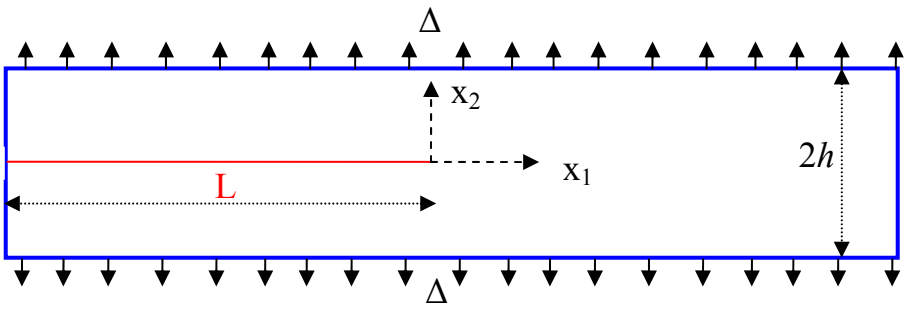

Figure 2.1a: Side view of Strip Specimen. The out of plane thickness is very small in comparison with h which is much less than L. Δ is the applied displacement.

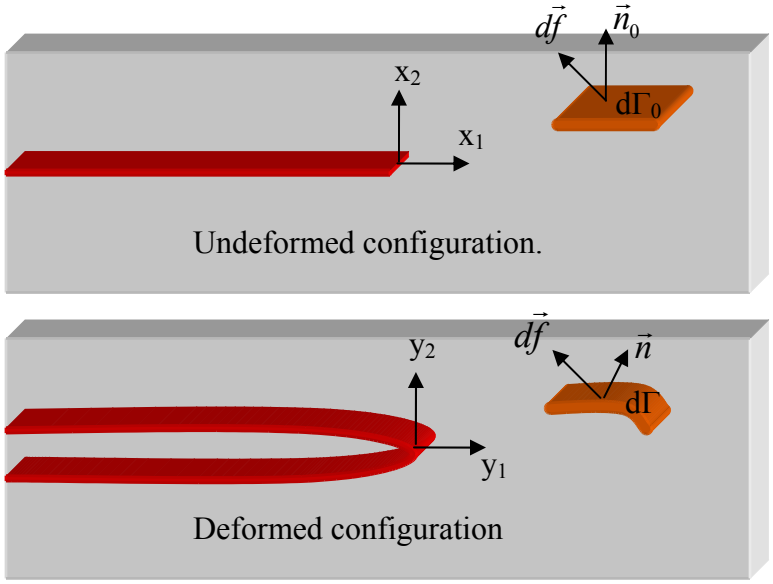

Figure 2.1b: Undeformed and deformed geometries of strip specimen showing first Piola Kirchoff stress (***S***) and true stress (***T***). Briefly, let $\vec{df}$ be the force acting on a material surface of area $d\Gamma_o$ in the undeformed configuration with the unit normal vector $\vec{n}_o$; after deformation, $d\Gamma_o$ becomes $d\Gamma$ with new unit normal vector $\vec{n}$. The first Piola Kirchoff stress tensor $\boldsymbol{S}$ is defined by $\vec{df} = \boldsymbol{S} \bullet \vec{n}_o d\Gamma_o$. The true (Cauchy) stress tensor $\boldsymbol{T}$ is defined by $\vec{df} = \boldsymbol{T} \bullet \vec{n} d\Gamma$. Here bold letter denotes a second order tensor.

2.2.2 Crack tip fields for a Neo-Hookean solid

Let $y_\alpha(\alpha = 1,2)$ denote the deformed coordinates of a material point located at x_α. Also, let $(r = \sqrt{x_\alpha x_\alpha}, \theta)$ be a polar coordinate system describing the position of a material point x_α in the reference un-deformed configuration. We place the origin of the deformed coordinates y_α at the deformed crack tip, that is, $y_\alpha(r = 0) = 0$. We will use the Einstein summation convention (sum over repeated indices) throughout this work. The displacements $u_\alpha(x_1, x_2)$ of a material point at x_α are related to y_α by

$$y_\alpha = x_\alpha + u_\alpha \tag{2.1}$$

In the following, we consider Mode I deformation where y_1 and y_2 are even and odd functions of x_2 respectively. This condition is satisfied by the loading of our strip specimen. In plane stress, the strain energy density of a Neo-Hookean solid *W* was first given by Rivlin [18]

$$W = \frac{\mu}{2} I_1 \tag{2.2}$$

where,

$$I_1 \equiv y_{\alpha,\beta} y_{\alpha,\beta} + \lambda^2 - 3 \tag{2.3}$$

In (2.3), λ is the stretch ratio in the out of plane direction.

2.2.3 Near tip displacement fields

Near the crack tip, Guebelle & Knauss [16] have shown that

$$y_\alpha(r\to 0,\theta)=\begin{cases} y_1 = C_1 r\cos\theta + o(r) \\ y_2 = C_2 r^{1/2}\sin(\theta/2) + o(r^{1/2}) \end{cases} \qquad -\pi\le\theta\le\pi, \tag{2.4}$$

Equation (2.4) can also be derived from a first order approximate full field solution in an earlier work by Wong and Shield [12]. C_α in (2.4) are unknown constants which depend on the external loads (in our case λ_a) and the specimen geometry. It is for this reason that these constants cannot be determined by asymptotic analysis. Note that C_2 has a unit of square root of length while C_1 is dimensionless. In fact, C_1 in (2.4) can be interpreted as the horizontal stretch ratio of a material element closed to the crack tip. Equation (2.4) implies that the deformed crack profile is

$$y_2 = \pm C_2\sqrt{\frac{-y_1}{C_1}} \qquad\qquad y_1\to 0^-. \tag{2.5}$$

2.2.4 Near tip stresses

The 1st Piola Kirchoff stress $S_{\alpha\beta}$ (figure 2.1b) in the reference configuration can be determined using (2.2) and (2.4). It is [16]:

$$\begin{aligned} &S_{11}=\mu C_1,\ S_{12}=0,\ S_{21}=-\frac{\mu C_2}{2}r^{-1/2}\sin(\theta/2), \\ &S_{22}=\frac{\mu C_2}{2}r^{-1/2}\cos(\theta/2) \end{aligned} \qquad r\to 0,-\pi\le\theta\le\pi \tag{2.6}$$

The physically relevant stress measure is the true (Cauchy) stress $T_{\alpha\beta}$ (figure 2.1b) in the deformed configuration. The true stress components are related to the 1st Piola Kirchoff stress by $T_{\alpha\beta}=S_{\alpha\xi}y_{\beta,\xi}$, where $,_\xi$ denotes $\partial/\partial x_\xi$. Using (2.4) and (2.6), the true stresses as $r\to 0$ are:

$$T_{11} = \mu C_1^2, \qquad T_{22} = \mu C_2^2 / 4r \tag{2.7a}$$

$$T_{12} = T_{21} = -\frac{\mu C_2 C_1}{\sqrt{2r}} \sin\left(\theta/2\right) \tag{2.7b}$$

For a *linear* elastic solid, the crack tip stresses in Mode I are [19]

$$\begin{pmatrix} T_{11} \\ T_{22} \\ T_{12} \end{pmatrix} = \frac{K_I}{\sqrt{2\pi r}} \cos\frac{\theta}{2} \begin{pmatrix} 1 - \sin\frac{\theta}{2}\sin\frac{3\theta}{2} \\ 1 + \sin\frac{\theta}{2}\sin\frac{3\theta}{2} \\ \sin\frac{\theta}{2}\cos\frac{3\theta}{2} \end{pmatrix} \qquad r \to 0 \tag{2.8}$$

where K_I is the Mode I stress intensity factor. For our strip geometry K_I is found to be $2\sqrt{3}\mu\Delta/\sqrt{h}$ (see (2.18) in section 2.2.5). In linear elastic fracture mechanics (LEFM), the deformation field for a Mode I crack depends on only one constant, K_I. Furthermore, *all* stress components have the *same* inverse square root singularity with distance from crack tip, with the singularity being independent of direction. Whereas, the nonlinear theory predicts that $T_{22} \propto 1/r$, T_{11} bounded and $T_{12} \propto 1/\sqrt{r}$. In particular, directly ahead of the crack tip, LEFM predicts $T_{11} = T_{22}$ whereas $T_{11}/T_{22} \approx 0$ in the nonlinear theory. The amplitudes of the true stress near tip fields in the nonlinear theory are governed by *two* independent parameters C_1, C_2 whereas in the linear theory, the amplitude is completely determined by a single parameter K_I. A comparison of (2.7a,b) and (2.8) shows that the angular distributions of the stresses are very different. For example, the normal stress T_{22} in the nonlinear theory is independent of orientation in the reference coordinates. Note that the shear stress in

the linear theory for positive angles less than 60^0 is *positive* whereas this stress is *negative* for all positive angles in the nonlinear theory. The fact that the shear stresses has a lower singularity than the normal stress implies material points near the crack tip is under a state of *uniaxial* tension. Finally, note that the LEFM predicts that the stress state directly ahead of the crack tip ($\theta = 0$) is that of hydrostatic tension.

The true stresses in (2.7a, b) are expressed in terms of the reference coordinates. In practice, it is useful to express them in terms of the deformed coordinates y_α. A straightforward calculation using (2.4) shows that, near the crack tip,

$$r = \frac{2}{C_2^2} y_2^2 + \frac{y_1}{C_1}, \qquad \cos\theta = \frac{C_2^2 y_1}{\left(2C_1 y_2^2 + C_2^2 y_1\right)} \tag{2.9}$$

Let (R, ϕ) denote a polar coordinate system located at the deformed crack tip, that is,

$$y_1 = R\cos\phi, \quad y_2 = R\sin\phi. \tag{2.10a}$$

Equation (2.5) implies that, near the crack tip

$$0 \le |\phi| < \frac{\pi}{2}. \tag{2.10b}$$

Using (2.7) and (2.9), the near tip true stresses, valid in the sector $0 \le |\phi| < \frac{\pi}{2}$, are:

$$T_{11} = \mu C_1^2, \tag{2.11a}$$

$$T_{22} = \frac{\mu C_1^2}{4\rho} f_{22}(\rho, \phi), \; f_{22}(\rho, \phi) = 1/\left(2\rho\sin^2\phi + \cos\phi\right), \tag{2.11b}$$

$$T_{12} = T_{21} = \frac{\mu C_1^2}{\sqrt{\rho}} f_{12}(\rho,\phi),$$

$$f_{12}(\rho,\phi) = \frac{-sign(\phi)2^{-3/2}}{\sqrt{2\rho\sin^2\phi + \cos\phi}}\left(1 - \frac{\cos\phi}{\left(2\rho\sin^2\phi + \cos\phi\right)}\right)^{1/2} \tag{2.11c}$$

where ρ is a dimensionless distance from the deformed crack tip defined by

$$\rho \equiv RC_1 / C_2^2 \tag{2.11d}$$

and

$$sign(\phi) = 1(-1)\ , \quad \phi > 0(<0)\ . \tag{2.11e}$$

Equations (2.11b,c) imply that, as long as $|\phi| < \frac{\pi}{2}$, T_{22} and T_{12} can be approximated by taking $\rho \to 0$ in f_{22} and f_{12}. This results in:

$$f_{22} \approx \sec\phi \qquad \frac{\pi}{2} - |\phi| << 2\rho \tag{2.12a}$$

$$f_{12}(\phi) \approx \frac{-\sqrt{\rho}\tan\phi}{2} \qquad \frac{\pi}{2} - |\phi| << 2\rho \tag{2.12b}$$

Using (2.10b), (2.11c) and (2.12b) the near tip shear stress is given by

$$T_{12} = T_{21} = -\frac{\mu C_1^2}{2}\tan\phi \qquad \frac{\pi}{2} - |\phi| << 2\rho \tag{2.13}$$

in the deformed coordinates. Equation (2.13) states that the asymptotic shear stress is *bounded* and *independent of radius* in the sector $|\phi| - \frac{\pi}{2} << \rho$! On the other hand, for $\rho > 0$, $|\phi| \to \pi/2$, we have

$$T_{22}(\rho,\phi \to \pi/2) = \mu \frac{C_1^2}{2\rho^2} \qquad |\phi| \to \pi/2 \tag{2.14a}$$

$$T_{12} = T_{21} = -sign(\phi)\frac{\mu C_1^2}{4\rho} \qquad |\phi| \to \pi/2 \tag{2.14b}$$

That is, the normal and shear stresses are extremely concentrated on the deformed crack faces. The singularity of the normal stress T_{22} directly ahead of the crack tip is lower than that along the crack face. Also, the near tip shear stress is bounded away from the crack face; hence the near tip stress field is approximately uni-axial.

2.2.5 Energy release rate and the determination of C_2

One of the constants C_2 can be determined using an energy argument. The energy release rate J for the strip geometry was first obtained by Sawyers and Rivlin [20]. For the case of a Neo-Hookean solid, it is

$$J = h\mu\left(\lambda_a - \frac{1}{\lambda_a}\right)^2 \tag{2.15}$$

J can also be obtained using the path independent integral of Eshelby [21],

$$J = \int_{\Gamma}\left(Wn_1 - S_{\alpha\beta}n_\beta u_{\alpha,1}\right)ds \tag{2.16}$$

where Γ is any simple close path which encloses the crack tip in the reference configuration, n_β is the outward unit vector normal to Γ and s denotes arc length. The path independence of the J integral allows us to choose Γ as a circular contour with arbitrarily small radius ε. The center of the circle coincides with the crack tip in

the reference configuration. Since ε is arbitrarily small, the asymptotic fields given by (2.4) and (2.6) are exact on the circular path. Using (2.4) and (2.6), the *J* integral is found to be:

$$J = \frac{\pi}{4}\mu C_2^2 \tag{2.17}$$

C_2 is found by equating (2.15) and (2.17), i.e.

$$C_2 = 2\sqrt{\frac{h}{\pi}}\left(\lambda_a - \frac{1}{\lambda_a}\right) \tag{2.18}$$

Note, for the special case of small applied strains, $\Delta / h << 1$,

$$C_2 \approx 4\sqrt{\frac{1}{\pi h}}\Delta, \qquad J \approx 4\mu\Delta^2 / h \tag{2.19}$$

According to LEFM [19], $J \approx \frac{K_I^2}{3\mu}$. Using (2.19),

$$K_I = 2\sqrt{3}\mu\Delta / \sqrt{h}\,. \tag{2.20}$$

The determination of C_1 requires a full field analysis and will be presented in section 2.2.8.

2.2.6 Region of validity of near tip fields

The stress fields given by (2.11) are valid in a small region Ω surrounding the crack tip. Let the linear dimension of Ω be denoted by d. To estimate *d*, consider the scenario of "small scale yielding" (SSY). SSY is satisfied when the applied stretch on the strip is small, that is, $\lambda_a \approx 1$ or $\Delta / h << 1$. Under SSY, the nonlinearity due to geometry changes and material behavior is confined to a very small region near the crack tip, that is, $d << h$. As a consequence, the LEFM solution (2.8) is valid at distances from the crack tip that is small compared with *h* but large compare with *d.* Using (2.8), the opening stress directly ahead of the crack tip is

$$T_{22} \approx \frac{K_I}{\sqrt{2\pi R}} \qquad \text{where} \quad d << R << h \tag{2.21}$$

We estimate *d* by equating (2.21) to (2.11b) at $R = d$ with $\phi = 0$ and using K_I given by (2.20). This gives

$$d \sim \frac{8C_1^2}{3\pi}\varepsilon_a^2 h \tag{2.22}$$

where $\varepsilon_a \equiv \Delta / h << 1$ is the applied strain. Equation (2.22) indicates that the region of dominance of the large strain asymptotic solution given by (2.11b) is proportional to the square of the applied strain. For example, for $\varepsilon = 0.1$ (marginally small strains), $d \sim 8.49 \times 10^{-3} h$ assuming that $C_1 = O(1)$. Since the region of dominance of the near tip fields must be less than d; very fine meshes are needed to resolve the near tip stresses in this limit.

2.2.7 Finite element Method (FEM)

We solve the strip problem numerically using ABAQUS [22], a nonlinear finite element software. Our goals are to determine C_1 and to obtain the full-field solution. In addition, checking against the asymptotic solution for the Neo-Hookean case is a stringent test of our FEM.

ABAQUS uses a total Lagrangian solution procedure for finite deformation hyperelastic material models. We implemented a python script to create the strip geometry and mesh for the FEM study (figure 2.2a). Our two dimensional FE model consists of quadrilateral elements (CPS4) with 2 degrees of freedom at each node. While ABAQUS has a material model for the Neo-Hookean solid, the exponentially hardening solid required a user material (U-HYPER) subroutine to be written in Fortran, which is called by the ABAQUS solver during the solution procedure. Symmetry allows us to model only half of the strip. We normalize all dimensions by *h*, half of the initial height of the strip.

Determining the stress fields near the crack tip is nontrivial. For small applied strains, the region of validity of the *1/R* singularity is very small and requires a very fine mesh near the crack tip to resolve the fields there accurately. In order to determine the near tip stresses, we follow a procedure known as submodeling [22]. The element size (*e*) in our FE mesh near the crack tip has to be on the order of $e \approx 10^{-6}$ in order to resolve the stresses. However, $e \approx 10^{-1}$ far away from the crack tip. Hence, using $e \approx 10^{-6}$ close to the crack tip gives rise to a large condition number for the FE solution matrix; resulting in large relative errors. This can be avoided using a fine mesh everywhere, but will result in millions of degrees of freedom making it intractable to solve on a single processor desktop.

To implement submodeling, we first run an analysis with a coarse mesh on the full model geometry, then reuse the results from the coarse mesh model as boundary

conditions for a submodel with a finer mesh (figure 2.2b). The submodel is a semi-circle of radius $r = 10^{-1}$ centered at the crack tip. A convergence study was carried out to ensure that the coarse mesh results are accurate at the boundary of the submodel. We also verified that the coarse mesh results agree with the submodel results at the boundary. A simple way to check the accuracy of our simulations is to note that, at distances sufficiently far away from the crack tip, the normal Cauchy stress is approximately independent of X and is given by [10]:

$$T_{22} = \mu\left(\lambda_a^2 - \frac{1}{\lambda_a^2}\right) \tag{2.23}$$

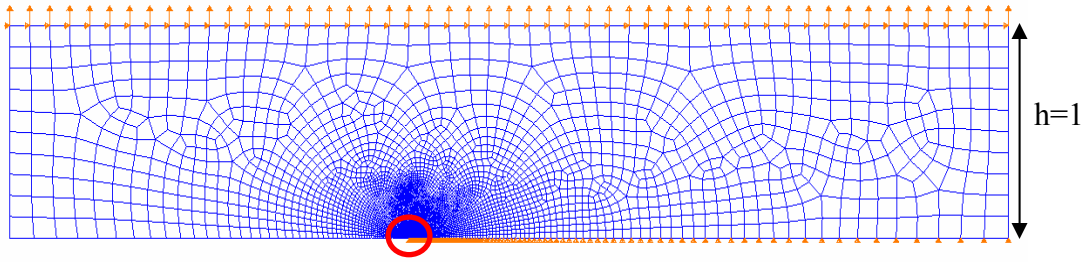

Figure 2.2a: FE model (coarse mesh) of half of the specimen. A uniform vertical displacement is applied on the top edge. The horizontal displacement on the top edge is constrained to be zero. The submodel region (r = 0.1) is highlighted.

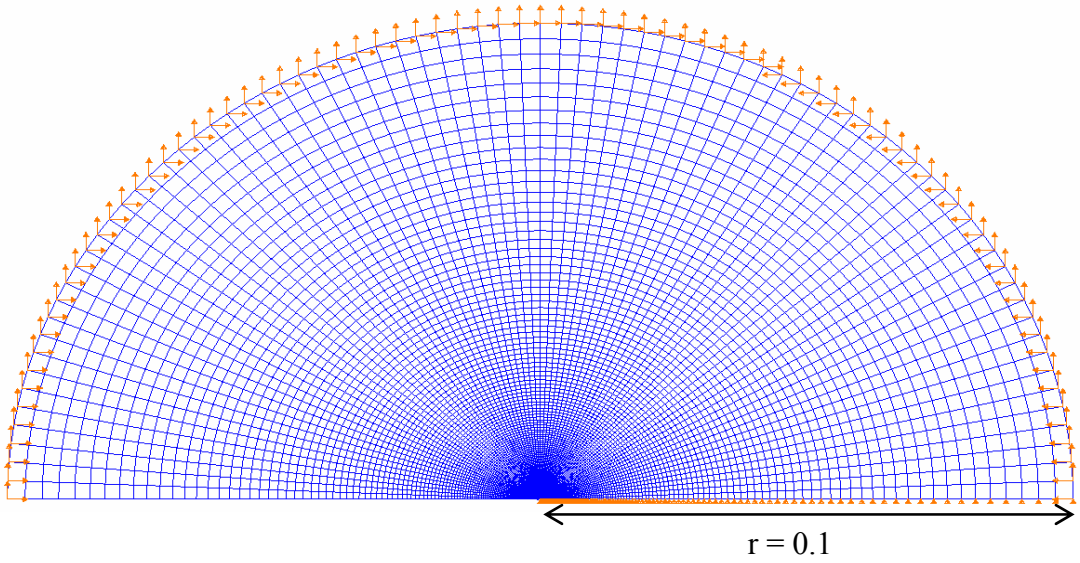

Figure 2.2b: Semicircular FE Submodel with fine mesh

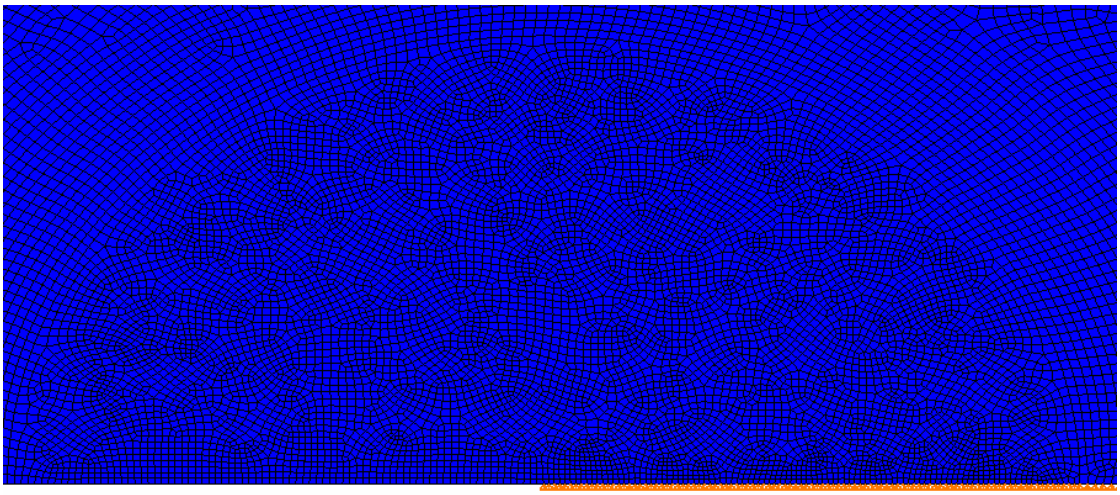

Figure 2.2c: FE mesh zoomed in near the crack tip

2.2.8 Numerical Results for Neo-Hookean solid

Recall from (2.5) that $y_2 = \pm C_2\sqrt{\frac{-y_1}{C_1}}$, where C_2 is given by (2.18) . This result allows us to determine C_1 from FEM analysis by fitting parabolas to the deformed crack profiles close to the crack tip at successive levels of λ_a.. The crack profiles and their parabolic fits are shown in figure 2.3a and the plot of C_1 vs. λ_a is shown in figure 2.3b. $C_1(\lambda_a)$ can also be determined by fitting the normal true stresses T_{22} ahead of the crack tip for different levels of applied deformation. The true stress T_{22}/μ predicted by the asymptotic theory can be obtained by combining (2.10c), (2.11b) and (2.17), which gives

$$T_{22}(R \to 0, \phi = 0) = \frac{C_1 J}{\pi R} \tag{2.24}$$

where $J = \mu h\left(\lambda_a - 1/\lambda_a\right)^2$ recalling (2.15). If the FE result is accurate near the crack tip, $C_1(\lambda_a)$ computed from fitting the crack profiles and the normal true stresses have to be the same. This is indeed the case as shown in Figs. 2.4a, where $C_1(\lambda_a)$ obtained from figure 2.3b is used to fit the normal true stress T_{22} ahead of the crack tip. Numerical result for the normal opening stretch λ_2 is plotted in a Ln-Ln plot in figure 2.4b. The local stretch near the crack tip is almost 150 times the applied far field stretch. The transverse normal opening stress (T_{11}/μ) directly ahead of the crack tip is plotted in figs. 2.4c which show that T_{11} ahead of the crack tip is about 3 orders of magnitude smaller than T_{22} and consistent with (2.10a), it approaches a constant value as dictated by the asymptotic analyses. Since the applied strip displacement λ_a is close to one, SSY condition is valid. From section 2.2.6, (for small applied stretch $\lambda_a \approx 1$), LEFM should apply so $T_{22} \propto 1/\sqrt{R}$ in the region $d << R << h$. In this

region, a log-log plot of the true stress T_{22} versus R is a straight line with a slope of $-1/2$. On the other hand, for $R << d$, (2.23) suggests that a log-log plot of the true stress versus R is a straight line with slope -1. This hypothesis is in good agreement with the result as shown in figure 2.5. Finally, the near tip shear stress field $\overline{T}_{12} \equiv 2T_{12}/\mu \tan\phi$ vs. *R/h* is shown in figure 2.6 for $\lambda_a = 2.0$ and for different angles ϕ. Consistent with (2.13), the shear stress normalized by $\mu \tan\phi$ is independent of ϕ and approaches a constant for $|\phi| < \pi/2$.

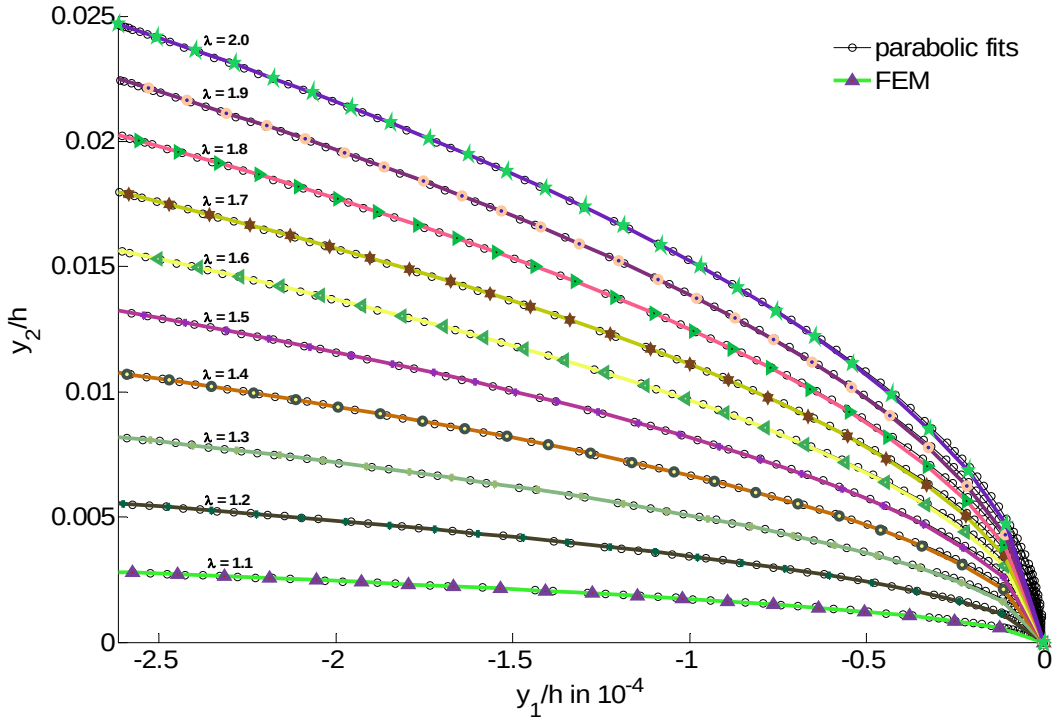

Figure 2.3a: Deformed crack opening profiles in Neo-Hookean solid and their parabolic fits.

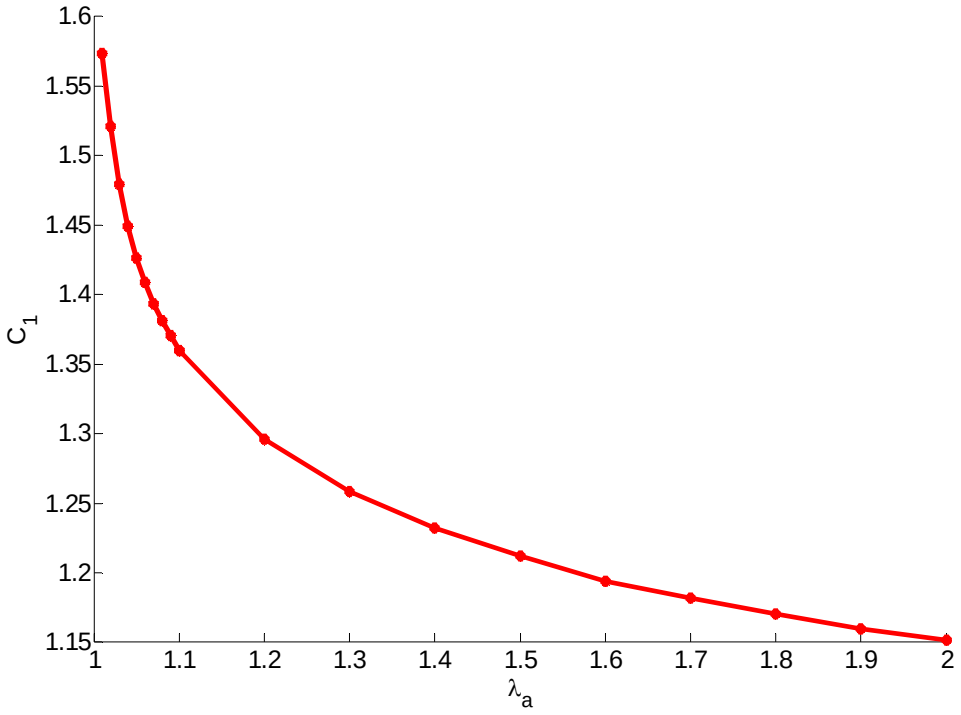

Figure 2.3b: Dependence of C_1 on λ_a

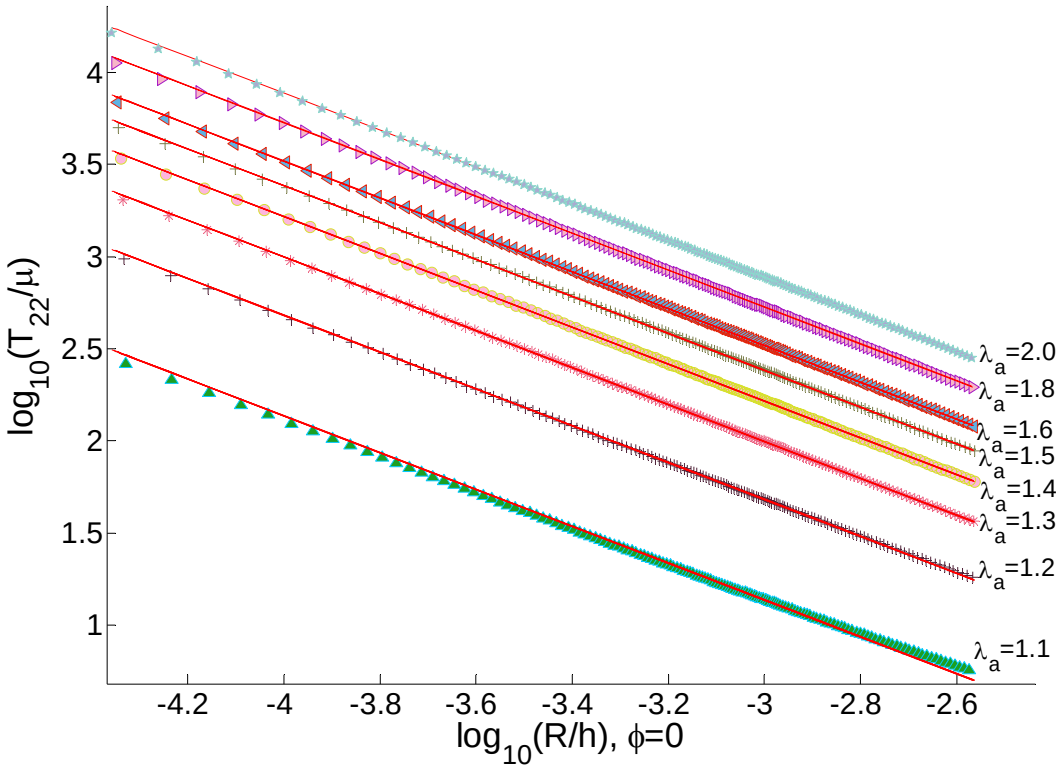

Figure 2.4a: Log-Log plot of T_{22} versus y_1/h shows a 1/R singularity as predicted by theory (2.24). Symbols show FEM result and solid lines show the fits with slope -1.

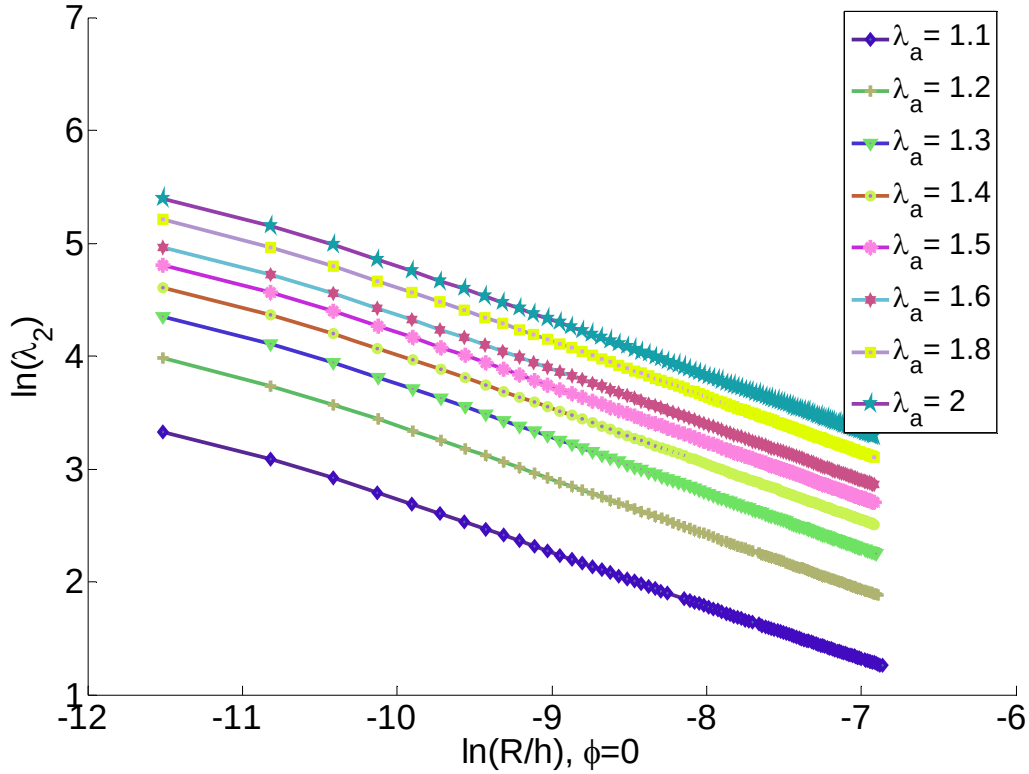

Figure 2.4b: Ln-Ln plot of normal opening stretch λ_2 directly ahead of the crack tip.

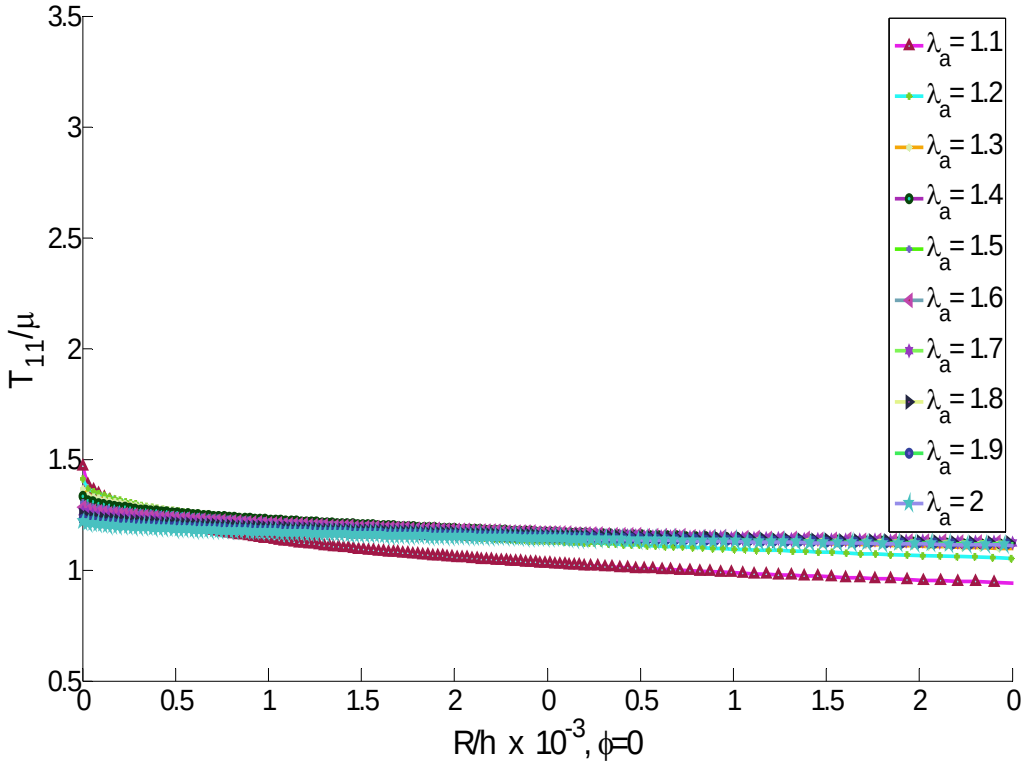

Figure 2.4c: T_{11} directly ahead of crack tip in deformed coordinates

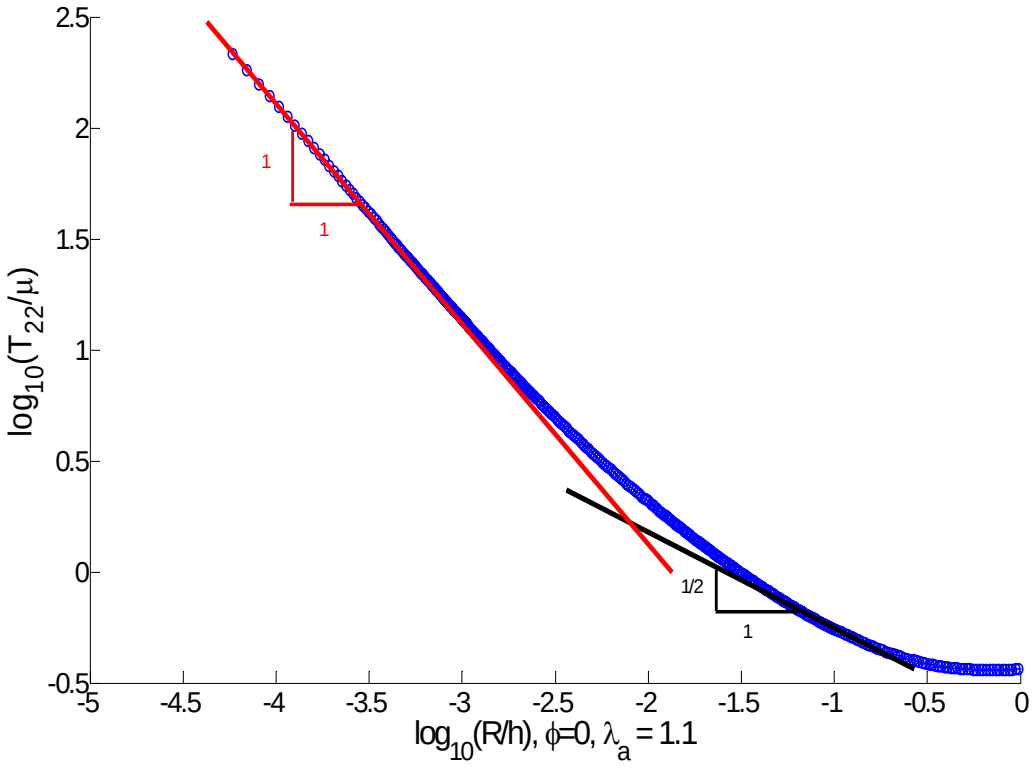

Figure 2.5: Log-Log plot of normal stress T_{22} vs. distance from crack tip, R (ϕ=0) under SSY ($\lambda_a = 1.1$). Close to the crack tip, it exhibits a $1/R$ singularity and away from it, the $1/\sqrt{R}$ singularity takes over.

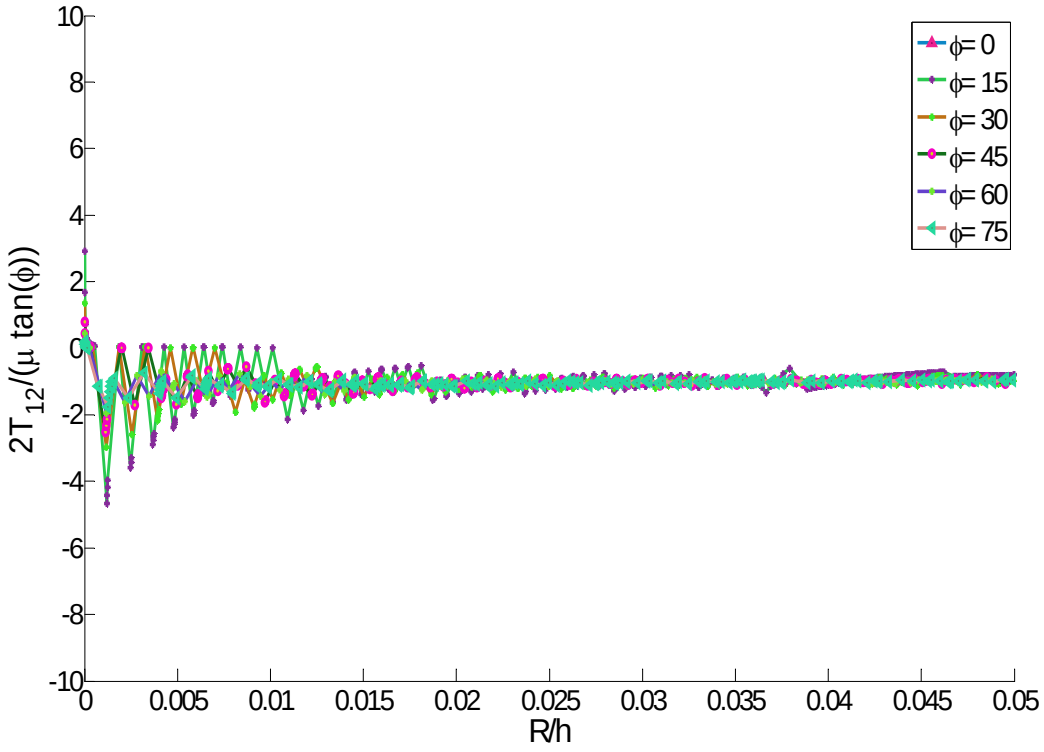

Figure 2.6: $\overline{T}_{12} \equiv 2T_{12} / \mu \tan\phi$ plotted along different angles ahead of crack tip or $\lambda_a = 2.0$. As predicted by (2.13), $\overline{T}_{12}$ is independent of R and ϕ.

2.3 Exponential Hardening Solid

2.3.1 Crack tip fields in a strain hardening material

The Neo-Hookean model underestimates the strain hardening of elastomers. This inadequacy motivates us to study the crack tip field of a material that exhibits very severe strain hardening. The constitutive model used in this study is motivated by the recent fracture experiments of Seitz et al [10]. Their fracture specimen is the strip geometry which is shown schematically in figure 2.1. The specimen is an elastic hydrogel which consists of acrylic triblock copolymers with poly(methyl methacrylate) [PMMA] endblocks and a poly(n-butyl acrylate) [PnBA] midblock. We found a strain energy density function W [10, 23] that fits their uniaxial compression data well. In plane stress, the strain energy density is given by

$$W = \frac{\mu}{2} I_m \left(\exp\left(\frac{I_1}{I_m} \right) - 1 \right); \tag{2.25a}$$

where μ is small strain shear modulus, I_1 is defined in (2.3) and I_m is a strain hardening parameter. Note that for small strains, this material behaves like a Neo-Hookean solid, i.e.,

$$W(I_1 << 1) \approx \frac{\mu}{2} I_1 \tag{2.25b}$$

For large strains (i.e., $I_1 / I_m >> 1$), the material hardens exponentially. This feature allows us use this model to study the nature of crack tip fields in materials with finite extensibility. Depending on the length of the midblocks and the weight percent of polymer used, the small strain shear modulus in their experiments varies from 2.7 to 6.4 kPa. Upon fitting, the strain hardening parameter I_m is found to vary from 3.5 to

17. The asymptotic behavior of the near tip fields in a material governed by this work function is not known. In fact, asymptotic analysis becomes much more difficult as strain hardening increases. For example, Guebelle and Knauss [16] considered a generalized Neo-Hookean model with energy density function

$$W = \frac{\mu}{2b}\left[\left(1+\frac{b}{n}I_1\right)^n - 1\right], \tag{2.26a}$$

where b is a material constant and $n > 1/2$ is a strain hardening parameter. In this model, strain hardening increases with n. They discovered their asymptotic analysis breaks down for $n > 7/5$. It is interesting to note that

$$\lim_{n\to\infty} \frac{\mu}{2b}\left[\left(1+\frac{b}{n}I_1\right)^n - 1\right] = \frac{\mu}{2b}\left[\exp\left(bI_1\right) - 1\right] \ . \tag{2.26b}$$

In this limit, the generalized Neo-Hookean model is the same as the exponential model for $b = 1/I_m$. In this section, we determine these near tip fields using our nonlinear finite element model.

2.3.2 Results for an Elastomer which strains hardens exponentially

The experiments of Seitz et al [10] were conducted in the range of moderately large applied stretches, i.e., $\lambda_a \approx 2$; therefore, simulations have been carried out for moderate and large deformations. A log-log plot of the true stress directly ahead of the crack tip ($\phi = 0$) is plotted in Figs. 2.7a,b for several applied stretches λ_a and for $I_m = 3.5$ and 17 respectively. We discovered that

$$T_{22}/\mu \propto -1/\left(R\ln R\right), \tag{2.27}$$

fits the FE results very well. Our numerical results suggest that

$$T_{22}(R\to 0,\phi=0) = -C(\mathrm{I_m},\lambda_a)J/[R\ln R] \tag{2.28}$$

where $C(\mathrm{I_m},\lambda_a)$ is a dimensionless function of λ_a, J is the energy release rate and is found to be

$$J = \mu h I_m\left(\exp\left(\frac{I_1}{I_m}\right)-1\right), \qquad I_1 = \lambda_a^2+\frac{1}{\lambda_a^2}-2 \tag{2.29}$$

for the strip specimen [10]. Note that C in (2.28) plays the same role as C_1 for the Neo-Hookean solid. As in the Neo-Hookean case, we determine $C(I_m,\lambda_a)$ by plotting $\log T_{22}$ versus $\log R$ and finding the intercepts of the resulting straight lines. These results are shown in figure 2.8. A comparison of Figs. 2.3b and 2.8 shows that $C(I_m,\lambda_a)$ is of order one and decreases to a constant value for large λ_a. Despite the large differences in strain hardening behavior, the near tip stress fields are very similar to the Neo-Hookean solid. For example, $T_{22} >> T_{11}$ (see Figs. 2.7 and 2.9). Also, the shear stress T_{12} is vanishingly small in comparison with the normal stress T_{22} in the sector $|\phi| < \pi/2$ (see figure 2.10). There is a slight difference between the two material models in that the shear stress on the deformed crack face $|\phi| = \pi/2$ is found to be very small, which is not the case for the Neo-Hookean solid. As a consequence, elements *everywhere* suffer very little shear distortion, and this fact allows us to obtain accurate results even at large applied λ_a. Note that the apparent oscillations in the shear stresses are spurious: they occur only because the stresses along the radial paths are determined using interpolation by ABAQUS, resulting in oscillations whenever there are no nodes along the path.

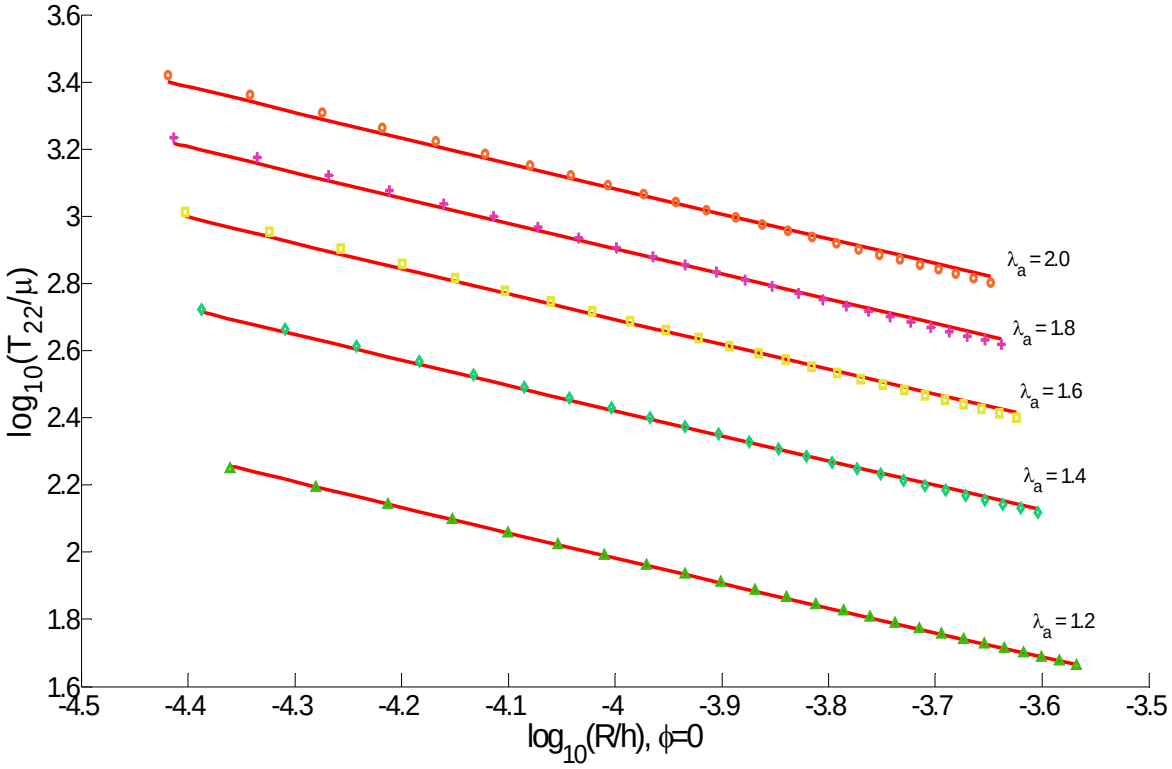

Figure 2.7a: Plot of T_{22}/μ versus y_1/h for $I_m = 3.5$ for different applied stretch λ_a. The fits (solid lines) are based on (2.26a). The finite element results are shown as symbols.

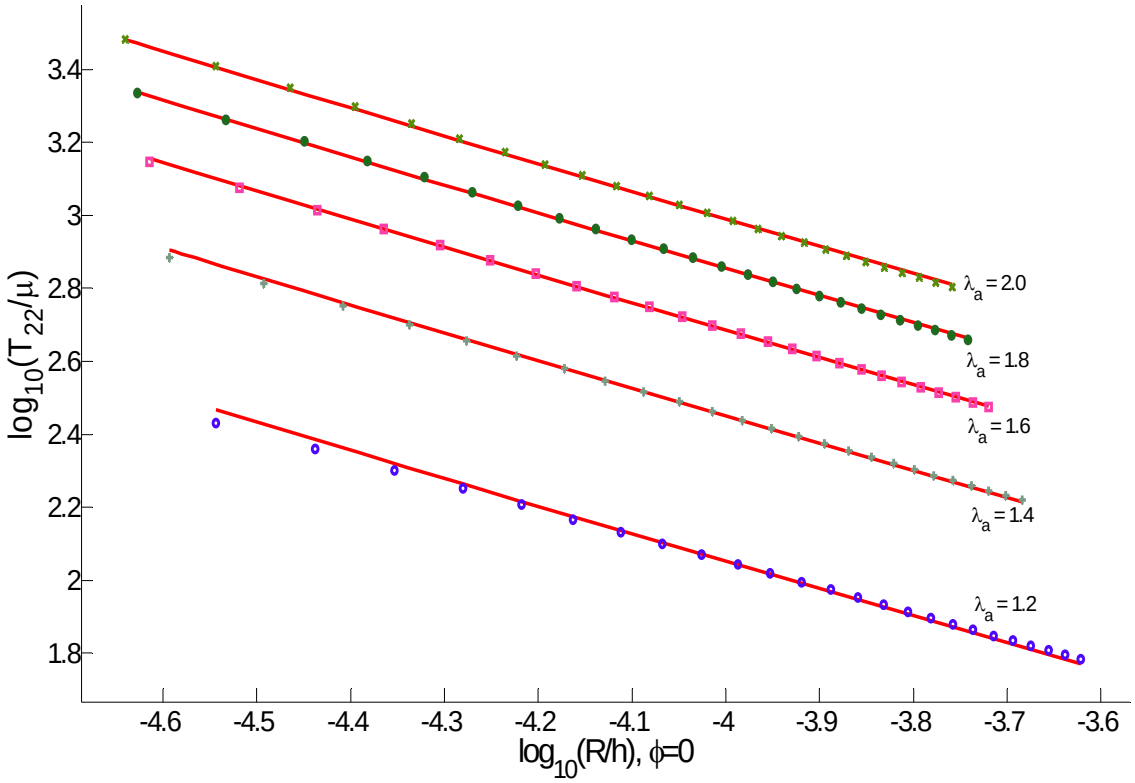

Figure 2.7b: Plot of T_{22}/μ versus X/h for $I_m = 17$ and for different applied stretch λ_a. The fits (solid lines) are based on (2.26a). The finite element results are shown as symbols.

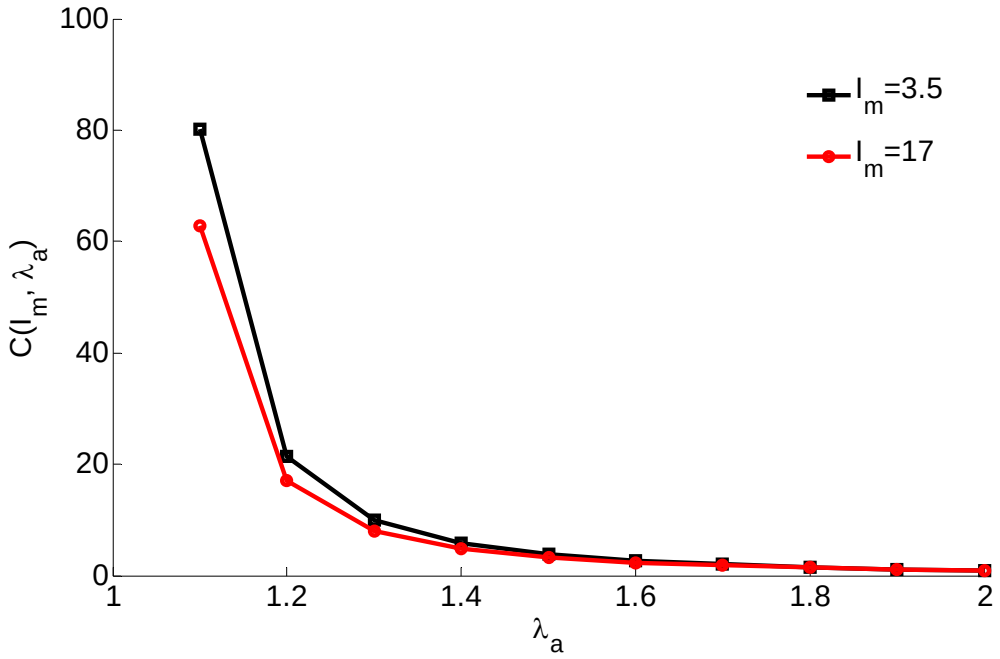

Figure 2.8: $C(I_m, \lambda_a)$ vs λ_a

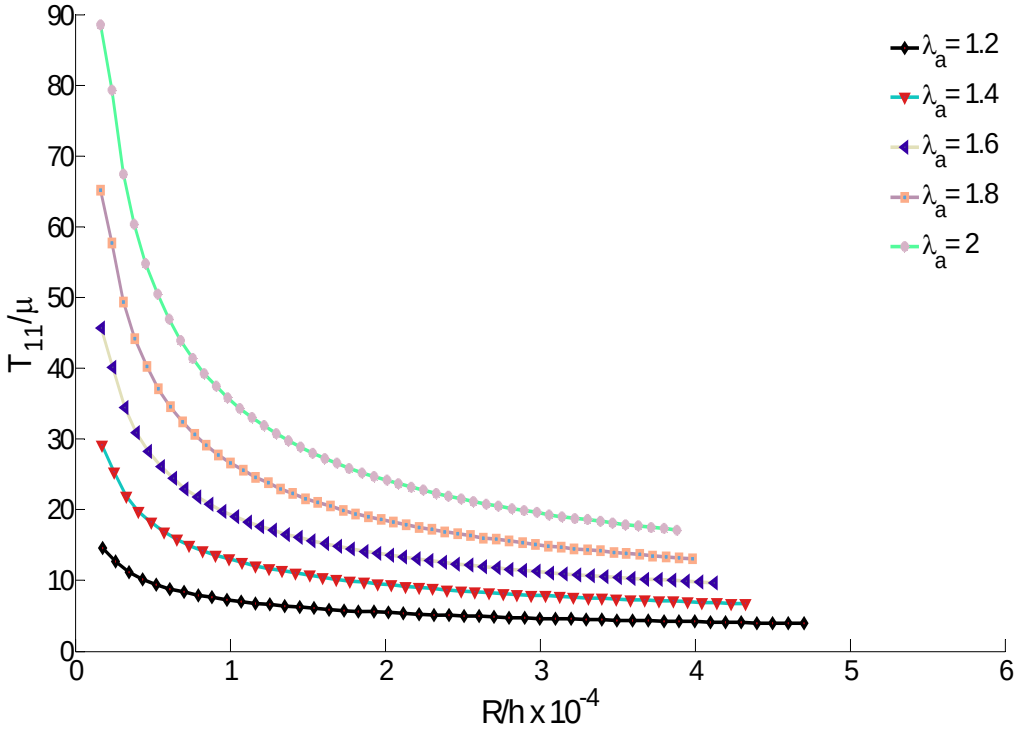

Figure 2.9: T_{11}/μ versus distance directly ahead of crack tip for $I_m = 3.5$

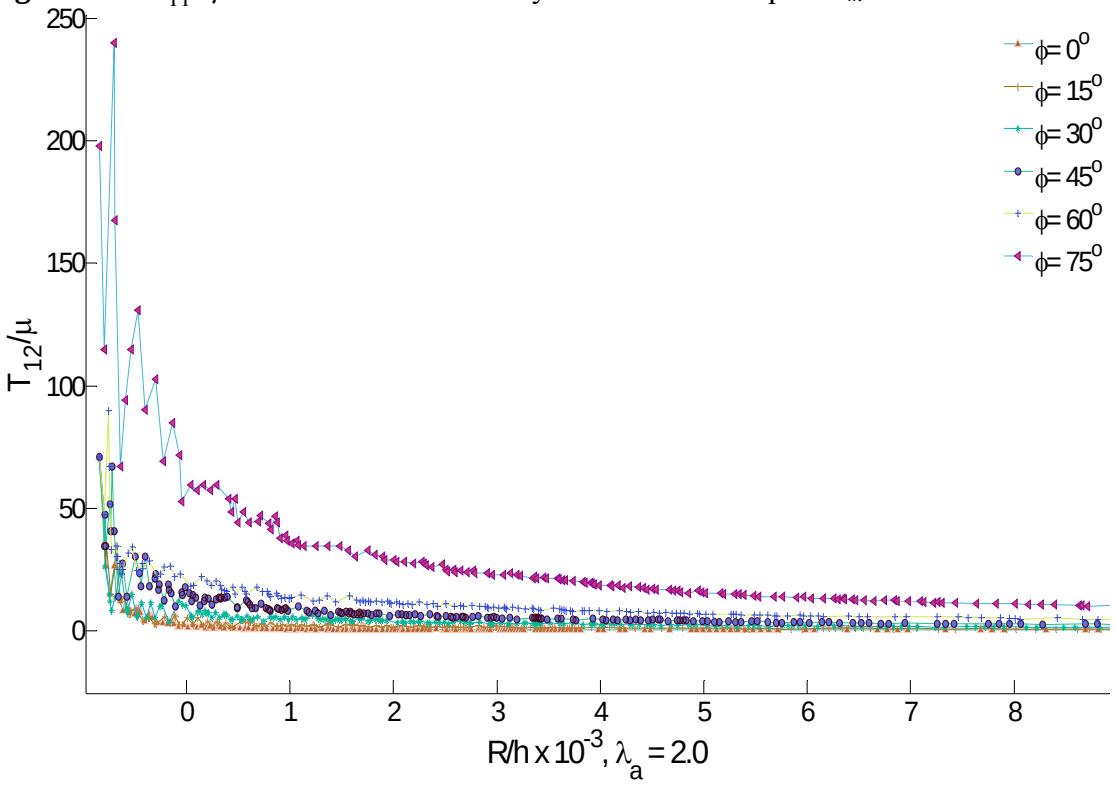

Figure 2.10: Plots of T_{12}/μ versus R/h for $I_m = 3.5$ along different radial path specified by ϕ. The shear stress increases only slightly with increasing ϕ.

2.4 Summary and Discussion

The stress field near the tip of a plane stress crack in a strip fracture specimen loaded in Mode I is studied for a Neo-Hookean solid and an elastomer that strain hardens exponentially. Our calculations show that the near tip stress fields behave in a similar way despite the very large difference in strain hardening behavior of the two material models. For example, the opening true stress (T_{22}) is much greater than the other normal stress component, T_{11}. In addition, the shear stresses are very small away from the crack face for both materials. However, there is a concentration of shear stress on the crack faces for the Neo-Hookean solid which is not present in the exponentially hardening material. This suggests that shear deformation decreases with increasing strain hardening. In both materials, a uni-axial state of stress exists near the crack tip. Our simulation confirms that the crack tip stress field in soft materials is very different from the prediction of the linear theory.

Our numerical results for the exponentially hardening solid show that T_{22} directly ahead of the crack tip has a $-1/RlnR$ singularity. Given that lnR is a very weak singularity, the opening stress singularities for the Neo-Hookean and the exponential model are very similar. Also, in both material models, $C_1(C)$ approaches one for large applied stretches. Therefore, the amplitude of the dominant singular stress T_{22} is directly proportional to the energy release rate in this limit. The fact that they are so similar given the very different strain hardening behavior suggests that this is a universal feature that is *approximately* satisfied for a wider class of soft materials, particularly for materials which exhibit high strain hardening. Exceptions will undoubtedly exist and further investigation to this hypothesis is necessary. Figure 2.11 shows that there is a much bigger region along the crack face where the opening stress (T_{22}) is high than directly ahead of the crack tip for the exponential solid. Recall, for the Neo-hookean solid, (14a) shows that the opening stress has a higher singularity

when approached along the crack face. This suggests that secondary cracks may initiate along the crack face. That is, it is possible for multiple crack fronts to develop ahead of the main crack. Crack tip splitting was indeed observed in some of the experiments of Seitz et al [10].

The fact that the dominant crack tip stress field for both material models is similar does not imply that the deformation fields are also similar. In fact, the exponential hardening material deforms much less. This can be quantified using the fact that T_{22} is

$$T_{22} = \mu W'(I)\left((y_{2,1} - \lambda^3 y_{1,2})y_{2,1} + (y_{2,2} - \lambda^3 y_{1,1})y_{2,2}\right) \tag{2.30a}$$

where $W' = dW/dI$. As one approaches the crack tip along $\phi = 0$,

$$T_{22} \approx \mu\left(y_{2,2}\right)^2 e^{\left(y_{2,2}\right)^2 / I_m}, \tag{2.30b}$$

for the exponential hardening model. Equation (2.30b) and (2.28) imply that

$$y_{2,2} \approx \sqrt{I_m \ln\left(T_{22}/\mu\right)} \propto \sqrt{-\ln R} \tag{2.30c}$$

Equation (2.30c) implies that the deformation gradient for the exponential hardening model has a very weak logarithmic singularity. Using (2.30a), it can be shown that the deformation gradient for the Neo-Hookean solid is $1/\sqrt{R}$. This means that exponential hardening solid deforms much less as expected.

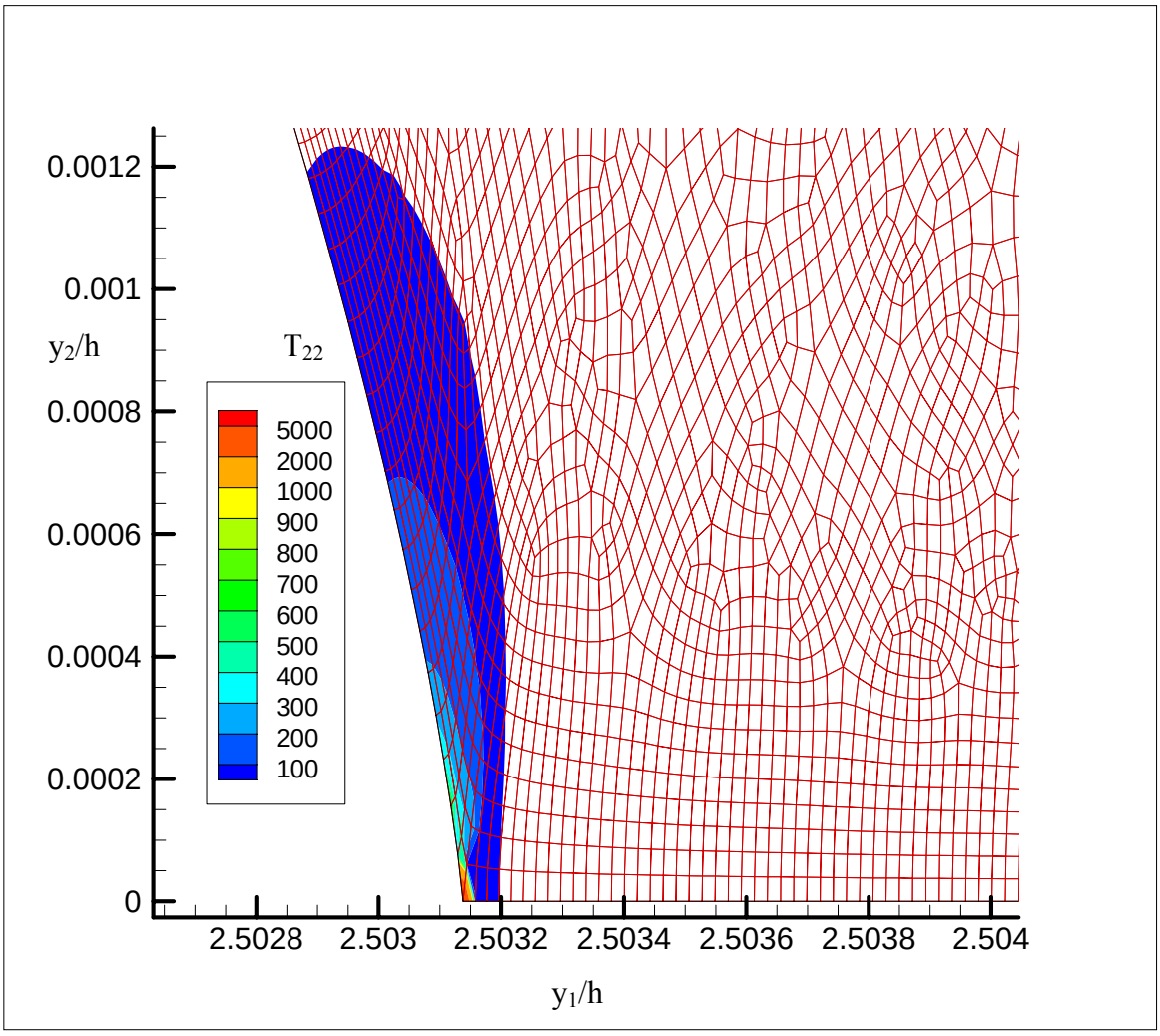

Figure 2.11: Normal opening stress (T_{22}) contour with FEM mesh is shown near the crack tip for $\lambda_a = 1.1$ in exponentially hardening solid ($I_m = 3.5$). The region where T_{22} is high is along the crack face rather than directly ahead of the crack tip, which suggests that secondary cracks may initiate from the crack face.

A few remarks on criterion for crack propagation. A standard hypothesis is to assume the applied energy release rate J is equal to the effective surface energy or fracture toughness of the material J_c. For the exponential hardening model, the crack growth criterion $J = J_c$ leads to

$$\lambda_a^* = \frac{\Gamma}{2} + \frac{\Gamma}{2}\sqrt{1+\frac{1}{\Gamma^2}} \qquad \Gamma = \sqrt{I_m \ln\left(1+\frac{J_c}{\mu I_m h}\right)}, \tag{2.31a}$$

where λ_a^* is the critical stretch for crack growth. For large Γ,

$$\lambda_a^* \approx \Gamma \approx \sqrt{I_m \ln\left(\frac{J_c}{\mu I_m h}\right)}. \tag{2.31b}$$

Equations (2.23) and (2.27) and the fact that $C_1(C)$ approaches a constant for large λ_a suggests that this energy based fracture criterion is equivalent to a local stress based fracture criterion.

REFERENCES

[1] Tanaka, Y.; Fukao, K.; Miyamoto, Y. Fracture energy of gels. European Physical Journal E. 2000, 3(4), 395-401.

[2] Tanaka, Y.; Fukao, K.; Miyamoto, Y.; Nakazawa, H.; Sekimoto, K. Regular patterns on fracture surfaces of polymer gels. Journal of the Physical Society of Japan, 1996, 65(8), 2349-2352.

[3] Livne, A.; Ben-David, O.; Fineberg, J. Oscillations in rapid fracture. Phys Rev Lett. 2007, 98(12), 124301.

[4] Livne, A.; Cohen, G.; Fineberg, J. Universality and hysterestic dynamics in rapid fracture. Phys Rev Lett. 2005, 94(22), 224301.

[5] Barrangou, L. M.; Daubert, C. R.; Foegeding, E. A. Textural properties of agarose gels. I &II. Food Hydrocolloids. 2006, 20(2-3), 184-203.

[6] Baumberger, T.; Caroli, C.; Martina, D. Fracture of a biopolymer gel as a viscoplastic disentanglement process. European Physical Journal E. 2006, 21(1), 81-89.

[7] Gong, J. P.; Katsuyama, Y.; Kurokawa, T.; Osada, Y. Double-network hydrogels with extremely high mechanical strength. Advanced Materials. 2003, 15(14), 1155

[8] Webber, R. E.; Creton, C.; Brown, H. R.; Gong, J. P. Large strain hysteresis and Mullins effect of tough double-network hydrogels. Macromolecules. 2007, 40(8), 2919-2927.

[9] Baumberger, T.; Caroli, C.; Martina, D. Solvent control of crack dynamics in a reversible hydrogel. Nat Mater. 2006, 5(7), 552–555.

[10] Seitz, M. E.; Shull, K.R.; Krishnan, V.R.; Hui, C.Y; Martina D.; Baumberger, T.; Fracture and high strain behavior of self-assembled tri-block copolymer gels, 2008, Accepted in J. of Soft Matter.

[11] Shull, K. R.; Fracture and adhesion of elastomers and gels: large strains at small length scales, J. Polym. Sci., Part B: Polym. Phys.,2006, 44, 3436–3439.

[12] Wong, F. S.; Shield, R. T., Large plane deformation of thin elastic sheets of Neo-Hookean material. ZAMP. 1969, 20(2), 176-199.

[13] Knowles, J. K.; Sternberg E., An asymptotic finite-deformation analysis of the elastostatic field near the tip of a crack. J. of elasticity. 1973, 3(2), 67-107.

[14] Knowles, J. K.; Sternberg E., Finite-deformation analysis of elastostatic field near tip of a crack- reconsideration and higher-order results. J. of Elasticity. 1974, 4(3), 201-233.

[15] Stephenson, R. A., The equilibrium field near the tip of a crack for finite plane strain of incompressible elastic materials. J. of Elasticity. 1982, 12(1), 65-99.

[16] Geubelle, P.H.; Knauss, W. G. - Finite strains at the tip of a crack in a sheet of hyperelastic material:I. Homogeneous case. J. of Elasticity. 1994, 35(1-3), 61-98.

[17] Ravichandran G.; Knauss, W.G.; A finite elastostatic analysis of biomaterial cracks. Int. J. Fracture, 1989, 39,235-253.

[18] Rivlin, R. Large elastic deformations of isotropic materials. Royal Society of London -- Philosophical Transactions Series A. 1948, 240, 509-525.

[19] Rice, J. R. A path independent integral and approximate analysis of strain concentration by notches and cracks. Journal of App. Mech. 1968, 35 (2): 379-386.

[20] Sawyers, K. N.; Rivlin, R. S. Trousers test for rupture. Engineering Fracture Mechanics, 1974, 6(3), 557-562.

[21] Eshelby, J. D. The determination of the elastic field of an ellipsoidal inclusion, and related problems. Proceedings of the Royal Society of London Series A-Math. and Physical Sci. 1957, 241 (1226): 376-396.

[22] Hibbit Karlsson and Sorensen Inc., ABAQUS Manuals, Hibbit Karlsson and Sorensen Inc., Providence, RI, 2007, Abaqus 6.6.

[23] Krishnan, V.R.; Hui, C. Y. Large deformation of soft elastic materials in adhesive contact with a rigid cylindrical flat punch. Soft Matter, 2008, 4, 1909 – 1915.

CHAPTER 3

FINITE STRAIN DEFORMATION FIELDS NEAR THE TIP OF AN INTERFACE CRACK BETWEEN A SOFT INCOMPRESSIBLE ELASTIC MATERIAL AND A RIGID SUBSTRATE

3.1 Introduction

3.1.1 Motivation

The problem of an interface crack between a soft elastic incompressible material and a rigid substrate is of importance to polymer physicists and chemists working with soft materials like Gels and Elastomers. Nucleation and growth of interface cracks are known to be precursors to failure of pressure sensitive adhesives [PSA] which are soft ($E \approx 1$ kPa) incompressible materials [1-2]. When these interface cracks grows along the interface, the PSA has little adhesion; on the other hand, in a good adhesive, these cracks grows into cavities followed by fibrillation [3]. Specifically, in a probe tack test, a cylindrical punch (e.g. a steel probe) is brought into close contact with the surface of an incompressible elastic layer and then retracted at a fixed rate (see figure 3.1a.). The extremely small thickness of the elastic layer coupled with its incompressibility, give rise to high hydrostatic stress during punch retraction, which usually cause cavity growth from small crack-like defects present on the interface between the rigid punch and the PSA (see figure 3.1b). Experiments have shown that when a good adhesive is detached from a high energy surface [4-5], the crack fronts of these defects do not propagate along the interface but are pinned. These pinned cracks eventually grow into cavities shown schematically in figure 3.1c. The details of this growth are shown in figure 3.1d: the deformed crack surface rotates about the pinned tip, so that the angle (θ) between the rotated crack face and the interface is almost

180^0. This is followed by cavity growth, resulting in the formation of a thin wall of material (fibrils) between neighboring cavities. The profile of the deformed crack face (or cavity) in figure 3.1d is referred to as "the foot of the fibril" in Glassmaker et al [3]. This picture is very different than the prediction of linear elastic fracture mechanics (LEFM) which predicts a $1/\sqrt{R}$ singularity resulting in a crack opening displacement that is proportional to $\sqrt{R}$, where R is the distance from the crack tip (figure 3.1c).

In a previous work, we study the problem of an axisymmetric punch retracting from a rigid infinite Neo-Hookean half space [6]. Using FEM, we demonstrated that the crack opening profile is similar to the "foot" observed by Glassmaker et al [3]. In addition, we found that the normal opening stress directly ahead of the interface crack tip is much smaller than the shear and the transverse normal stress. However, if the interface is frictionless, the normal opening stress is the dominant stress component. These results suggest that crack pinning and friction plays an important role in interfacial fracture. In this work we explore this phenomenon further by considering a more realistic material model which exhibits severe strain hardening behavior. In addition, we study the differences between a pinned crack and a frictionless interface crack in both plane stress and plane strain deformations.

The finite strain deformation fields near the tip of planar cracks in hyperelastic solids have been a subject of interest to the mechanics community, see for example Knowles & Steinberg [7-8], Stephenson [9], Hermann [10], Guebelle and Knauss [11] and the references within. The works of Knowles and Steinberg [7, 8] focus primarily on a class of compressible materials loaded under plane stress and strain. Later, Stephenson studied the same problem assuming that the material is incompressible. Hermann studied the problem of an interface crack between two compressible hyperelastic solids loaded in plane strain. Guebelle and Knauss [GK] performed

asymptotic analyses on a plane stress interface crack between a rigid solid and an incompressible generalized Neo-Hookean solid under plane stress conditions.

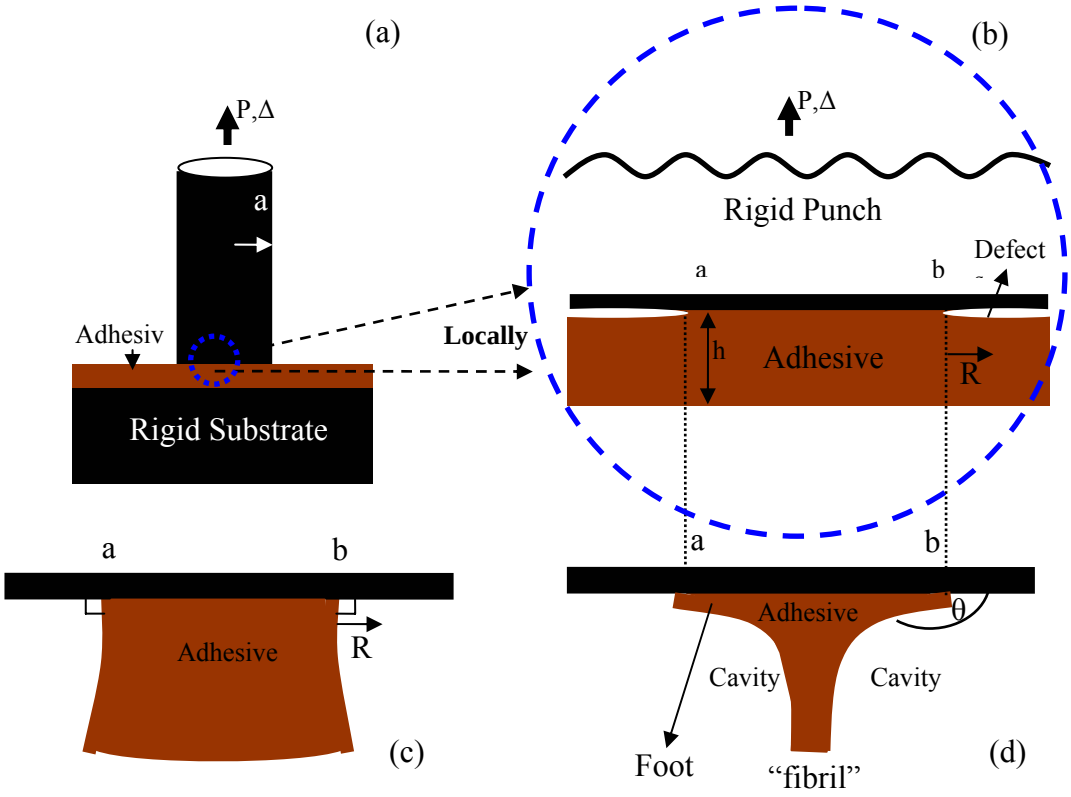

Figure 3.1: a: Tack test. A rigid flat punch is in adhesive contact with a thin layer of soft adhesive. It is then pulled upwards (retraction) in the vertical direction. b: A closer view of the interface region: the applied load causes crack-like defects on the punch–adhesive interface to grow. In good adhesives, the tips of these defects are pinned between points a and b. (*R* is the distance behind the crack front). c: A close up view of the deformation near the pinned crack predicted by SSLE theory, note that the angle θ made by the adhesive with the punch surface is 90°. d: Observed deformation, the angle θ made by the adhesive with the punch surface is close to 180°. The foot refers to the thin layer of material attached to the interface.

Although the details of the crack tip deformation fields are quite different, cracks in *homogeneous* solids loaded in plane stress and plane strain share several common features. For example, the crack face opens up smoothly and the normal opening stress (T_{22}) is the dominant stress field ahead of the crack tip. Therefore, it is surprising that we observe just the opposite from our FEM simulations on a pinned interface axisymmetric crack [6]. Firstly, the normal opening stresses (T_{22}) are not dominant, they are much smaller than the shear and transverse normal stresses. Of particular relevance is the deformed crack profile: the crack face flips over, compressing the material directly ahead of the crack tip. More concretely, a typical assumption for the crack opening profile has the form

$$y_2 = c\left|y_1\right|^{\alpha}, \tag{3.1}$$

where c is a constant that depends on the specimen geometry and external loads, y_1 and y_2 are the Cartesian coordinates of a material point in the deformed geometry (see Figure 3.2a,b). In (1), the deformed crack tip is located at $y_1 = y_2 = 0$. Figure 3.2a shows that the crack opens up smoothly for the case of $0 < \alpha < 1$, $y_1 < 0$. However, what is observed in experiments and in our simulations are shown schematically in figure 3.2b, where $\alpha > 1$ and $y_1 > 0$.

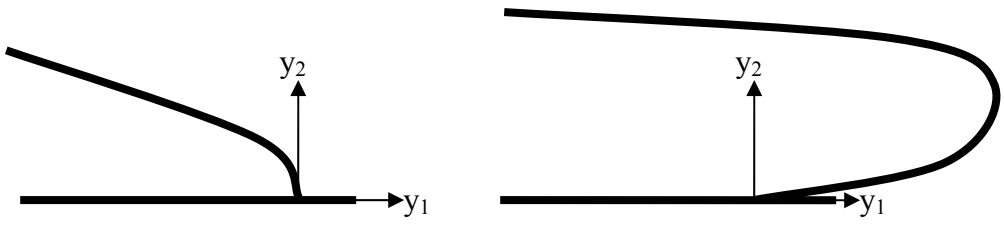

Figure 2a: $\alpha < 1$ Figure 2b:

Figure 3.2: Dependence of crack opening profiles on α.

There is a surprising lack of numerical (FEM) work in the area of finite strain elasticity for crack problems. The exceptions are [11, 12, and 13]. The deformation fields near crack tips are extremely difficult to compute because of the excessive mesh distortion at the crack tip which causes the analyses to fail for very small applied external loads. In [6], we performed a large deformation numerical study on an axisymmetric model of a punch retracting from an infinite elastic half-space using a re-meshing procedure. Note that the surface of the elastic half space outside the punch can be viewed as the face of an interface crack. The crack front is the punch edge. Since the three dimensional constraint at a crack tip under plane strain conditions is similar to that arising from axisymmetry, we use the same remeshing scheme to resolve the stresses in this work. Unless other specified, all stresses reported in this paper are true (Cauchy) stresses given with respect to the deformed configuration. Summation convention will be used throughout.

The paper outline is as follows: In section 3.2 we present the model geometry and the material model. Section 3.3 has details of the finite element method, including the remeshing scheme. We also present our validation of the plane stress and plane strain FEM in this section. Specifically, we compare our FEM result with known asymptotic solution of the crack tip field. In section 3.4, we present results from our FEM analyses for cracks (both full friction interface and frictionless interface) in an exponentially hardening material loaded in plane stress or plane strain. In section 3.5 (Summary and discussion), we give further insight to the relation between friction and adhesion by connecting our result with the experiments of Newby et al [14] and is given in section 3.5.

3.2 Material Model & Model Geometry

3.2.1 Model geometry

In both plane stress and plane strain deformation, a material point can be specified by two coordinates. Details of finite strain plane strain or plane stress formulations can be found in the classical papers of Knowles and Steinberg [7, 8]. In both cases, we specify a material point in the undeformed reference configuration by the Cartesian coordinates (x_1, x_2). After deformation, this material point moves to (y_1, y_2). The displacements are denoted by $u_\alpha = y_\alpha - x_\alpha$, $\alpha = 1, 2$.

Although the nature of the crack tip fields does not depend on specimen geometry, we used two geometries in this study. All the plane stress analyses were carried out using the strip geometry in figure 3.3a. This geometry is motivated by recent fracture experiments conducted by Seitz et al [15] and Baumberger et al [16]. The elastic strip has height *h* and width *w*, with $w >> h$. The bottom half of the strip is in contact with the rigid substrate along $x_1 \geq w/2$, $x_2 = 0$. The rest of the strip is not in contact, representing an interface crack of length $w/2$ occupying $-w/2 < x_1 < 0, x_2 = 0$. Since $w >> h$, this geometry approximates an semi-infinite interface crack in an infinite bimaterial strip. A uniform vertical displacement $u_2 = \Delta$ is applied on the top surface of the strip. At distances far ahead of the crack tip, this displacement causes a uniform vertical stretch $\lambda_a = \Delta / h$. We shall call λ_a the applied stretch. The horizontal displacement u_1 is prescribed to be zero on this surface, representing a clamped boundary.

The geometry used for plane stress analysis is not appropriate for plane strain. The incompressibility condition places severe restriction on the amount of deformation possible. To avoid this difficulty, all plane strain calculations are carried out using the geometry shown in figure 3.3b: A finite crack of length *a* lies on the interface between two rectangular blocks. The out of plane dimensions of the both

blocks are infinite (plane strain). The widths and height of the blocks are denoted by w and h respectively. Since our goal is to simulate a finite interface crack in an infinite solid, loaded under uniform traction at infinity, we choose $w, h >> a$. The upper block is an incompressible elastic solid while the lower block is rigid. A uniform vertical displacement $u_2 = \lambda_a h$ is applied on $x_2 = h$; λ_a can be interpreted as the far field stretch ratio when $h >> a$.

For the loadings consider in this work, the solutions of the frictionless interface crack problems in both plane stress and plane strain are identical to the solutions of the problems obtained by replacing the rigid substrate by the same elastic material, loaded symmetrically. For example, if the rigid substrate in our plane stress specimen is replaced by a strip of the same elastic material with the same height and a vertical displacement of $\pm\Delta/2$ is applied to the upper and lower surfaces of the strip at $\pm h$, then by symmetry, these boundary conditions will give a zero shear stress on $x_2 = 0$; thus satisfying the frictionless boundary condition.

3.2.2 Material Model

In this work we focus on an exponentially hardening solid whose strain energy density function W is given by

$$W = \frac{\mu \mathrm{I_m}}{2}\left[\exp\left(\frac{\mathrm{I_1}}{\mathrm{I_m}}\right) - 1\right] \tag{3.2}$$

where μ is the small strain shear modulus, $\mathrm{I_m}$ is a strain hardening parameter, I_1 is a scalar invariant and is the sum of the square of the principal stretches. This constitutive model was motivated by the recent experiments of Setiz et al [15] who performed fracture experiments on an elastic gel which consists of acrylic triblock

copolymers with poly(methyl methacrylate) [PMMA] endblocks and a poly(n-butyl acrylate) [PnBA] midblock. This model was found to accurately describe their compression data.

For small strains, the exponential solid behaves like a Neo-Hookean solid which has a strain density function given by

$$W = \frac{\mu \mathrm{I}_1}{2} \tag{3.3}$$

For large strains, $\mathrm{I}_1 / \mathrm{I}_m >> 1$, the material hardens exponentially. This feature allows us to study the nature of crack tip fields in materials with finite extensibility. In plane strain deformation,

$$I_1 = y_{\alpha,\beta} y_{\alpha,\beta} - 2 \ , \tag{3.4}$$

where $y_{\alpha,\beta} = \partial y_\alpha / \partial x_\beta$. In plane stress,

$$I_1 = y_{\alpha,\beta} y_{\alpha,\beta} + \lambda^2 - 3 \qquad \lambda = 1/\left(y_{1,1} y_{2,2} - y_{1,2} y_{2,1}\right) \tag{3.5}$$

3.3 Finite Element Model and validation

The finite element model was implemented in ABAQUS [17], a finite element software. ABAQUS uses a total Lagrangian solution procedure for finite deformation hyperelastic materials. While ABAQUS has a material model for the Neo-Hookean solid, the exponentially hardening solid required a user material (U-HYPER) subroutine (Appendix 3C) to be written in FORTRAN, which is called by the ABAQUS solver during the solution procedure.

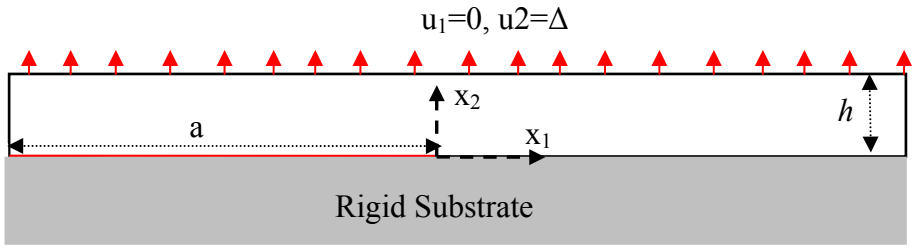

Figure 3.3a: Strip geometry used for plane stress simulations, the crack length *a* is much greater than *h*, the height of the strip.

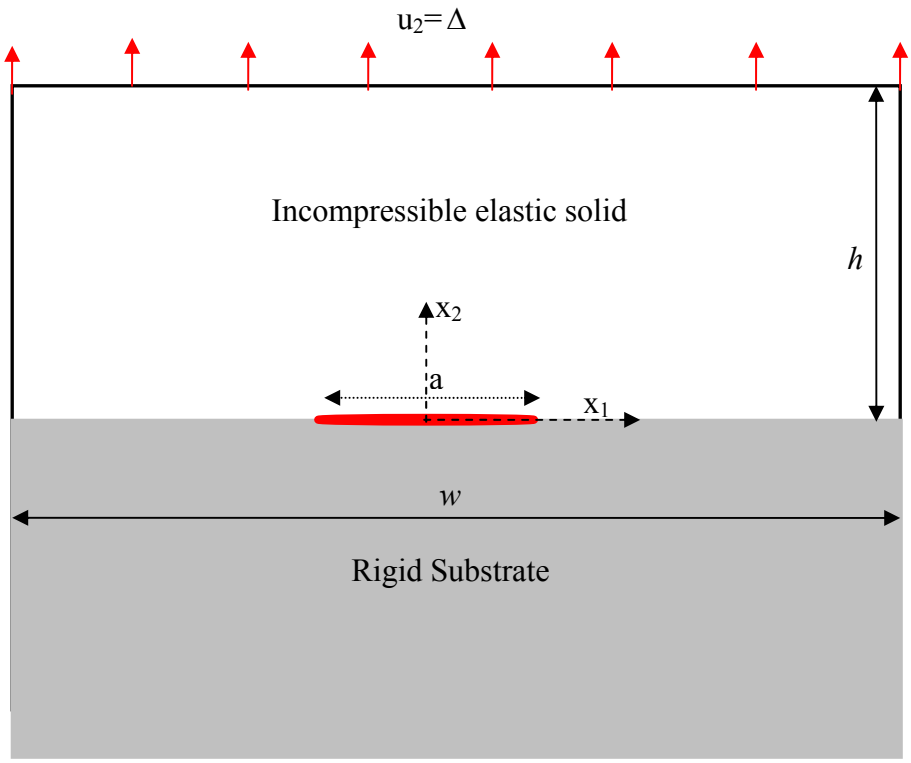

Figure 3.3b: Plane strain geometry: An interface crack between an elastic solid and a rigid substrate. The out of plane thickness is infinite in both blocks. The rectangular blocks have width *w* and height *h*, with *w*, *h*>>*a*.

3.3.1 FE model and Boundary conditions

All lengths in our simulations are normalized by the crack length a. This allows us to set the crack length $a = 1$ in all plane strain simulations. For the plane strain problem, symmetry allows us to model only one fourth (upper quadrant) of the geometry. The width and height of the elastic block are $w = 10$ and $h = 20$ respectively. The vertical displacement Δ on the top edge $(x_2 = h)$ is applied in increments till the desired amount of far field stretch λ_a is reached. Increasing the block dimensions does not affect the near tip field for the same λ_a. A symmetric boundary condition is imposed on the left edge of the FE model. On the interface, the horizontal and vertical displacements are both prescribed to be zero for the full friction case. For the frictionless case, only the vertical boundary condition is prescribed to be zero while zero shear traction is imposed. The FE mesh consists of four node linear quadrilateral elements (CPE4RH) in plane strain with reduced integration. There is also an additional pressure degree of freedom in each element (hybrid element) to take into account the incompressibility constraint. In plane stress, we use regular four node quad elements (CPS4) since there is no difficulty with incompressibility.

3.3.2 Mesh & Remeshing scheme

The mesh is progressively refined from the far tip region to the near crack tip region, with the smallest element size around the crack tip of the order of 10^{-5}. A spider web configuration is used for the mesh, consisting of rings of concentric circles around the crack tip with mesh density decreasing with distance from the crack tip. This is known to give accurate results near regions of singularity [18]. Approximately *40000* nodes are used in both plane stress and plane strain models. Due to the high degree of constraint at the crack tip under plane strain, there is excessive mesh distortion in the elements near the crack tip which causes premature analysis failure. Distortion also

causes severe lose of accuracy in quadrilateral elements and we attend to this issue by using a remeshing scheme that we presented in an earlier paper [6]. A Python script was implemented to automate the adaptive meshing. The remeshing procedure is done as follows and is shown schematically in figure 3.4.

1. A far field displacement is applied taking care not to distort the elements at the crack tip beyond the permissible element aspect ratio (for accuracy).
2. The deformed geometry is then extracted from the finite element results file. Further, the deformed geometry is now meshed again, making sure that the mesh is fine near the crack tip where the stress gradients are high and all the elements have an acceptable aspect ratio.
3. The solutions (stresses and strains) from the integration points in the elements of the old FEM mesh are now mapped on to the integration points of the elements in the new mesh. Hence the new mesh carries the stress history before the new incremental displacement is applied on the boundary
4. A new far field displacement step is applied similar to step 1 and this is carried on successively till the desired degree of far field stretch is achieved. We thus apply the far field displacement boundary condition in incremental steps.

We have validated this procedure for some simple problems e.g. simple tension experiment. In plane stress problems, the remeshing procedure was not used since we could obtain accurate results even without this procedure. We however used a procedure known as submodeling [17] to obtain accurate results very close to the crack tip. The model and mesh is implemented again using a python script. For further details on this numerical technique the reader is referred to our earlier work [19].

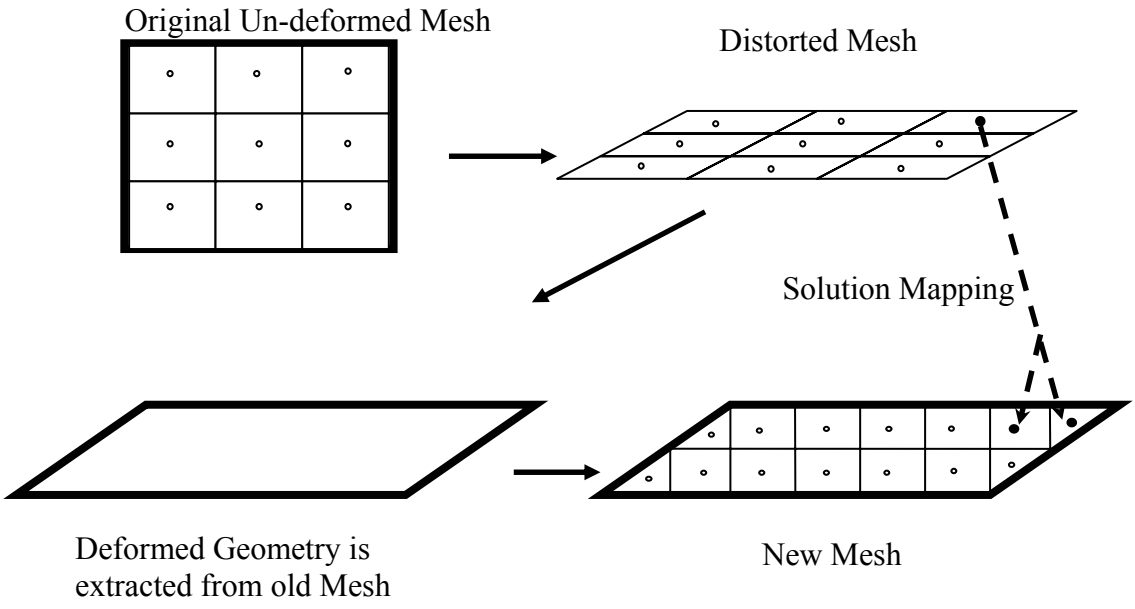

Figure 3.4: Illustration of Remeshing scheme

3.3.3 Plane Strain Validation

Ideally, we would like to validate our FEM results for both pinned and frictionless boundary conditions. However to the best of our knowledge, there exists no asymptotic solution in the literature for a pinned plane strain interface crack between an incompressible elastic solid and a rigid substrate, even for the special case of a Neo-Hookean material. Therefore, we validated our FEM results and the remeshing scheme by solving a plane strain crack problem in a homogeneous incompressible Neo-Hookean solid and comparing the near tip stress fields with the asymptotic solutions of Stephenson [10]. As mentioned earlier, the solution of this problem is the same as that of a crack on a frictionless interface. In appendix 3A, we show that the normal opening stress T_{22} directly ahead of the crack tip, expressed in terms of the deformed coordinates, has the form (see appendix 3A):

$$T_{22}(y_1, y_2 = 0)/\mu = A\left(y_1/a\right)^{-2/3} \tag{3.6}$$

where A is a function of the applied stretch. Physically, A determines the strength of the singularity. In general, A can not be determined using the asymptotic method of Stephenson [10]. Equation (3.6) states that a log-log plot of $T_{22}(y_1, y_2 = 0)/\mu$ versus y_1/a should be a straight line with slope $-2/3$. This prediction is confirmed by our numerical results in figure 3.5. The unknown function A can be determined numerically by finding the intercepts of the straight lines in figure 3.5. Figure 3.6 shows that A is proportional to the applied stretch λ_a. Also the deformed crack profiles from the FEM results are parabolas as predicted by asymptotic analysis.

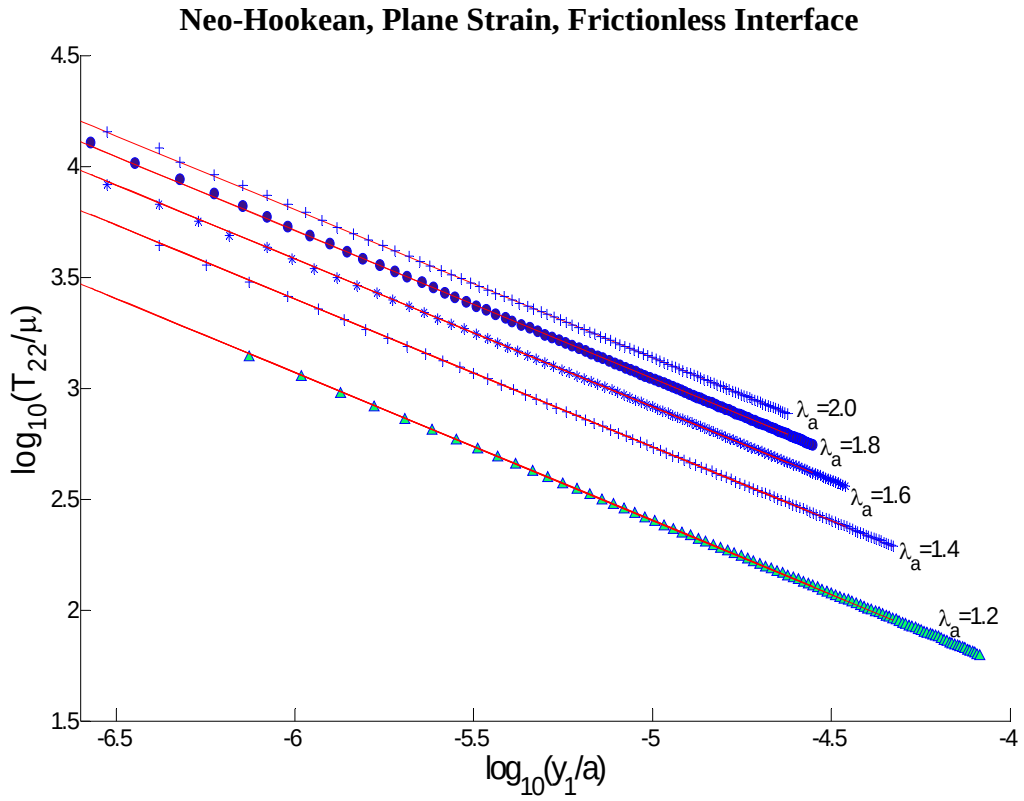

Figure 3.5: Log-Log plot of normalized opening normal stress field T_{22}/μ ahead of crack tip in a homogeneous Neo-Hookean material under plane strain shows a $1/R^{2/3}$ singularity. FEM results are plotted alongside asymptotic fits (red lines with slope *-2/3*) for different values of λ_a.

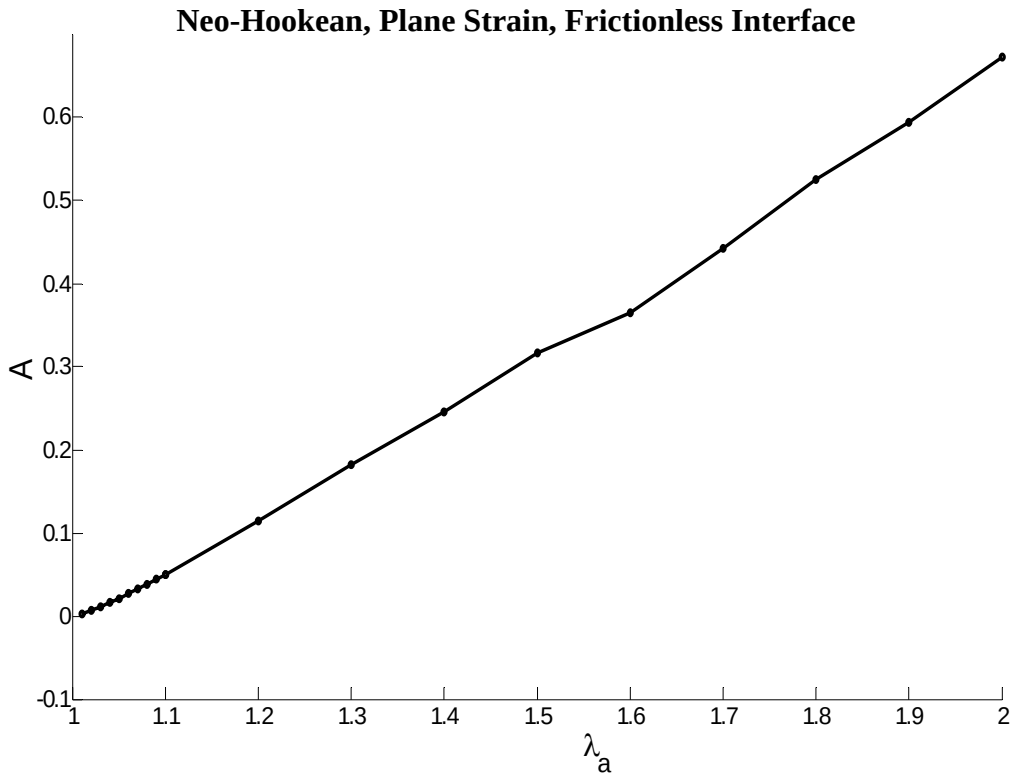

Figure 3.6: Amplitude (A) of normal opening stress (T_{22}) versus applied far field stretch λ_a, for a finite crack in an infinite homogeneous Neo-Hookean solid.

3.3.4 Plane Stress validation

Since there are no analytical results for the exponential hardening solid, we use the asymptotic results of [GK] for a pinned plane stress interface crack between a Neo-Hookean solid and a rigid substrate to validate our FEM analyses. For the case of a frictionless interface (e.g. a Mode I crack in homogeneous solid), we have validated our finite element results in a previous work [19].

For a pinned crack in a Neo-Hookean material, GK predicts that the normal opening stress directly ahead of the crack tip should have the form:

$$\frac{T_{22}}{\mu}(y_1, y_2 = 0) = \frac{B}{(y_1 / h)} \tag{3.7}$$

where B is a function of the applied stretch. Physically, B determines the strength of the singularity. In general, B can not be determined using the asymptotic method of GK [11]. Equation (7) states that a log-log plot of $T_{22}(y_1, y_2 = 0)/\mu$ versus y_1 / h should be a straight line with negative slope -1. This prediction is confirmed by our numerical results in figure 3.7. The unknown function B can be determined numerically by finding the intercepts of the straight lines in figure 3.7. Figure 3.8 plots B as a function of the applied stretch λ_a. The crack opening profile is plotted in figure 3.9 for different values of applied far field stretch. The asymptotic analysis of GK states that the crack opens up according to $y_2 = c\left|y_1\right|^{1/2}$ as $y_1 \to 0^-$. For small values of λ_a the local crack opening profiles are consistent with their analysis, but the FEM results deviate from the asymptotic results for $\lambda_a < 1.5$. For applied load $\lambda_a > 1.5$, the angle made by the crack face with the interface is less than 90^o. If our finite element method is correct, this result suggests that the asymptotic solution of GK may not be unique. However, the normal opening stress directly ahead of the

crack tip is still well predicted by GK's analysis. We have checked our finite element result by further refining the mesh using submodeling.

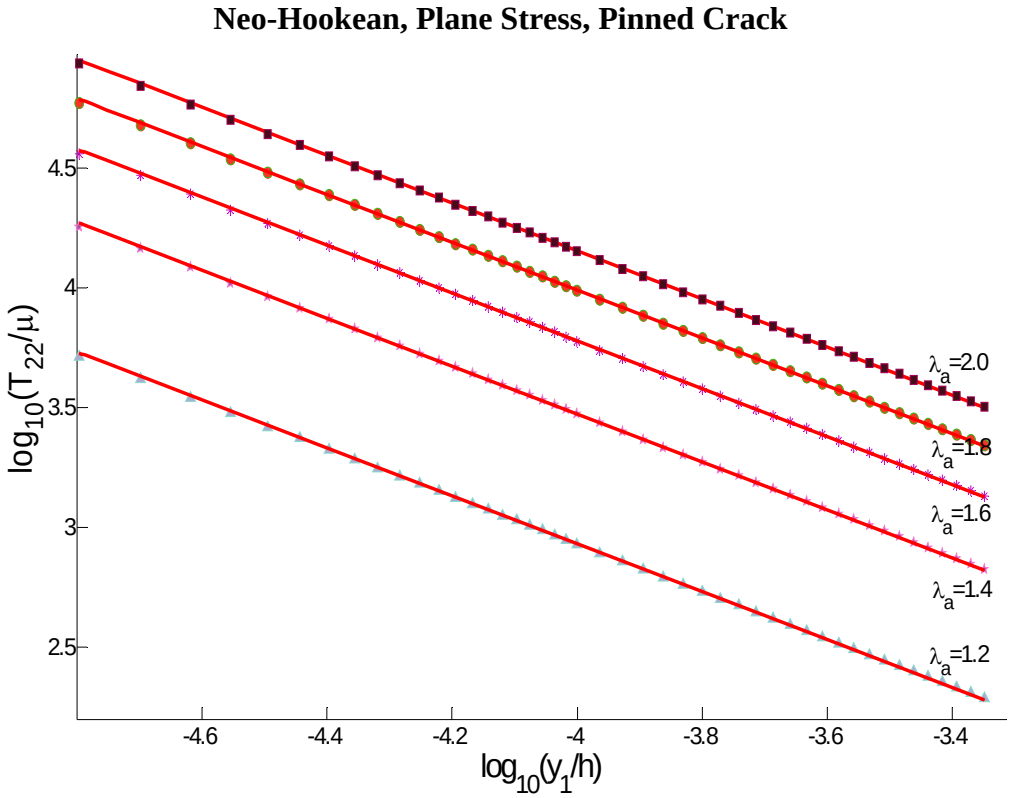

Figure 3.7: Log-log plot of the normalized opening normal stress T_{22}/μ directly ahead of the crack tip in a Neo-Hookean strip specimen in plane stress, for a pinned interface crack, shows a *1/R* singularity. The symbols are finite element results and the straight lines (red) are fits with slope of -1.

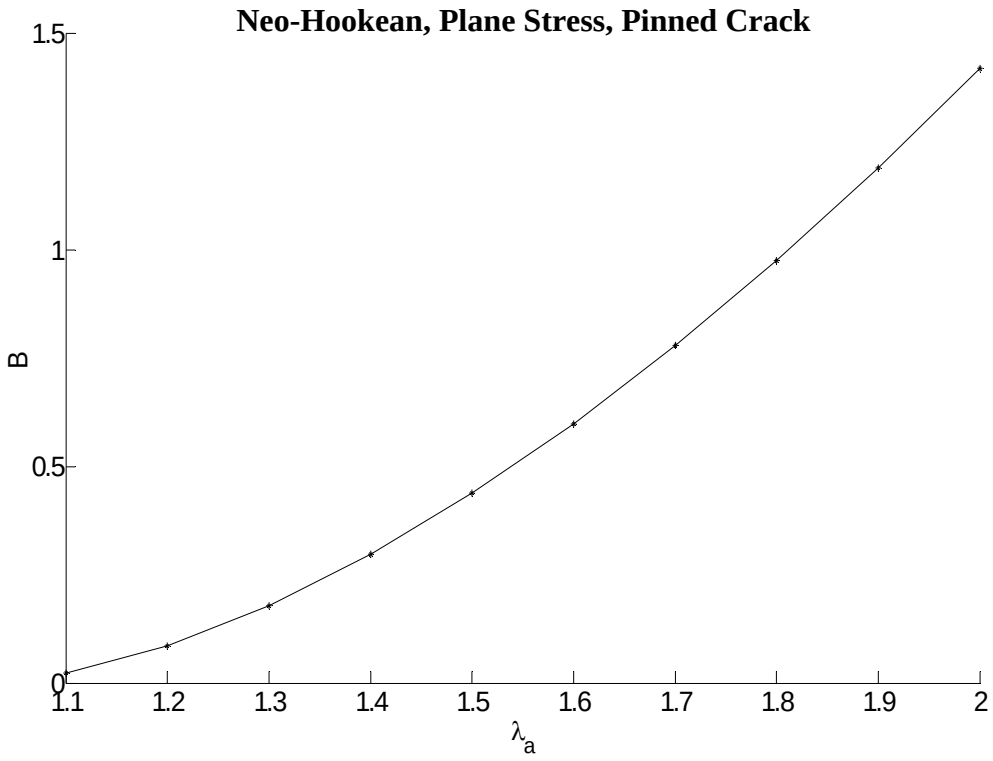

Figure 3.8: Amplitude (B) of normal opening stress (T_{22}) versus applied far field stretch λ_a in a Neo-Hookean strip specimen under plane stress for a pinned interface crack.

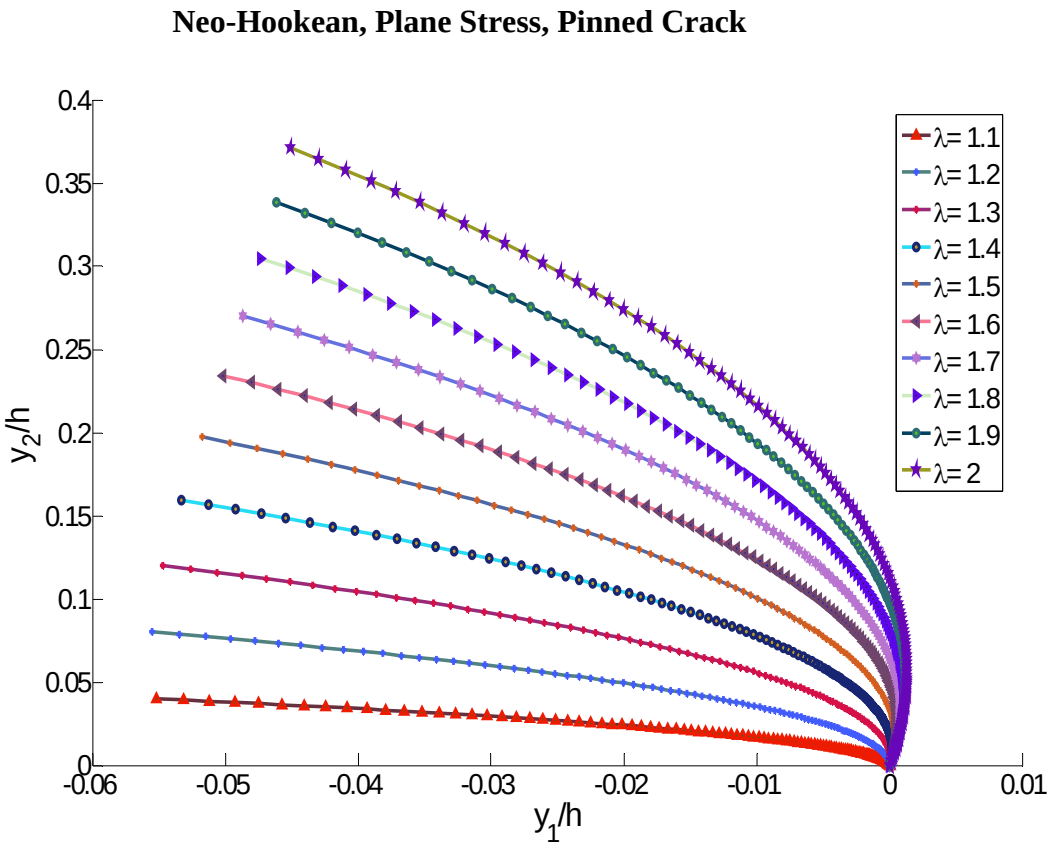

Figure 3.9: Crack opening profiles in a Neo-Hookean strip specimen under plane stress for a pinned interface crack, for $1.1 \le \lambda_a \le 2.0$.

3.4 Finite element results for exponential hardening solid

3.4.1 Frictionless Interface (Plane Stress Results)

We first study the case of a frictionless interface. The work function of the elastic solid is specified by (3.2) with I_1 given by (3.5). The value of the hardening parameter I_m is set equal to 3.5 in all our simulations since this value gave a good fit to the compression data obtained by Seitz et al [15]. As mentioned earlier, the solution of the frictionless interface crack problem remains unchanged if the rigid substrate is replaced by a strip of the same elastic solid with the same height, provided that the applied displacement is scaled down by a factor of ½. Since the solution of this problem was obtained in a previous work [19], we briefly summarize the key findings that are relevant to this work. They are:

1. The normal true stress T_{22} directly ahead of the crack tip exhibits a $1/(y_1|\ln y_1|)$ singularity. The normal stress (T_{22}) has a higher order singularity than the shear stress (T_{12}) and the transverse stress (T_{11}). In other words, the near tip stress state ahead of the crack tip is in a state of uni-axial tension.

2. The crack opening profile was smooth and is consistent with $y_2 = c|y_1|^{\alpha}$ with $\alpha < 1$.

3.4.2 Pinned Interface crack (Plane Stress Results)

Next, we consider the case of a pinned interface crack. Qualitatively, the crack tip fields were very similar to the frictionless case. The interfacial stresses directly ahead of the crack tip are shown in Figs. 3.10a, c-d. These figs. show that the normal opening stress (T_{22}) dominates the shear (T_{12}) and the transverse normal stresses (T_{11}) by at least an order of magnitude. The normal opening stress directly ahead of the crack tip can be fitted using

$$T_{22}(y_1, y_2 = 0)/\mu = Ch/\left(y_1|\ln y_1/h|^p\right) \tag{3.8}$$

where p is a numerical constant ≈ 1.5. We find that there is a range of p ($1<p<2$) which depends on λ that can fit the data well. The amplitude 'C' of the T_{22} singularity is plotted in figure 3.10b and is quadratic with the applied far field stretch λ_a. The shear stress directly ahead of the crack tip is negative for small applied far field stretch and becomes positive for $\lambda_a \geq 1.3$. This suggests that pinning the crack tip constrains the interface from moving in the $-x_1$ direction for small applied load. The crack opening profile is shown in figure 3.11. The crack opens up smoothly, similar to the case of a frictionless interface. Note that the crack opening displacement for the same applied stretch is much less than the Neo-Hookean material. This is due to the high strain hardening of the exponential model. Also, the deformed crack faces makes an obtuse angle with the interface.

3.4.3 Frictionless Interface, Plane Strain Results

First we consider the case of a frictionless interface between an exponential solid and a rigid substrate. Qualitatively the results are similar to the Neo-Hookean case (plane strain and plane stress), that is, the transverse normal stress is much smaller than the opening normal stress – the crack tip is in uniaxial tension. The normal stresses are shown in Figs. 3.12a, c. The normal opening stress directly ahead of the crack tip can be fitted using

$$T_{22}(y_1, y_2 = 0)/\mu = Da/\left(y_1 \left|\ln y_1/a\right|^p\right) \tag{3.9}$$

where p is a numerical constant ≈ 2.5. We find that there is a range of p ($2<p<2.5$) which depends on λ_a that can fit the data well. The amplitude 'D' of the T_{22} singularity is plotted in figure 3.12b and is a quadratic function of applied far field stretch λ_a. The crack opening profile is shown in figure 3.13. The crack opens up smoothly as expected. Note that the results are only given for $\lambda_a \leq 1.5$, since the remeshing procedure failed to work for higher λ_a.

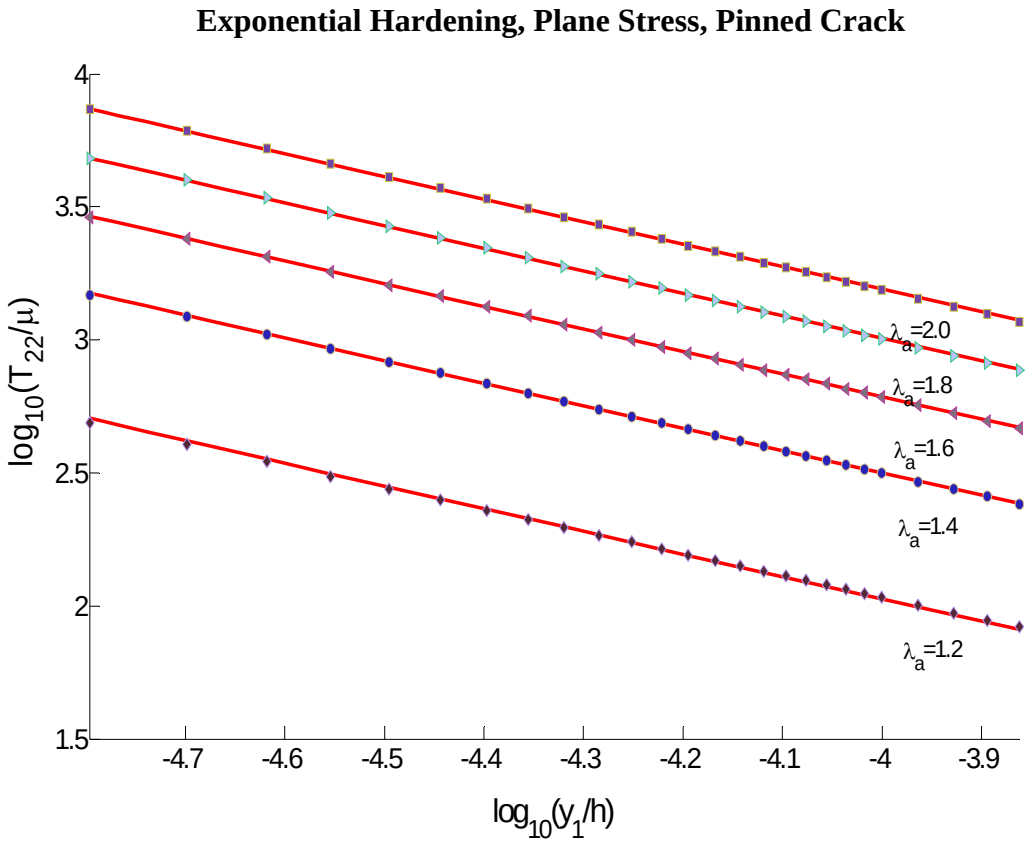

Figure 3.10a: Log-log plot of the normalized opening normal stress T_{22}/μ directly ahead of the crack tip in an exponential hardening strip specimen under plane stress, for a pinned interface crack. The symbols are finite element results. Note that the straight lines (red) are not exactly parallel due to the presence of the $\left(-\log y_1/h\right)^{1.5}$ term.

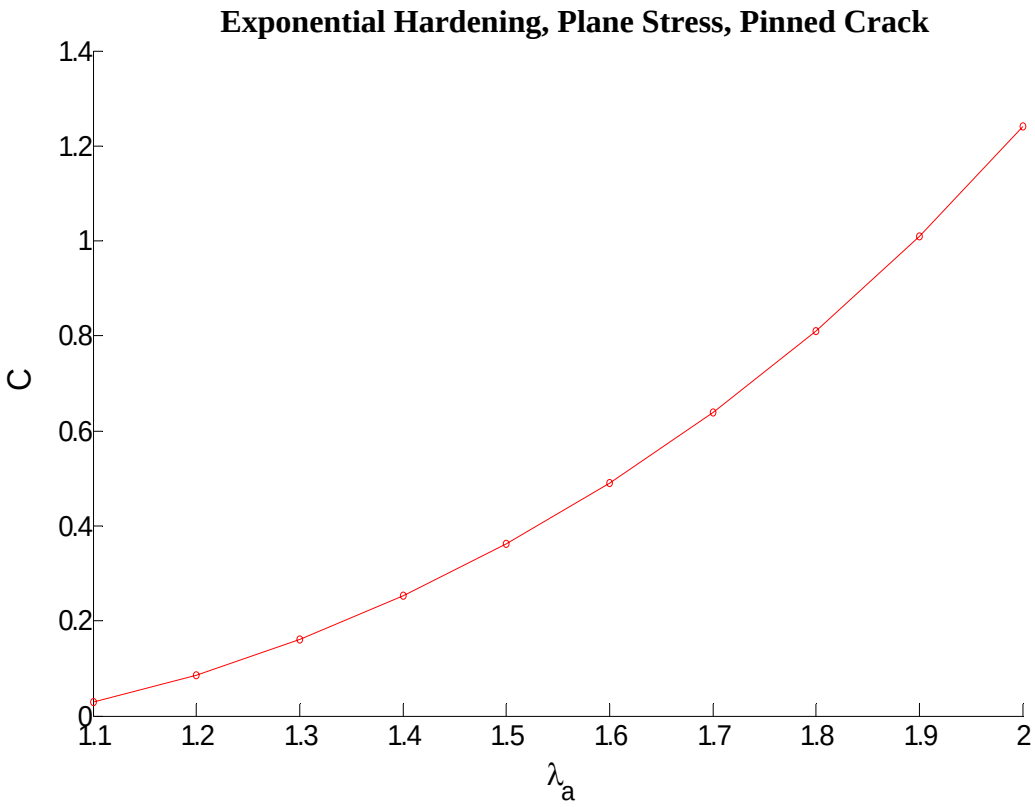

Figure 3.10b: Amplitude (C) of normal opening stress (T_{22}) versus applied far field stretch λ_a in an exponential hardening strip specimen under plane stress for a pinned interface crack.

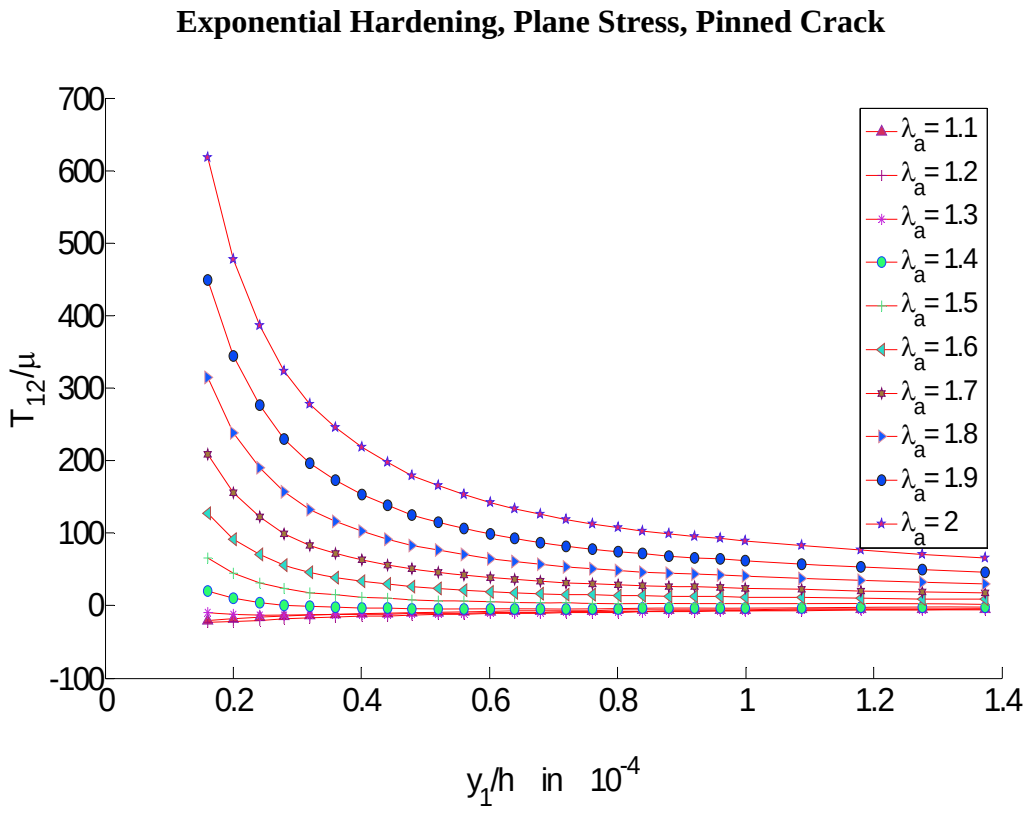

Figure 3.10c: Normalized shear stress T_{12}/μ directly ahead of the crack tip in an exponential hardening strip specimen under plane stress, for a pinned interface crack. Note that T_{12} is negative for small applied far field stretch and becomes positive for $\lambda_a \geq 1.3$

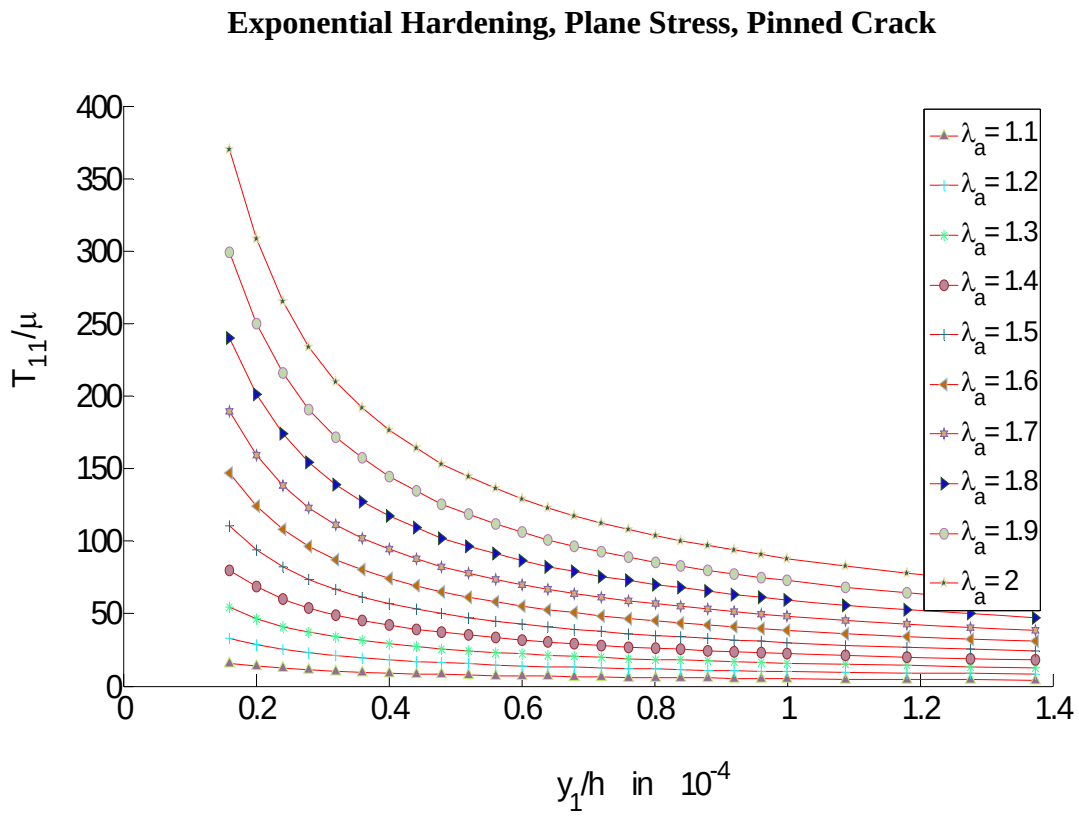

Figure 3.10d: Normalized transverse normal stress T_{11}/μ directly ahead of the crack tip in an exponential hardening strip specimen under plane stress, for a pinned interface crack. T_{11} is one order of magnitude smaller than T_{22}.

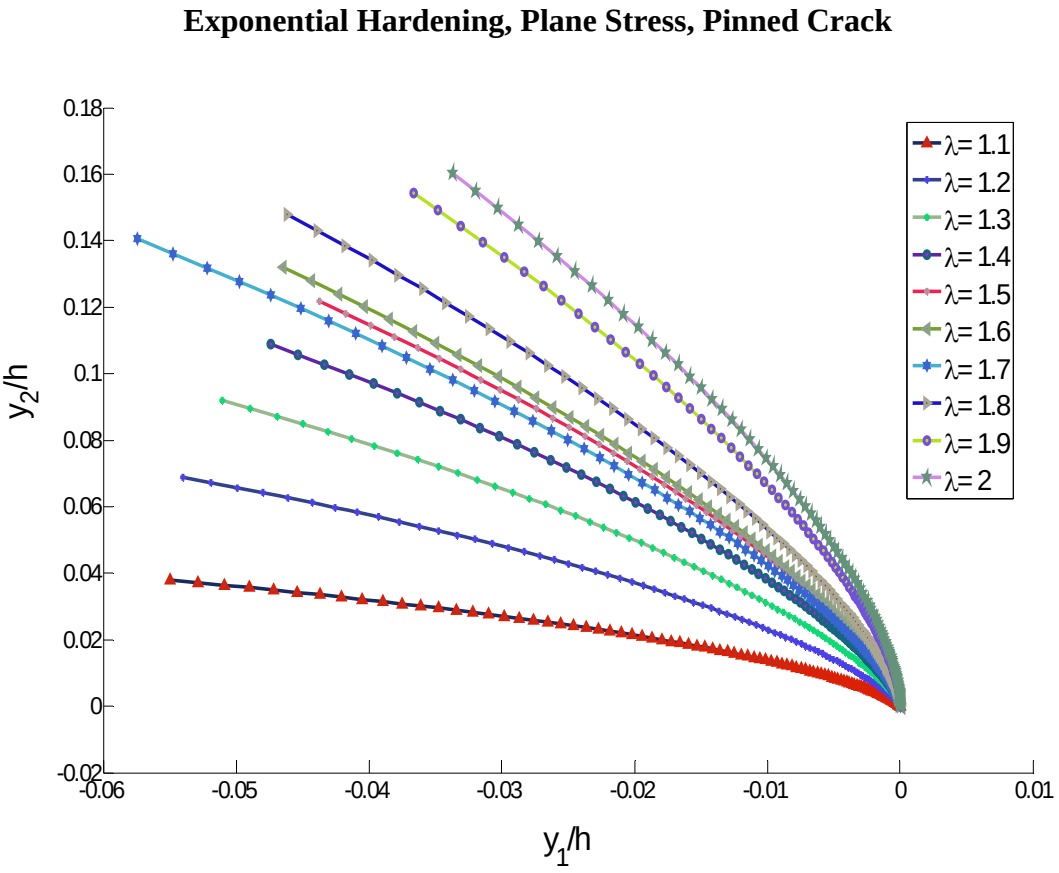

Figure 3.11: Crack opening profiles in an exponential hardening strip specimen under plane stress, for a pinned interface crack. $1.1 \le \lambda_a \le 2.0$.

Exponential Hardening, Plane Strain, Frictionless Interface

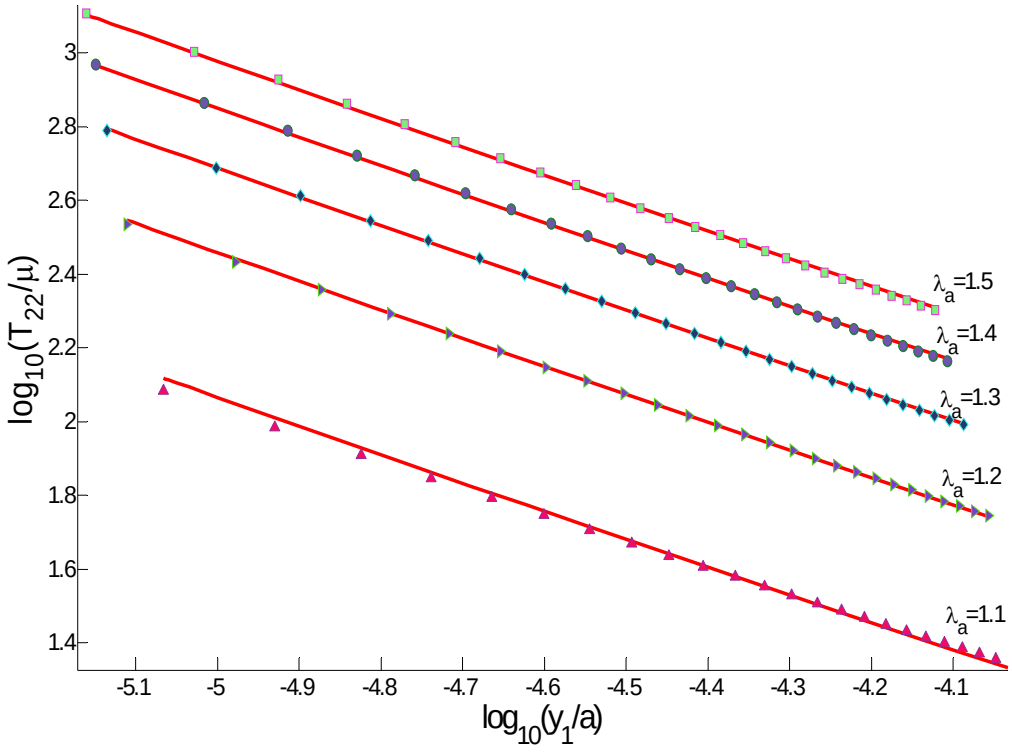

Figure 3.12a: Log-log plot of the normalized opening normal stress T_{22}/μ directly ahead of the crack tip in an exponential hardening solid under plane strain, for a frictionless interface. The symbols are finite element results. Note that the straight lines (red) are not exactly parallel due to the presence of the $\left(-\log y_1/a\right)^{2.5}$ term.

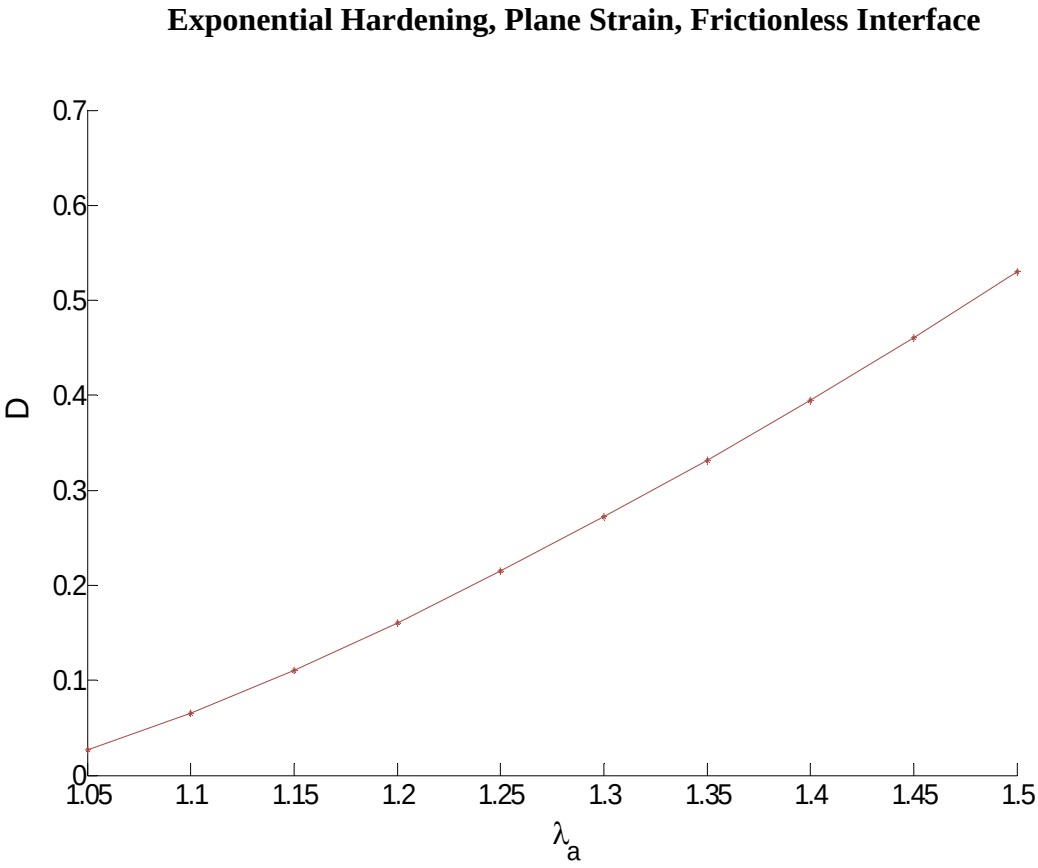

Figure 3.12b: Amplitude (D) of normal opening stress (T_{22}) versus applied far field stretch λ_a in an exponential hardening solid under plane strain, for a frictionless interface.

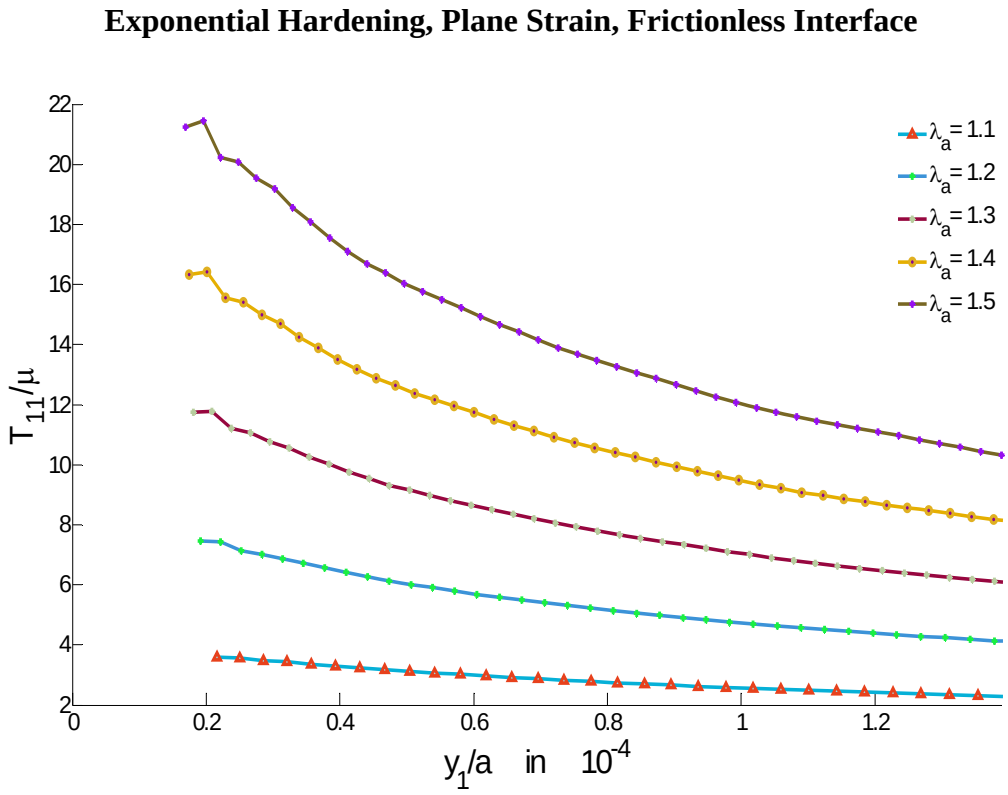

Figure 3.12c: Normalized transverse normal stress T_{11}/μ directly ahead of the crack tip in an exponential hardening solid under plane strain, for a frictionless interface.

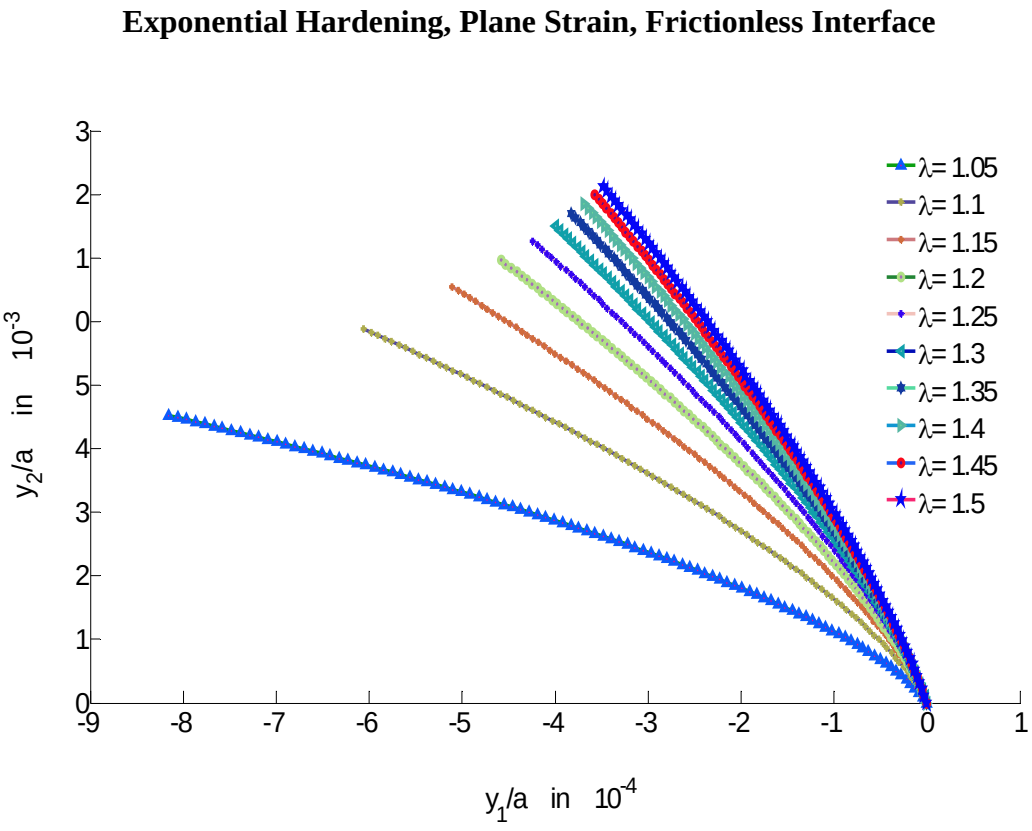

Figure 3.13: Crack opening profiles in an exponential hardening solid under plane strain, for a frictionless interface. $1.05 \le \lambda_a \le 1.5$.

3.4.4 Pinned interface crack, Plane Strain Results

Our results above show that interface cracks under plane stress and plane strain conditions behave in a similar way. Specifically, the normal opening stress dominates over other stress components. Also, the crack opens up smoothly. Therefore, one may well expect the same behavior in pinned cracks. Our result above shows that this is indeed true for plane stress deformation. Surprisingly, this is not true in plane strain. As in the axisymmetric punch problem, we found that the crack face flips over, almost touching the fixed interface directly ahead of the crack tip, with the crack tip angle almost tangent to the interface. This is true for both the Neo-Hookean and the exponential hardening solid. This is also consistent with experiments on pressure sensitive adhesives by Glassmaker et al [3], who observed the occurrence of a "foot" prior to cavitation. Figure 3.14 shows the deformed crack face profile in the exponential solid, even at very small applied loads ($\lambda_a = 1.05$), resembles a foot.

There is a definite element size effect seen in the FEM results since reducing the element size at the crack tip causes the crack face "flipping over" to occur at a smaller value of λ_a. The element size near the crack tip is less than 10^{-5} in our FEM simulations and reducing it further will not change the qualitative nature of the results presented here. This element size was sufficient to capture the normal opening stress singularities reported by Stephenson [10] and Guebelle & Knauss [11] for plane strain and plane stress respectively, in Neo-Hookean solids. For a pinned crack under plane strain, the interfacial stresses are quite different. The normal opening stress (T_{22}) was lesser than the shear and the transverse normal stresses with the transverse normal stress (T_{11}) being the highest. Also, the normal opening stress (T_{22}) shows oscillations directly ahead of the crack tip, with the amplitude of the oscillations increasing towards the crack tip (figure 3.15a). Oscillations also occur in the normal stress (T_{zz}) at the interface of a rigid cylindrical punch retracting from an incompressible Neo-

Hookean substrate to which it is perfectly bonded [6]. For the axisymmetric problem in [6] however, the normal stress (T_{zz}) peaks at a finite distance from the punch edge (crack front), the oscillations appear after the peak, then decrease in amplitude as one approach the punch edge, suggesting that the opening stress at the tip is bounded. This is not the case for a pinned plane strain crack; the amplitude of the oscillations in the opening normal stress (T_{22}) increases monotonically towards the crack tip as shown in figure 3.15a. From figure 3.15a, it seems that these oscillations do not occur for small λ_a. However, they are actually present even for very small applied loads; but the region where oscillations occur is too small to be captured by our finite element mesh. Indeed, we did see oscillations in T_{22} for small λ_a by further reducing the element size around the crack tip. Figure 3.15b shows that T_{22} increases monotonically towards the pinned crack tip and has approximately the same magnitude as the absolute value of the amplitude of the normal stress (T_{22}). Also, the transverse normal stress (T_{11}) has the highest magnitude as shown in figure 3.15c. These results are quite different from the case of a frictionless interface where the opening normal stress (T_{22}) dominates.

In the axisymmetric punch problem in [6], the shear stress (T_{rz}) on the interface increases to a peak value directly above the blunted crack tip, before it decreases to a bounded value at the punch edge. This result differs from our plane strain pinned crack simulations in that the shear stress (T_{12}) on the interface (figure 3.15b) increases monotonically towards the pinned crack tip. It should be noted that the elastic substrate in the punch problem is Neo-Hookean whereas the plane strain calculations are obtained using an exponential hardening solid. Nevertheless, the fact that the stress distribution near the crack tip is different is cause of concern. Therefore, we perform a consistency check on our finite element results for the pinned

interface plane strain crack by noting that on the interface (see appendix 3B for details),

$$\frac{T_{11}(y_1,0)-T_{22}(y_1,0)}{T_{12}(y_1,0)}=\frac{\left(\left(u_{1,2}(y_1,0)\right)^2-1\right)}{u_{1,2}(y_1,0)}\approx u_{1,2}(y_1,0) \tag{3.10}$$

Using our FE element results for $T_{11}(y_1,0), T_{12}(y_1,0)$ and $T_{22}(y_1,0)$, we can solve equation (3.10) for $u_{1,2}(y_1,0)$. Since $T_{12}(y_1,0)$ is (see appendix 3B)

$$T_{12}(y_1,0)=\mu e^{I/I_m}u_{1,2}(y_1,0) \tag{3.11}$$

where $I\equiv I_1(x_1,0)=\left(u_{1,2}(x_1,0)\right)^2$, we can check for consistency by substituting $u_{1,2}(y_1,0)$ obtained from (3.10) into (3.11) and compare with $T_{12}(y_1,0)$ obtained from FEM. Note that the strain invariant I_1 directly ahead of the crack tip (i.e., $y_2=0$) is $\left(u_{1,2}(y_1,0)\right)^2$. Since the energy density W depends only on I_1, the strain energy of the material points lying along the interface is due only to interfacial shear. In appendix 3C, we show that the interfacial true stress components $T_{\alpha\beta}$ must satisfy the condition

$$\left|T_{11}\right|>>\left|T_{12}\right|>>\left|T_{22}\right| \tag{3.12}$$

which is also supported by our simulation.

Exponential Hardening, Plane Strain, Pinned Crack

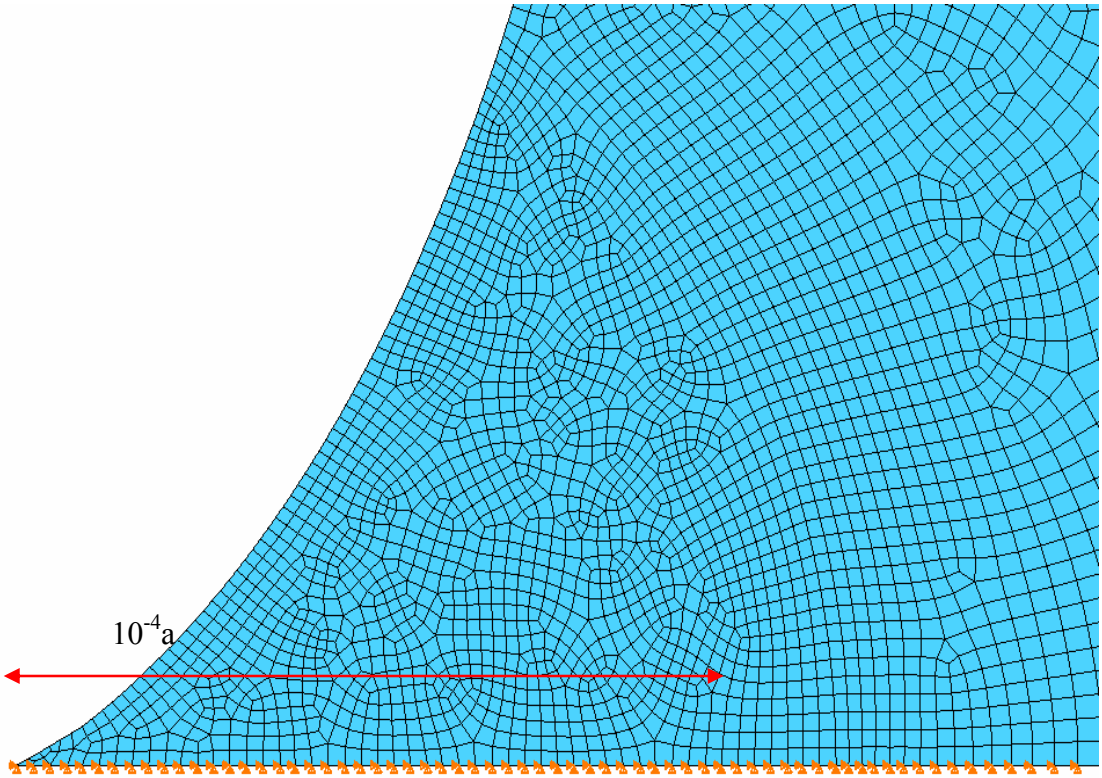

Figure 3.14: Crack opening profile from finite element simulation for $\lambda_a = 1.05$ in exponential hardening solid showing the foot seen in experiments of Glassmaker et al [3]. The crack face flips over, almost touching the pinned interface directly ahead of crack tip. The local mesh is indicated. The arrow shows the scale $(10^{-4}a)$. The smallest element is less than $10^{-5}a$.

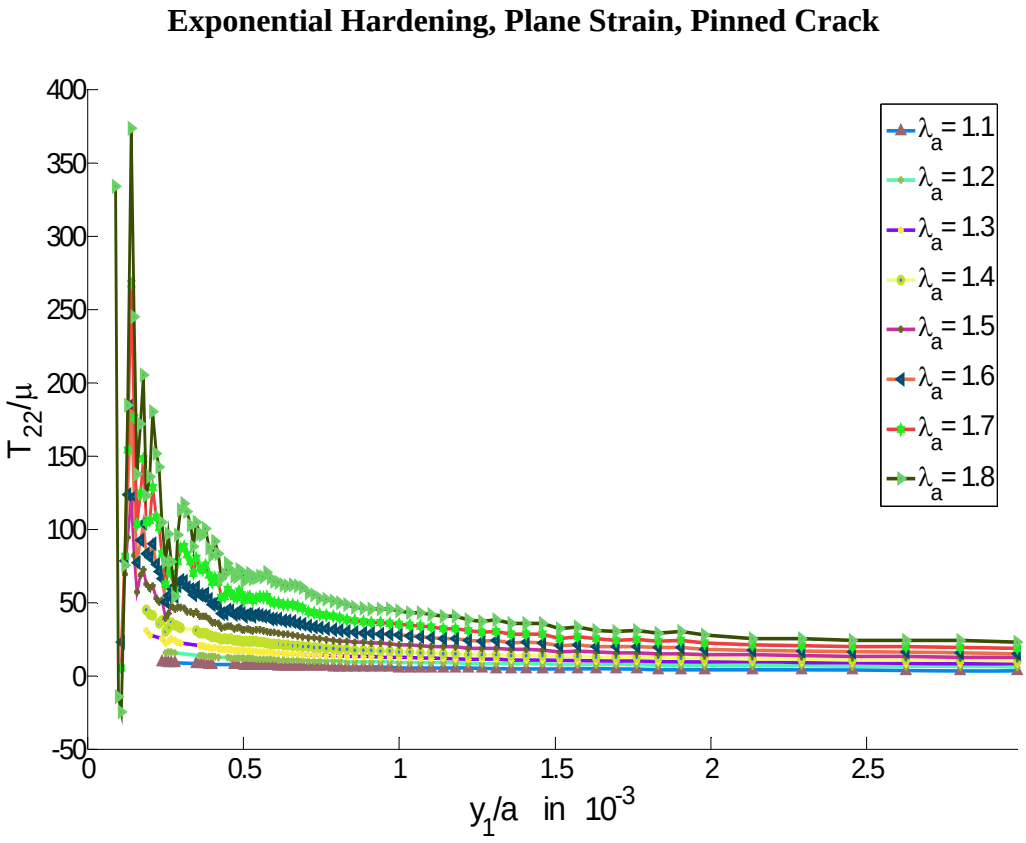

Figure 3.15a: Normalized opening normal stress T_{22}/μ directly ahead of the crack tip in an exponential hardening solid under plane strain, for a pinned interface crack. T_{22} is lesser than the other stress components. The opening normal stress oscillates. The amplitudes of these oscillations increase towards the crack tip.

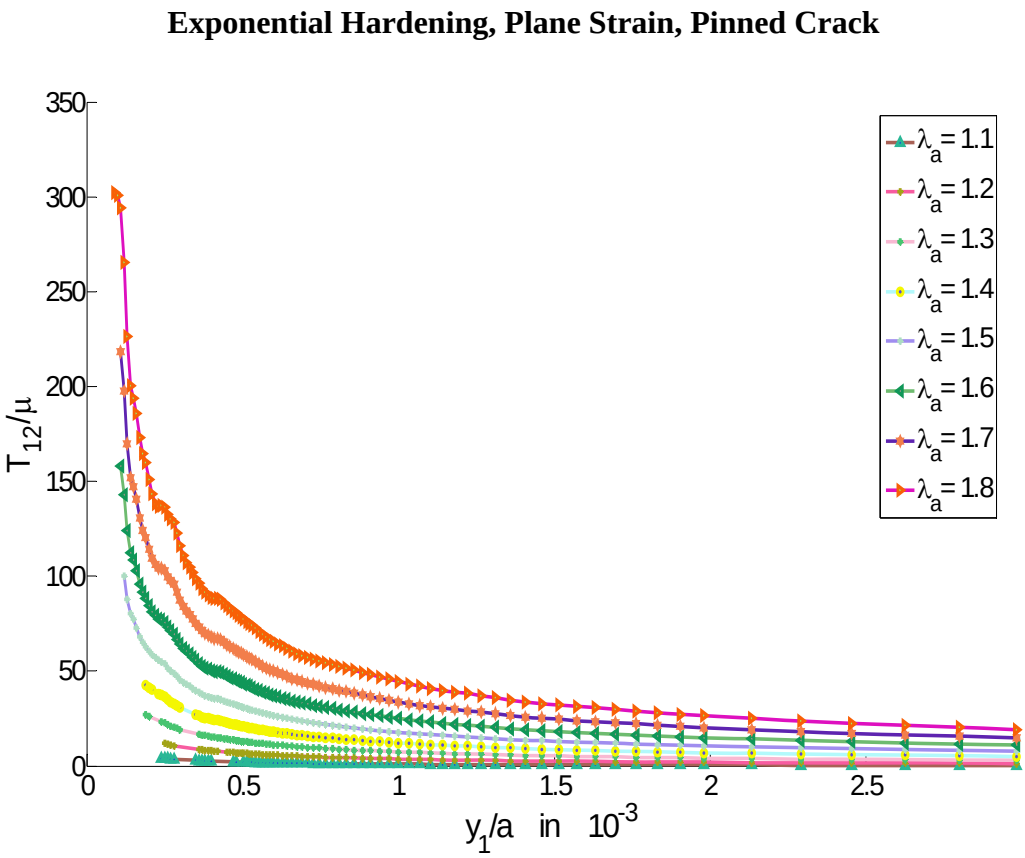

Figure 3.15b: Normalized shear stress T_{12}/μ directly ahead of the crack tip in an exponential hardening solid under plane strain, for a pinned interface crack.

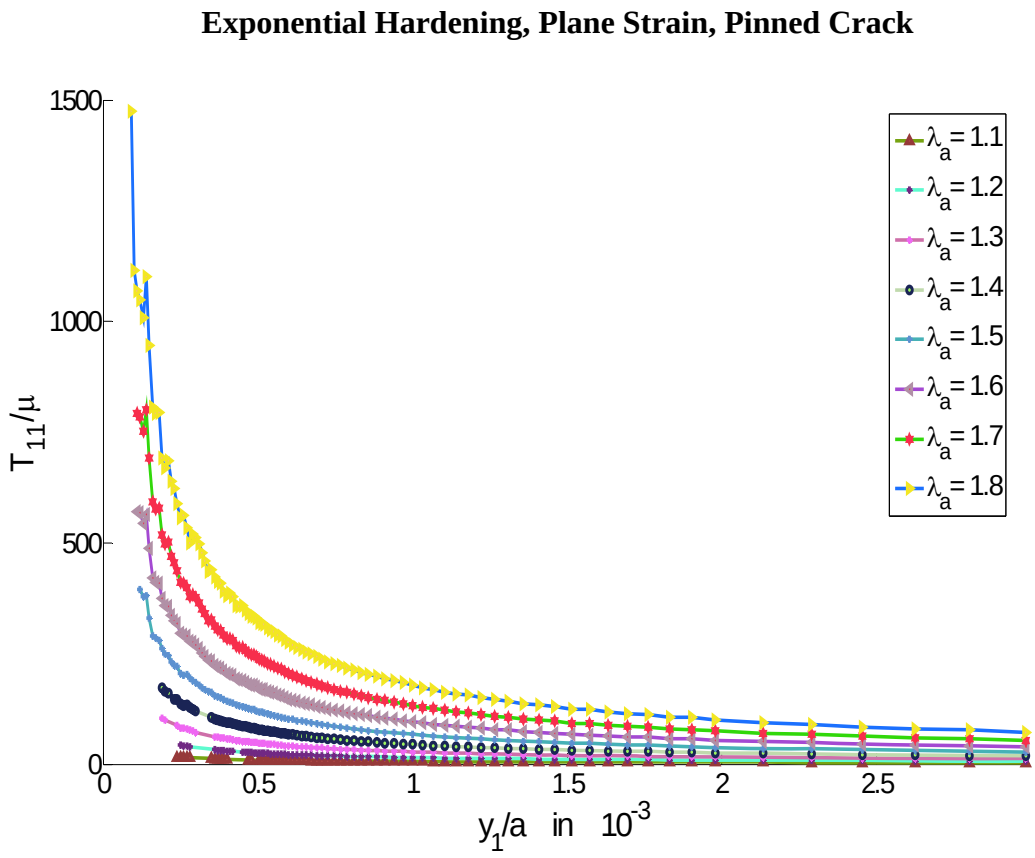

Figure 3.15c: Normalized transverse normal stress T_{11}/μ directly ahead of the crack tip in an exponential hardening solid in plane strain, for a pinned interface crack. T_{11} is the higher than the other stress components.

3.5 Discussion and conclusions

We carried out finite strain simulations for an interface crack between a rigid substrate and an infinite incompressible elastic half space. Our results suggest that geometric constraint can play an important in the shape of the deformed crack as well as the interfacial stress ahead of the crack tip. For example, both the pinned and frictionless crack in plane stress exhibits same qualitative behavior, i.e., the crack opens up smoothly and the opening normal stress is the dominant stress component. In contrast, the normal stress (T_{22}) directly ahead of a pinned interface crack tip in plane strain is less than the shear stress (T_{12}) and the transverse normal stress (T_{11}) and it shows oscillations. Furthermore, the crack face flips over and the tip angle is almost tangential to the interface. We believe that the oscillations are real and not numerical instabilities since they persist despite using a very fine mesh size (10^{-5}). We believe that our numerical result is accurate since the same FEM has been able to reproduce asymptotic results in the literature.

It is well known that linear elastic fracture mechanics (LEFM) predicts an oscillatory stress field ahead of the crack tip for a planar bi-material interface crack as shown by Williams [20], Erdogan [21], Shih & Asaro [22]. This is because the near tip stresses and strains turn out to be of mixed mode character no matter what the far field loading conditions are, unlike in a homogeneous case. These oscillations however disappear if one of the bimaterial is incompressible and the other rigid. For example, for the plane strain interface crack problem we study in this work, it has been shown that the stress intensity factor is pure Mode I, and is given by Rice [23]

$$K_I = \sigma_\infty \sqrt{\pi a / 2} \tag{3.13}$$

where σ_∞ is the applied tension at infinity. This result is valid whether or not the interface crack is pinned, or whether the crack is loaded under plane stress or plane strain.

This result is clearly at odds with our finite strain results. Therefore, one needs to be particularly careful when applying LEFM results to interpret experiments. For finite strain elasticity under plane stress deformation, Knowles and Sternberg [7] (compressible materials) and later Guebelle & Knauss (GK) [11] (incompressible materials) showed that the stress field ahead of a bi-material interface crack tip are free of the oscillatory singularities predicted by the linear theory. Hermann [9] showed that this is also true for an interface crack between two compressible hyperelastic solids under finite plane strain deformation. Their results suggest that non-oscillatory crack tip fields should be expected on a bi-material interface between a soft incompressible material and a rigid substrate. However, our numerical results seem to indicate the contrary. The normal stress field (T_{22}) ahead of an interface crack between a soft incompressible hyperelastic material and a rigid substrate, under plane strain conditions, is oscillatory. However, unlike the case of a rigid punch retracting from an elastic substrate in [6], where the oscillations in T_{zz} are found to be bounded, the magnitude of the oscillations in our plane strain problem increase towards the crack tip and seems to be unbounded.

Our numerical analysis shows that there are important differences in the interface stresses under plane strain deformation, between the "full friction" and frictionless boundary conditions, in contrast to the prediction of LEFM. Specifically, for the "full friction" or a pinned crack, the normal stress oscillates and is of the same order of magnitude as the shear stress, as opposed to the frictionless case, where the opening normal stress dominates. Furthermore, our numerical results shows that the normal opening stress at the same distance directly ahead of the crack tip and for the

applied λ_a in the frictionless case is at least one order of magnitude higher than the pinned crack case.

This result may also explain why interface cracks in a tack test on a sticky surface get pinned, which is a necessary condition for stable cavity growth in the direction of the applied displacement. Our result that the opening stress ahead of an interface crack is higher on a slippery surface is also consistent with the experimental observation that fibrils between cavities eventually fail due to sliding of the "foot" along the interface [3]. Indeed, our analysis shows that crack blunting initially reduces stress concentration at the interface, allowing stable cavity growth. As deformation continues, shear stress builds up at the interface, which eventually slides. Finally, sliding enhances normal stress at the receding contact line, which subsequently causes the detachment of fibrils from the interface. This conclusion is entirely consistent with recent experiments [24-26].

To make further connection with experiments, we note the novel experiments on friction and adhesion by Newby and Chaudhury [27-28]. These experiments demonstrate that there is a connection between interfacial slip and adhesion; namely, debonding is more likely to occur on a slippery interface even though the interface may have a higher work of adhesion! Their experiments are consistent with our result that a frictionless interface promotes higher normal opening stress, hence is easier to fail. A schematic (figure 3D) of the local crack opening profile in the paper of Newby et al [14] is particularly revealing. These authors hypothesize that the crack must open as a low angle wedge near the tip, very similar to the deformed crack profile shown in figure 3.14. Their hypothesis clearly violates standard results in fracture mechanics and can only be reconciled using finite strain theory.

Our finite element analysis suggests that the standard assumption in finite deformation crack profile, namely, (3.1) with $0 < \alpha < 1$ may not be the only choice.

For example, our plane stress simulations for a pinned interface crack indicate that the local crack profile deviates from the theoretical prediction for larger applied loads. This result suggests that there may be other solutions than those considered in the literature. Further theoretical work is needed to resolve this issue. Likewise, the existence of oscillatory interface crack tip field needs to be reconsidered.

APPENDIX 3A

Stephenson's result [10] in deformed coordinates

Equation (3.6) can be derived using (4.37), (5.9) and (5.11) in Stephenson's work. According to (4.37), directly ahead of the crack tip, $\theta = 0$, y_1 is (4.37)

$$y_1 = \frac{4}{3a} r^{3/2} + o(r^2) \tag{3.A1}$$

where a is a constant that can not be determined by asymptotic analysis. The normal component of the true stress field, T_{22}, is given by (5.9) and (5.11). It is

$$T_{22} = Cr^{-1} + o(r^{-1}) \tag{3.A2}$$

where C is a constant. Combining (3.A1) and (3.A2) gives:

$$T_{22} \approx K y_1^{-2/3} \tag{3.A3}$$

where $K = C\left(\frac{3a}{4}\right)^{-2/3}$ and is a constant that depends on the geometry and far field applied load.

APPENDIX 3B

A consistency check on our numerical results ahead of the pinned interface crack tip under plane strain deformation for the exponential hardening solid is presented here. For an incompressible isotropic elastic solid with a strain energy density function that depends only on I_1, the true stresses $T_{\alpha\beta}$ is related to the displacement gradients by

$$T_{\alpha\beta} = -p\delta_{\alpha\beta} + 2W'(I_1)\begin{bmatrix} (y_{1,1})^2 + (y_{1,2})^2 & y_{1,1}\,y_{2,1} + y_{1,2}\,y_{2,2} \\ y_{1,1}\,y_{2,1} + y_{1,2}\,y_{2,2} & (y_{2,1})^2 + (y_{2,2})^2 \end{bmatrix} \tag{3B.1}$$

where $W'(I_1) = dW/dI_1$ and p is the "pressure" required to satisfy the incompressibility condition. Since one of the materials is rigid, the displacements directly ahead of the crack must satisfy

$$u_1(x_1 > 0, x_2 = 0) = u_2(x_1 > 0, x_2 = 0) = 0\,. \tag{3B.2}$$

In 3B.2, we have assumed that the origin of the coordinate system (x_1, x_2) coincides with the crack tip and the interface occupies $x_1 > 0, x_2 = 0$. Equations (3B.2) and (3.4) imply that

$$y_{1,1}(x_1, 0) = 1, \qquad y_{1,2}(x_1, 0) = u_{1,2}(x_1, 0) \tag{3B.3}$$

$$y_{2,2}(x_1, 0) = 1 + u_{2,2}(x_1, 0), \qquad y_{2,1}(x_1, 0) = 0 \tag{3B.4}$$

$$I(x_1, 0) = \left(u_{1,2}(x_1, 0)\right)^2 + \left(1 + u_{2,2}(x_1, 0)\right)^2 - 1 \tag{3B.5}$$

Directly ahead of the crack tip, the incompressible condition is

$$\underbrace{y_{1,1}\,y_{2,2}}_{1+u_{2,2}(x_1,0)} - \underbrace{y_{1,2}\,y_{2,1}}_{0} = 1 \Rightarrow y_{2,2}(x_1, 0) = 1 \Leftrightarrow u_{2,2}(x_1, 0) = 0 \tag{3B.6}$$

Combining (3B.3), (3B.4) and (3B.6) gives

$$T_{\alpha\beta}(y_1,0) = -p\delta_{\alpha\beta} + \mu e^{I/I_m}\begin{bmatrix} 1+\left(u_{1,2}(y_1,0)\right)^2 & u_{1,2}(y_1,0) \\ u_{1,2}(y_1,0) & 1 \end{bmatrix} \tag{3B.7}$$

where W is given by (3.2) and $I \equiv I_1(x_1,0) = \left(u_{1,2}(x_1,0)\right)^2$. Equation 3B.7 enables us to perform a consistency check using the stresses derived from the finite element analysis directly ahead of the crack tip (note that $y_1 = x_1$ on the interface). Specifically, (3B.7) implies

$$\frac{T_{11}(y_1,0) - T_{22}(y_1,0)}{T_{12}(y_1,0)} = \frac{\left(\left(u_{1,2}(y_1,0)\right)^2 - 1\right)}{u_{1,2}(y_1,0)} \approx u_{1,2}(y_1,0) \tag{3B.8}$$

Since we expect $\left|u_{1,2}(y_1 \to 0^+,0)\right| \to \infty$, (3B.7) implies that $|T_{11}| >> |T_{12}| >> |T_{22}|$ which is consistent with our numerical result.

APPENDIX 3C

UHYPER FORTRAN CODE used with ABAQUS for exponential hardening solid

```
      SUBROUTINE UHYPER(BI1,BI2,AJ,U,UI1,UI2,UI3,TEMP,NOEL,
     1 CMNAME,INCMPFLAG,NUMSTATEV,STATEV,NUMFIELDV,FIELDV,
     2 FIELDVINC,NUMPROPS,PROPS)

      INCLUDE 'ABA_PARAM.INC'
      CHARACTER*80 CMNAME
      DIMENSIONU(2),UI1(3),UI2(6),UI3(6),STATEV(*),FIELDV(*),
      2 FIELDVINC(*),PROPS(*)
      REAL G, I_M, I

      ! User coding to define U, UI1, UI2, STATEV
      ! WRITE(*,*) "INCMPFLAG ,G ,I_M", INCMPFLAG,G,JM
      ! WRITE(*,*) "CMNAME", CMNAME
      ! EXPONENTIAL HARDENING INCOMPRESSIBLE MODEL
      ! U = (G*I_M/2.0)*[exp(I_1/I_M) – 1]; I_1 = BI1 -3

      G = PROPS(1)  ! shear modulus
      I_M = PROPS(2)  ! Hardening parameter
      I_1 = BI1 - 3.0

      U(1) = G*(I_M/2.0) * (exp(I_1/I_M) - 1)    ! Strain Energy density function
      UI1(1) = (G/2.0)*  exp(I_1/I_M)            ! 1st derivative w.r.t I_1
      UI2(1) = (G/(2.0*I_M))* exp(I_1/I_M)       ! 2nd derivative w.r.t I_1
```

UI1(2) = 0 ; UI1(3) = 0 ; UI2(2) = 0 ; UI2(3) = 0 ; UI2(4) = 0.

UI2(5) = 0 ; UI2(6) = 0 ;

RETURN

END

REFERENCES

[1] Creton, C., "Materials science of pressure-sensitive adhesives," Mater. Sci. Technol., 1997, 18, 708–740.

[2] Crosby, A. J. and K. R. Shull, "Adhesive failure analysis of pressure-sensitive adhesives," J. Polym. Sci., Part B: Polym. Phys., 1999, 37, 3455–3472.

[3] Glassmaker, N, J., Hui, C. Y., Yamaguchi, T., and Creton, C., Detachment of stretched viscoelastic fibrils, Eur. Phys. J. E, 2008, 25 (3), 253-266.

[4] Lakrout, H., Sergot P., and Creton, C., Direct observation of cavitation and fibrillation in a probe tack experiment on model acrylic pressure-sensitive adhesives, J. Adhes., 1999, 69(3-4), 307-359.

[5] Brown, K., Hooker, J. C. and Creton, C. Micromechanisms of Tack of Soft Adhesives Based on Styrenic Block Copolymers, Macromol. Mat. and Eng., 2000, 287, 163-179.

[6] Krishnan, V.R.; Hui, C. Y. Large deformation of soft elastic materials in adhesive contact with a rigid cylindrical flat punch. Soft Matter, 2008, 4, 1909 – 1915.

[7] Knowles, J. K. and Sternberg, E.: Large deformation near a tip of an interface-crack between two Neo-Hookean sheets, J. Elast., 1983, 13, 257-293.

[8] Knowles, J. K. and Sternberg, E. An asymptotic finite-deformation analysis of the elastostatic field near the tip of a crack. Journal of Elasticity, 1973, 3, 67-107.

[9] Hermann, J. M.: An asymptotic analysis of finite deformation near the tip of an interface-crack. J. Elast., 1989, 21, 227-269.

[10] Stephenson, R. A. The equilibrium field near the tip of a crack for finite plane strain of incompressible elastic materials. Journal of Elasticity, 1982, 12, 65-99.

[11] Geubelle, P. and Knauss, W. G.: Finite strains at the tip of a crack in a sheet of hyperelastic material: I. Homogeneous case, II. Special bimaterial cases, III. General bimaterial case. J. Elast., 1994, 35, 61-98, 99-138, 139-174.

[12] Chang, J. H., Li, J. F., Evaluation of asymptotic stress field around a crack tip for Neo-Hookean hyperelastic materials, International Journal of Engineering Science, 2004, 42(15-16), 1675-1692.

[13] Lund R. A., Westmann, R. A. Finite element analysis of hyperelastic large deformation crack tip fields, Int. J. of Fracture, 1990, 43 (4), 257-270.

[14] B. Zhang Newby, M. K. Chaudhury, H. R. Brown, "Macroscopic Evidence of the Effect of Interfacial Slippage on Adhesion", Science, 1995, 269.

[15] Seitz, M. E.; Shull, K.R.; Krishnan, V.R.; Hui, C.Y; Martina D.; Baumberger, T.; Fracture and high strain behavior of self-assembled tri-block copolymer gels, 2008, Accepted in J. of Soft Matter.

[16] Baumberger, T.; Caroli, C.; Martina, D. Solvent control of crack dynamics in a reversible hydrogel. Nat Mater., 2006, 5(7), 552–555.

[17] Hibbit, Karlsson and Sorensen Inc., ABAQUS Manuals, Hibbit Karlsson and Sorensen Inc., Providence, RI, 2007, Abaqus 6.6.

[18] Anderson, T.L, Fracture Mechanics, Fundamentals & Applications, 3rd Edition, Taylor & Francis group, 1994.

[19] Krishnan, V.R., Rong, L. and Hui, C. Y., Finite Strain Crack Tip Fields in Soft Incompressible Elastic Solids, 2008, Accepted in Langmuir.

[20] Williams, M. L., The stresses around a fault or crack in dissimilar media. Bull Seismol Soc, 1959, Am 49 2, 199–204.

[21] Erdogan, F., Stress distribution in a nonhomogeneous elastic plane with cracks. J Appl Mech, 1963, Trans ASME 30, 232–236.

[22] Shih, C.F., and Asaro, R.J., Elastic–plastic analysis of cracks on bimaterial interfaces: Part I – small scale yielding. J Appl Mech, 1988, Trans ASME 55, 299–316.

[23] Rice, J. R., Elastic Fracture Mechanics Concepts for Interfacial Cracks, Journal of Applied Mechanics, 1988, 55, 98-103.

[24] Léger, L., and Creton, C., Adhesion mechanisms at soft polymer interfaces, Philos. Trans. R. Soc. London, Ser. A: Math. Phys. Eng. Sci., 2008, 366, 1425–1442.

[25] C. Creton, J. C. Hooker and K. R. Shull, Bulk and interfacial contributions to the debonding mechanisms of soft adhesives, Langmuir, 2001, 17, 4948–4954.

[26] G. Josse, P. Sergot, M. Dorget and C. Creton, Measuring interfacial adhesion between a soft viscoelastic layer and a rigid surface using a probe method, J. Adhes., 2004, 80, 87–118.

[27] B. Zhang Newby, M. K. Chaudhury, “Friction in Adhesion”, Langmuir, 1998, 14(17).

[28] B. Zhang Newby, M. K. Chaudhury, “Effect of Interfacial Slippage on Viscoelastic Adhesion”, Langmuir, 1997, 13(6).